Teijin Aramid/ Delft University of Technology

Master's Thesis

Manufacturing and impact characterisation of aramid fibre reinforced high-performance thermoplastics

Camill de Vos

Supervised by

Dr. Julie Teuwen
Dr. Walter Nijhuis
Dr. Ileana de Kleuver

September 2022

Abstract

While aramid fibre composites are generally said to have excellent impact properties, this has not yet been translated to the aerospace sector, where impact prone secondary structures remain to be made from metals or glass fibre reinforced polymer. Aramid fibre reinforced engineering thermoplastics could combine the stiffness of thermoset resins with the ductility of commodity thermoplastics in a novel composite with both high structural and impact properties. In the following thesis work, Twaron and Technora fibres are evaluated for their suitability in such a material.

Processing aramid reinforced materials is a trade-off between the composite consolidation quality and tensile strength retention in the fiber. Good consolidation is required to achieve the required bending properties in structural laminates and requires a low polymer melt viscosity. Strength loss in the yarn is caused by the high temperatures needed to achieve such levels of viscosity, which induce a number of degradation mechanisms if no countermeasures are taken. Oxidation, hydrolysis and a purely thermal component are identified as the main mechanisms causing deterioration. Using a Kapton vacuum bag as well as drying the reinforcement and matrix material greatly improves strength retention during processing. Purely thermal degradation cannot be counteracted and makes Twaron or other para-aramid homopolymers unsuitable for reinforcing polymers with processing temperatures above 250°C. Technora is shown to be more resistant against both hydrolysis and thermal degradation, with only minor strength losses well beyond 320°C. The high toughness of Technora attributes these fibres a high energy absorption potential.

Various Twaron and Technora reinforced engineering thermoplastics are produced to evaluate the influence of the fibre-matrix interface and matrix material on the low-velocity impact response. Higher interfacial adhesion is achieved by using epoxy sizing on Twaron yarn and appears to improve the energy absorbed during perforation through increased fracture toughness. Technora reinforced PPS and PEI appear to have a high energy absorption potential but relatively low out-of plane performance. The eventual feasibility of the novel material will eventually depend on its high impact performance with respect to other, conventional laminates such as aramid-epoxy.

Contents

List of Figures

Chapter 1

Introduction

Despite finding application in countless high-performance applications, aramid fibres remain a niche product in the aerospace sector when compared to carbon and glass fibres. While the fibre and its composites bring their own unique set of advantages with them, aircraft manufacturers remain hesitant in applying the material due to its distinctive drawbacks. The main disadvantages are low compressive strength, poor fibre matrix-adhesion resulting in debonding problems and rapid deterioration due to exposure to water or UV-light [3]. As carbon and glass fibres face neither of these problems, they generally remain the preferred option for structural components. On the other hand, aramid does provide some unique advantages, most notably its high fibre toughness. These unique properties give aramid some niche applications, where its composite could outperform competitor reinforcements. The prospect of weight savings make exploring its potential in specific aerospace structures worthwhile, as manufacturers strive to decrease fuel consumption on their path towards more sustainable aviation. A prominent example of widespread aramid use are engine blade containment units as seen in Figure 1.1, which protect fuselage during catastrophic engine failure but have no structural purpose [4].

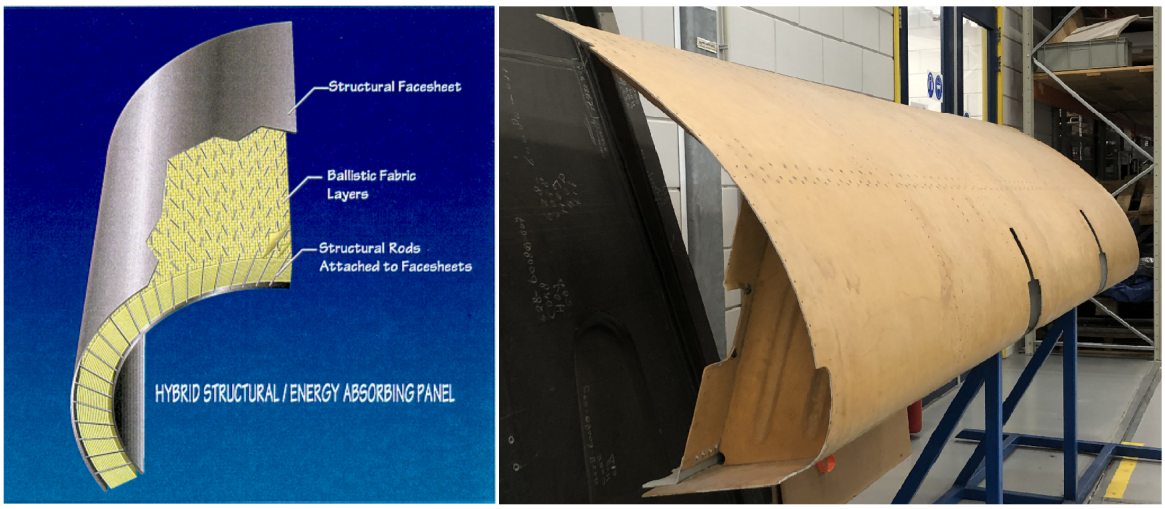

Figure 1.1: Dry aramid fibre jet engine casing [5] and glass fibre-PPS composite leading edge

Its impact properties are the main advantage aramid fibre has over competitor materials, as confirmed by widespread application in soft ballistic protection. Soft ballistics may either employ a small amount of matrix material to keep the fibres in place or use no matrix at all. Structural laminates distinguish themselves from ballistic composites in their requirement to transfer static loads. Nonetheless, impact performance is an important property in these materials as minor impacts only

may drastically reduce the loading capability. Aramid possesses high fibre toughness and moderate strength and stiffness at a very low density. These properties make it a promising reinforcement material for lightweight structures under light loads and with risk of high energy impact. Despite the favourable properties, use of aramid in structural composites is very rare. Notably in the aerospace sector, impact-prone structures such as fairings and leading edges remain to be made from GFRP or metals [6]. A reason for the limited application of aramid fibre reinforced polymer (AFRP) could be that scientific research has thus far failed to show widespread experimental evidence of the material performing advantageously in energy absorbing structures.

The impact strength of fibres is largely related to the area under their stress-strain curve [7]. Indeed, fibres used in impact applications such as S2-glass and aramids posses the highest toughness, both absolute and normalized in terms of their densities, with Technora and Kevlar KM2 performing exceptionally well. Figure 1.2 compares aramid to other common fibre types for their specific fibre toughness, clearly showing the specific property ranges. Apart from fibre toughness, matrix material

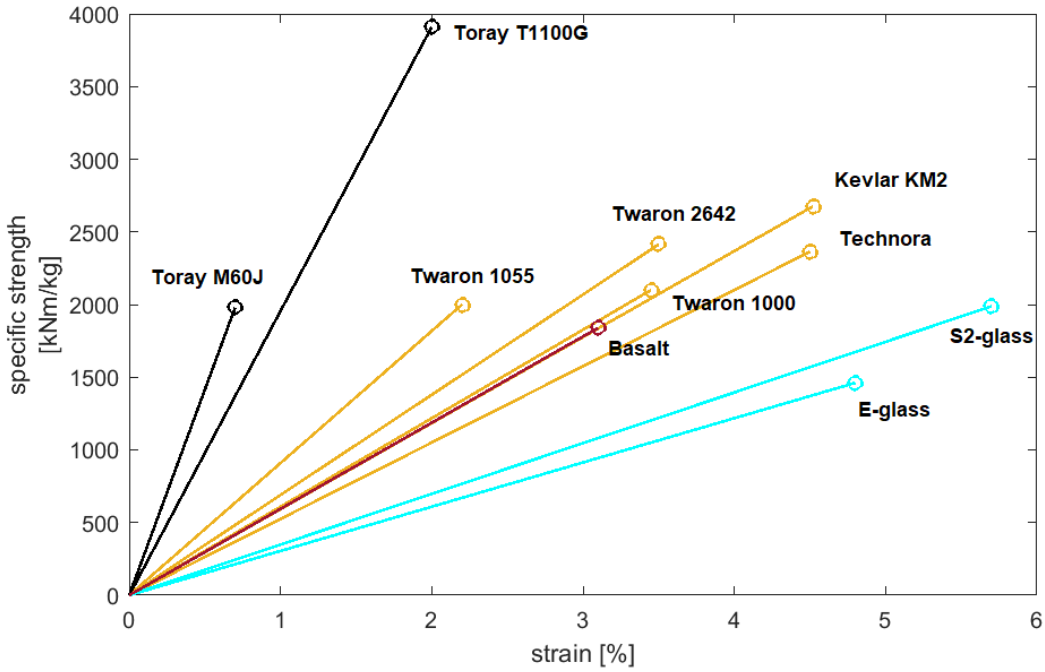

Figure 1.2: Specific toughness of some carbon, aramid, basalt and glass fibres [8],[9][1]

and fibre-matrix interface play a crucial role in structural composites. Extensive research has been conducted on improving the adhesion to aramid fibres [12]. Research on suitable polymer matrices is largely limited to thermosets and commodity thermoplastics. Thermosets provide stiffness and strength at relatively low cost. They appear to adhere moderately well to aramids, making them an excellent matrix material for structural composite use. Their brittle nature however restricts energy absorption in thermoset aramid composites to a point where they are frequently outperformed by glass fibre reinforced plastics (GFRP) [13]. The thermoplastics used in ballistic composites exhibit ductile behaviour but low strength and poor interfacial adhesion, making them unsuitable for structural use. High performance thermoplastics such as PEEK, PPS and PEI have recently seen increased use in composites as they offer faster processing times, better durability and recyclability over thermoset matrix materials. Furthermore, engineering thermoplastics posses comparable mechanical properties to thermosets but are much more ductile in nature due to the absence of crosslinks. Using these

[1]Values for Kevlar, Glass and Basalt fibre were obtained from the specified sources, values for Toray fibres were retrieved from https://www.toraycma.com and data on Twaron and Technora were obtained from internal unpublished documents. The data must be treated with care as the standard test method for evaluating fibre tensile strength differs accross the material types. While glass and carbon fibre data is generally measured from resin impregnated fibres, aramid tensile strength is obtained using twisted, dry yarn. Research by both Teijin and DuPont indicates that the tensile strength of resin impregnated yarn may be up to 25% higher than that of twisted yarn [10, 11].

polymers with aramid reinforcement could combine the properties of structural and ballistic aramid composites into a single material with both high mechanical and impact properties. A limited body of research on aramid reinforced high-performance thermoplastics is available but to the knowledge of the author, no feasible material has been produced or is being used on an industrial scale today.

This thesis project comprises two parts of research. Initially, the feasibility of manufacturing aramid fibre reinforced high-performance thermoplastics is explored using Twaron and Technora aramid yarn as produced by Teijin Aramid. The goal of this stage was to produce a viable composite, as well as to optimise the processing cycle in order to obtain the best properties possible. The limitations on the processing parameters were also defined. In the second stage, the impact characteristics of the novel material were explored. The effects of the fibre material, thermoplastic matrix type and fibre-matrix interface on impact performance were evaluated to some extent.

The literature review conducted before the experimental part of the project is presented in chapter 2, The experimental approach is elaborated in chapter 4, followed by the research proposal (chapter 3). The results are discussed in chapter 5. Finally, conclusions and recommendations regarding further research are presented in chapter 9.

1.1 Company Background

Teijin Aramid is a producer of various high-strength engineering fibres, most notably the para-aramid Twaron. Other products include meta-aramid Teijinconex and Twaron derivative Technora, famous for its use on parachutes for Mars rovers. Recently, an ultra-high molecular weight polyethylene (UHMWPE) film Endumax was introduced. The most prevalent applications protective and heat resistant clothing such as body armour, ballistic shielding, air cargo containers, ropes, cables and tyres, as well as reinforcement in conveyor and drive belts. The aramid fibres may also be ground to pulp, which finds extensive usage in brake pads and honeycombs, for which the pulp is further processed to aramid paper.

What is now Teijin Aramid was originally known as the Akzo Industrial Fibre branch, developing its first para-aramid in the 1970's, with commercial production starting in the 1980's. A fierce competition with American chemical company DuPont erupted soon after, due to the similarity of Akzo product Twaron with the more famous Kevlar. This dispute resulted in a patent war spanning over the next decade but the relationship between the rivals has improved significantly after Teijin Aramid was allowed to use the spinning process patented by DuPont, which in reverse was granted the right to use the solvent developed by Teijin. The Akzo branch became an independent company in 1989 but was bought up by Japanese holding group Teijin Ltd. in 2000. The Japanese chemical, healthcare and IT company had its own history of aramid research and eventually merged all these branches under the brand name Teijin Aramid. The company is also a producer of other performance polymer products such as films, fibres and resins. Furthermore, Teijin is one of the major global manufacturers of carbon fibres, which are produced by subsidiary Toho Tenax, as well as thermoplastic and thermoset carbon fibre pre-pregs.

Teijin Aramid produces and sells only the four products Twaron, Technora, Teijinconex and Endumax. Since their introduction, aramid mechanical properties have have improved massively, mostly due to process improvements resulting in gains in polymer quality and crystallinity. A large share of company resources is still aimed at increasing the performance of the existing products as well as to make the production more cost and energy efficient, which is done by the Research Physical and Chemical analysis (RPC) and Research Process Technology (RPT) departments. In addition, some efforts are aimed at increasing demand for the company's products. This strategy involves marketing departments across the world which remain in close contact with the major clients. Noteworthily however the company invests a large part of its assets into finding new possible applications for its products as well as helping clients optimize their applications using aramid fibres. The responsible branch is the Research Product and Application Development Department (RPA) which forms the Research and Development Center of Teijin Aramid along with the previously mentioned RPC and RPT branches. Overall however, Teijin Aramid remains a chemical rather than an engineering

company. The company products are presented in the following.

1.1.1 Twaron

Twaron is the company's oldest and by far the best selling product due to the wide range of everyday applications. The para-aramid is synthesized in a polycondensation reaction of para-phenylene diamine (PPD) and terephthaloyl dichloride (TDC), which bind together to form poly paraphenylene terephthalamide (PPTA) after the omission of HCl. Note that the para- prefix denotes the positioning of the aromatic ring within the group with the links being opposite to each other [1]. Both high molecular weight and low dispersity between chain lengths are required to obtain high mechanical properties, which necessitates that the polymerization occurs in solution. AKZO developed the method which is now the standard, using calcium chloride and n-methyl pyrrolidone (NMP) as co-solvents. After completion of the reaction, solvent and polymer are separated by washing and drying.

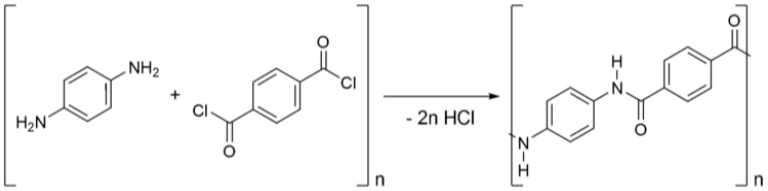

Figure 1.3: Polycondensation of PPTA [1]

It now possesses the chemical properties of Twaron but has low mechanical strength due to the random alignment of the molecules. In the following wet-spinning process, the polymer is initially dissolved in sulfuric acid, producing a dope. Inside the dope, the molecular chains align locally, forming a liquid crystalline polymer. During extrusion of the dope through a spinneret, the crystalline regions are forced to align along the axis of the formed filament. The high strength of aramid fibre originates from the hydrogen bonds between the oxygen and hydrogen atoms of neighbouring chains, which result in very high intermolecular forces. The filaments have a diameter of around 12 μm . Finally, the fibre is washed again and undergoes a heat treatment which further increases tensile strength.

Twaron is generally sold as wound filament yarn which naturally has a golden colour unless dyed black during the spinning process. The continuous fibres are found in a wide range of applications where high tensile strength is required. These include ballistic armour and helmets, cut and abrasion proof clothing, sail cloth, tire and belt reinforcement, cables, drumskins, sporting equipment such as hockey sticks, canoes, snow- and surfboards, loudspeaker diaphragms and jet engine enclosures. Within composites, it is used as a reinforcement for concrete, asphalt and polymers, notably thermoplastic pipes. In the form of short fibre, staple fibre and pulp, Twaron possesses several further applications, most notably as an asbestos replacement. Fibrillation drastically increases the materials surface to volume ratio, making it an excellent although expensive insulator. Pulp retains the high abrasion resistance of a para-aramid and is used in automotive brake pads to enhance friction at low temperatures. Further processing of pulp allows for the manufacturing of aramid paper, which is used as a thin insulator layer in batteries and in honeycombs, most notably for sandwich panels.

Health risks such as Fibrosis and cancer which occur when inhaling asbestos or carbon fibrils have been studied in Aramid Fibres in the past. While aramid fibres pose some risk during exposure to large quantities of dust, the product is generally accepted to be of very low risk to humans [14].

1.1.2 Technora

Technora is the company's other para-aramid product and performs quite similarly to Twaron. It was commercialized in 1985 by Teijin Ltd. as their para-aramid competitor to Kevlar. During the time, many competitors of DuPont chose to develop technical fibres with a different molecular structure to avoid patent disputes. Several other copolymer aramid fibres exist today but Technora is the only one to still be actively marketed.

Like Twaron, it is synthesized from PPD and TDC but with the addition of Oxidianiline (ODA) to form the copolymer, as both the amine groups of PPD and ODA bind to the TDC monomer (see Figure 1.4). The same solvents as those applied in the polymerization process of Twaron are used

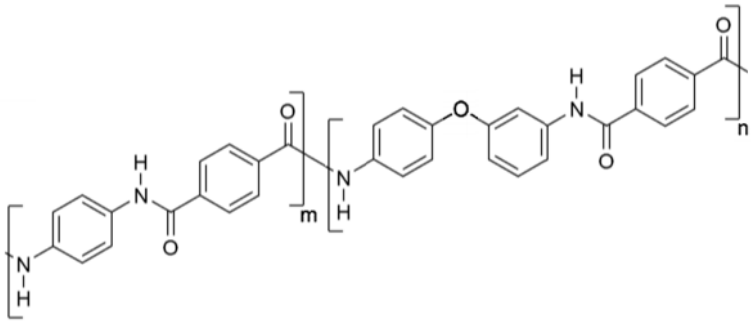

Figure 1.4: Chemical structure of Technora

for Technora but the second solution stage using sulfuric acid may be omitted as the polymer can be spun directly from the polymerization solution. However the crystallinity level reached during spinning is much lower than in Twaron meaning that a drawing process is required to fully align the polymer chains. This makes Technora more expensive to produce than homopolymeric aramids.

Compared to Twaron, Technora has a higher strain to failure, outperforming it in applications where higher elongation is desired along with high strength. Use cases which profit the most of this property are cables, ropes and umbilicals, with a prominent example being the parachute and suspension lines of Mars rovers Opportunity and Perseverance.

Chapter 2

Literature review

A literature review was conducted to obtain an overview of research investigating the effects of composite design parameter modification on the energy absorption behaviour of laminates. The scientific approach towards the experimental investigation of impact was also evaluated. Special focus went out on research covering aramid fibre, notably the manufacturing methods and characteristics of aramid fibre reinforced thermoplastics.

2.1 Introduction

Test results on composite impact strength vary quite drastically due to the lack of material and test standardisation. Numerous test methods and standards characterize material impact behaviour and are used as the comparative measure by researchers. Charpy and Izod tests quantify the ability of a material to absorb energy during failure. Both methods are standardized and often used to produce a single value for a materials impact strength but their comparative validity is limited [15]. Impact strength is compared with ballistic performance by [13]. Low velocity tests are generally carried out using a drop weight tower setup according to the ASTM-D7136 standard [16]. Apart from performance after impact, research also compares materials for their energy absorption capabilities. High velocity tests are carried out using a gas or powder gun. Medium velocity impact research and experiments in particular are quite scarce as the test setup is much less readily available. A large-caliber gas gun may be used [17]. Previous research by the author has also shown similar relative performance between materials across low and high velocity impact so these may be used to draw conclusions regarding medium velocity impact [18]. Apart from the perforation energy, impact behaviour may be categorised via the load-displacement or load-time curve of the event [19].

Optimising for an impact resistant composite comprises six modifiable laminate design parameters. Fibre material and volume fraction, matrix material, fibre architecture, layup, and the fibre matrix interface by means of fibre treatment [20]. Changing any of these parameters will greatly affect the material properties and some of the parameters are highly co-dependent. For example, changing matrix or fibre material will affect the interface and changes in fibre architecture will require revaluation of the layup. Material optimisation therefore requires analysis not only of the parameter effects on impact behaviour but also parameter interplay. A large body of research is available on increasing composite impact strength and damage resistance, although usually based on experimental data from GFRP or CFRP. These findings may hold to some degree for AFRP but cannot be universally accepted.

Next to the material properties, the impact conditions have a great effect on material behaviour. Vaidya defines the following three velocity regimes: Low ($<$20 m/s), medium (20 to 100 m/s) and high velocity or ballistic impact ($>$ 100 m/s) [17]. This classification is usually done to determine the influence of the boundary conditions on behaviour of the structure, where the response becomes material dominated at higher velocities. However, the mass and shape of the projectile as

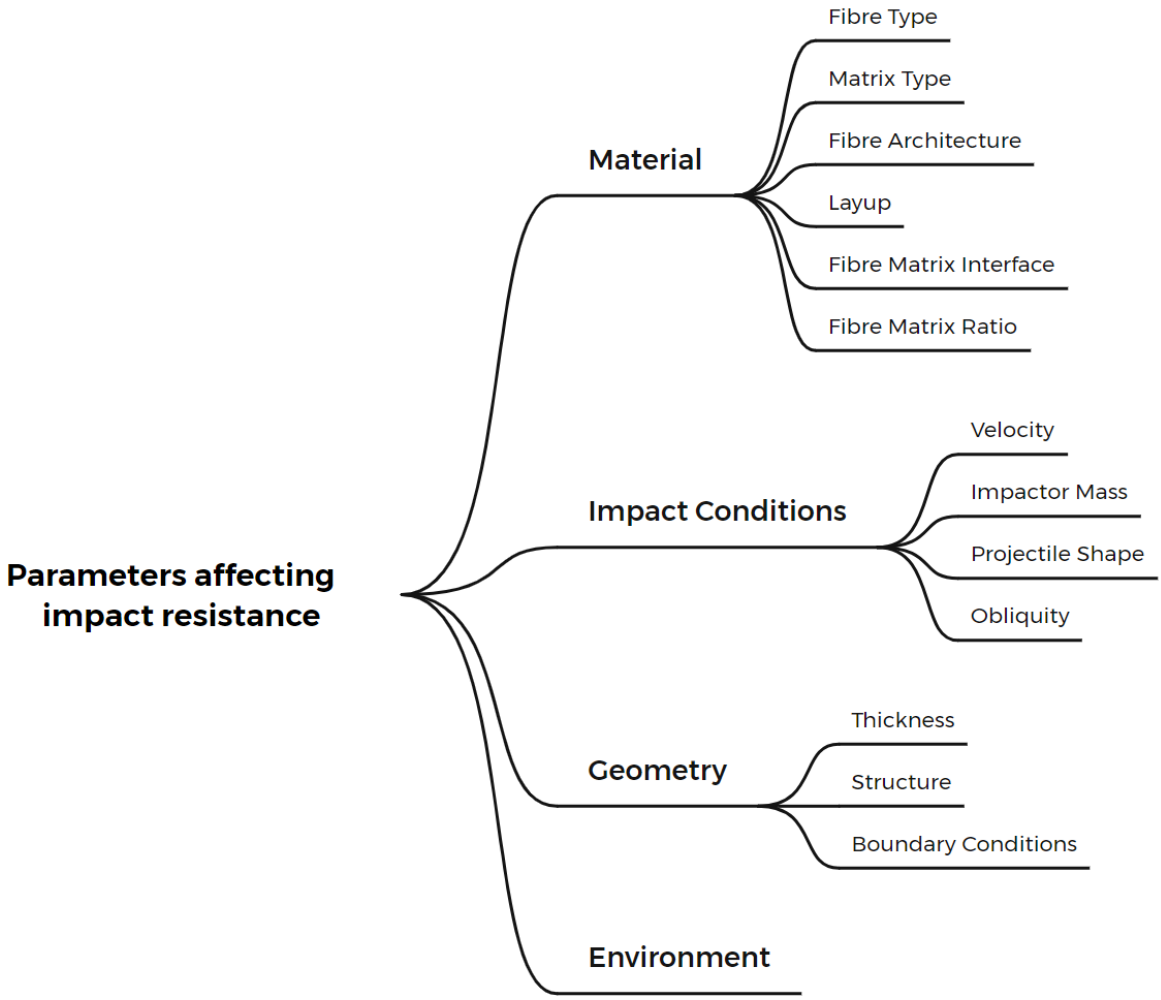

Figure 2.1: Factors in the impact resistance of composites

well as the stiffness of the structure influence this behaviour and a clear distinction between regimes is impossible. Most impacts in aviation applications are expected to be in the medium velocity regime, which is by far the least well investigated [21].

At low velocities, the response of the structure may be modelled quasi-statically [22] with multiple wave reflections from the boundaries. Medium-velocity impact is characterised by flexure and shear waves distributing the load over the structure [20]. High-velocity impact is a local phenomenon with transverse wave propagation. As the influence of the structure decreases with higher impact velocities, the material properties become the dominant factor in the response of the structure. Large bodies of research are available for both low and high velocity impact but not for the medium velocity regime. Low-velocity impact is a particular interest in structural composites due to its high probability of occurrence and for causing barely visible impact damage (BVID) [23] which may drastically reduce structural perfromance. High-velocity impact is often researched due to its importance for military applications. Most impacts in aviation applications however are expected to be in the medium-velocity regime.

As seen in Figure 2.1, next to the impact conditions, the geometric parameters also play a large role in the material response. Impact and geometric conditions are highly co-dependent and both have to be considered during testing. The following chapter covers the experimental approaches towards composite impact and the according analytical frameworks, while highlighting typical behaviour seen accross all composite materials.

2.2 Experimental approaches and theoretical concepts

2.2.1 Low-velocity impact

Low velocity impact is the most researched form of impact on composite laminates. Experimental equipment is widely available in the form of a drop tower and the material behaviour is quite similar to the response under quasi static loading [24]. Low-velocity impact is of great importance to structural composites due to the possibility of inflicting BVID. Composites and CFRP in particular may experience decreases in their strength properties of more than 50% after only minor impacts [25]. Researchers attempt to decrease the risk from BVID by increasing the damage resistance and damage tolerance of the laminate. Rather than addressing the material's ability to absorb energy or the resistance to perforation from a projectile, these properties influence the structure's integrity after one or several impacts. Response to low-velocity impact is dominated by the impact energy rather than impacter mass or velocity [26], [27].

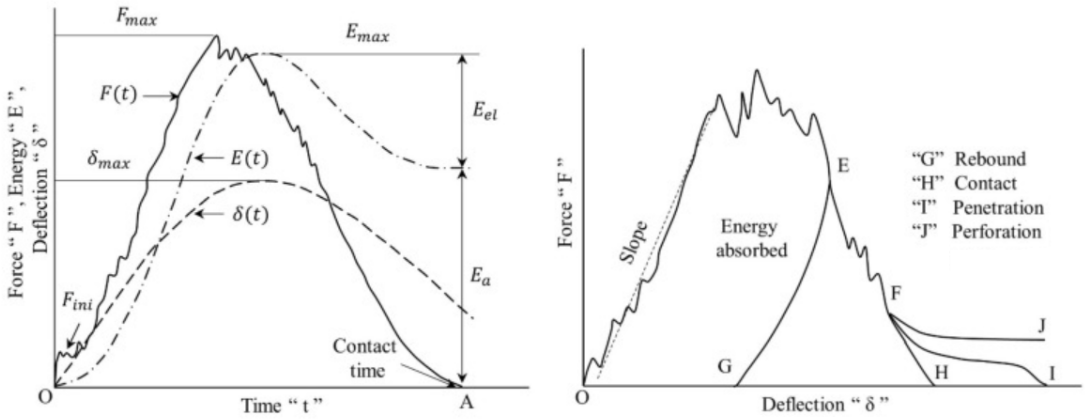

Figure 2.2: Schematic force-time and displacement behaviour of a composite [28]

The energy equilibrium is characterised by a global quasi-static component and a Hertzian contact force as

$$\frac{1}{2}mv^2 = \int_0^{\delta_{\max}} F d\delta + \int_0^{\alpha_{\max}} F d\alpha \tag{2.1}$$

with m and v the impacter mass and velocity. The contact force components are defined as

$$\begin{aligned} F &= k\delta \\ F &= n\alpha^{3/2} \end{aligned} \tag{2.2}$$

where δ and α denote the global deformation and the contact indentation and k and n the spring constant of the plate and the Hertzian contact stiffness, respectively. The contact stiffness depends on the effective impacter radius r_i and the transverse in-plane modulus E_2 with

$$n \approx \frac{4}{3} r_i^{1/2} E_2 \tag{2.3}$$

substituting Equation 2.3 and Equation 2.2 into Equation 2.1 yields

$$\frac{1}{2}mv^2 = \frac{1}{2}\frac{F_{\max}^2}{k} + \frac{2}{5}\frac{F_{\max}^{5/3}}{n^{2/3}} \tag{2.4}$$

using the maximum contact force F_max as an input value to obtain the energy absorption [29].

Most experiments are conducted according to the ASTM D-7136 standardization [30]. The material response during low-velocity impact is characterised by its load-time and load-displacement

history as seen in Figure 2.2. The graphs hold detailed information about the impact stiffness, damage initiation and progression of the sample. Furthermore, the absorbed energy may be calculated from fully fractured specimens to determine the perforation limit or maximum energy absorption [31].

Laminates dissipate the total impact energy E_{tot} through both elastic deformation and damage, or a conservative and an absorbing component E_{el} and E_a. The coefficient of restitution (COR) is defined by Feraboli and Kedward [32] and denote the ratio between the conservative and the total energy component. It is defined as

$$COR = \frac{v_{in}}{v_{out}} = \sqrt{\frac{E_el}{E_tot}} = \sqrt{\frac{E_{tot} - E_a}{E_{tot}}} \tag{2.5}$$

Initially, dissipated energy increases quadratically with the impact energy until it reaches the same value, at the point of penetration (see Figure 2.3). This is followed by a linear region, where all impact energy will be dissipated through damage. When the impact energy damages the panel beyond perforation, the energy absorbed will remain constant for impacts that perforate the target, though other authors state that the energy absorption during destructive high-velocity impact is different from that in the low-velocity regime [33]. The COR plot then contains additional information on the energy absorbing properties of both material and setup. The authors attribute the initial difference in elastic behaviour seen in Figure 2.3 to the boundary condition effects, which may dissipate energy non-conservatively. The initial sharp drop in the elastic response marks the onset of damage in the panel, which is followed by linear decay. After this, the COR drop follows power law behaviour [32], denoting the transition from matrix damage to fibre failure and a sudden drop to zero at penetration.

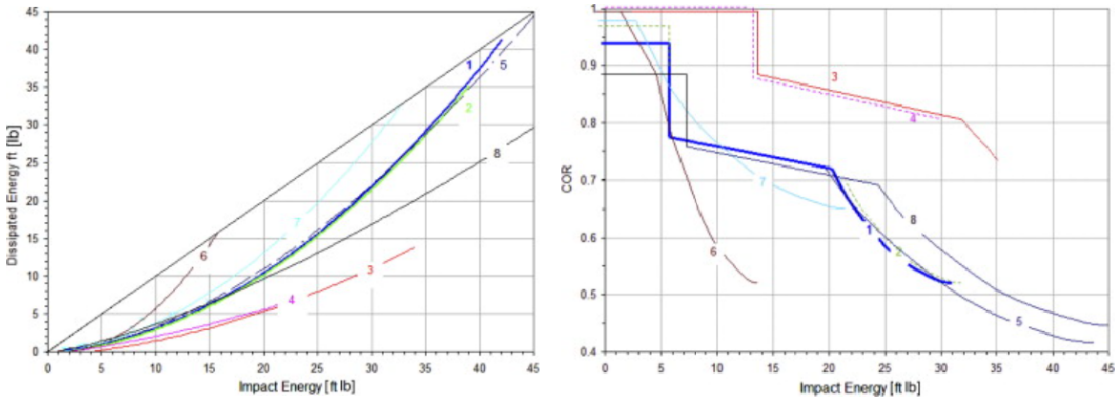

Figure 2.3: Dissipated vs impact energy for some various laminates and according COR plots [32]

Composite materials, notably AFRP may produce ductile behaviour during impact. Park and Seo [34] distinguish between elastic initiation energy E_i and propagation energy E_p absorbed through fracture. The sum of both is the total energy absorbed. E_i marks the initial, linear elastic region of the force deflection diagram (see Figure 2.2) and E_p denotes the area loaded beyond the maximum force. The ductility index DI is defined as

$$\mathrm{DI} = \frac{E_\mathrm{p}}{E_\mathrm{i}} \tag{2.6}$$

and becomes larger with the proportion of energy dissipated through damage rather than elastic behaviour.

2.2.2 High-velocity impact

A large body of research covers high-velocity impact by studying the response of composites and fabrics to ballistic impact from projectiles or shrapnel. Ballistic studies also incorporate a notably large

body of research on aramid fibre composites as the material is widely applied in armour applications. Researchers often aim to identify and improve the v_{50} - the impact velocity of some projectile on a yarn, fabric or composite which will result in penetration in 50% of the cases [35]. It marks the ballistic limit of an armour material. Determining it on yarn level is a way of directly comparing the energy absorption potential of armour fibres. Most setups identify the energy absorption through the difference in projectile velocity before and after impact v_i and v_r. The absorbed energy E_a is calculated as

$$\begin{aligned} E_a &= \frac{1}{2}m\left(v_i^2 - v_r^2\right) \\ &\approx \frac{1}{2}mv_{50}^2 \qquad\qquad \text{if} \quad v_i \sim v_{50} \end{aligned} \tag{2.7}$$

according to Reid and Wen [24]. The second relation indicates that the energy absorbed during destructive impact will be equal to that at the v_{50}. Hazell et al. [36] agree with this approach but add that at velocities well beyond the v_{50}, the ratio between impact energy and absorbed energy remains constant meaning that the absorbed energy increases. Simultaneously, the damage area decreases slightly with increasing velocity as failure shifts from delamination to shear plugging (see Figure 2.4).

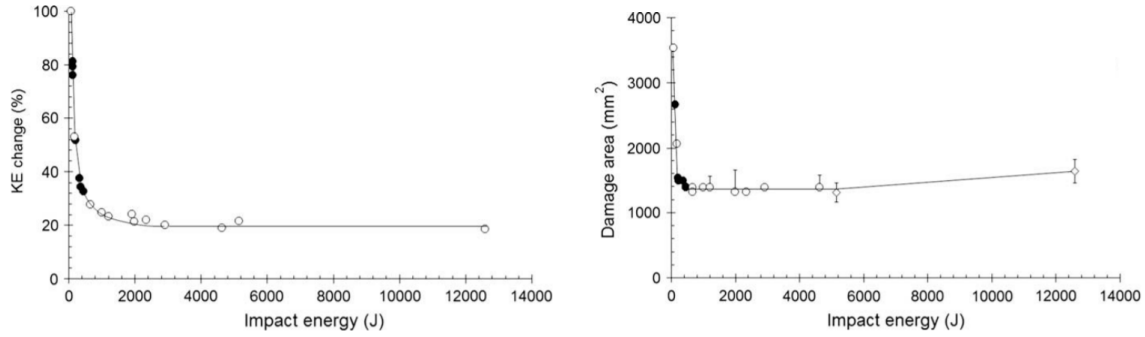

Figure 2.4: Kinetic energy change and damage area in terms of impact energy [36]

During HVI, boundary conditions have little to no effect as the wave cannot propagate the distance before the end of the impact event [37]. The energy absorption in composite panels is found to increase superlinearly with the laminate thickness [13], [38], [39], making material thickness an important design parameter. Concretely, this means that thicker materials should be preferred in design for impact. Lighter materials can be made thicker at the same weight, making the material density an important parameter. On the other hand, this means that the thickness of a material must be taken into account when rating its impact performance. Normalising the energy absorption by the thickness or areal density is commonly done but ideally, materials of similar thicknesses should be compared. Superlinear increase in energy absorption with the thickness was observed by Shrivastava et al. [40] in aluminium, suggesting that this relation holds for both composites and metals.

While LVI material response is similar to the quasi-static case, HVI behaviour can be described by multiplying the quasi-static perforation energy with some dynamic enhancement factor [24]. The static perforation energy E_f is defined as a combination of the local and global deformation energies E_l and E_g, where E_l is dependent on the impacter shape.

$$E_f = E_l + E_g \tag{2.8}$$

The dynamic perforation energy E_{pi} is correlated to E_f by the dynamic enhancement factor ϕ through

$$E_{pi} = \phi \mathrm{E}_f \tag{2.9}$$

The energy absorbed during impact is higher than during static indentation due to the wave propagation effects. ϕ increases linearly with the impact velocity v_i up to a transition velocity v_o, after

which the energy absorption plateaus.

$$\begin{aligned} \phi &= 1 + \beta \left(\frac{v_i}{V_o} \right) \quad (v_i < v_\mathrm{o}) \\ \phi &= 1 + \beta \qquad\qquad\quad (v_i > v_\mathrm{o}) \end{aligned} \tag{2.10}$$

β is determined empirically, whereas v_o depends on the speed of sound in the laminate C_L and its failure strain ε_u.

$$v_\mathrm{o} = C_{Lf}\varepsilon_u = \sqrt{\frac{E_{s1}}{\rho}}\varepsilon_u \tag{2.11}$$

E_{s1} and ρ denote the in-plane elastic modulus and the material density.

Reid and Wen's model suggests that material properties and impacter shape have a greater and less predictable effect on impact performance than the projectile velocity. The findings give designers much greater freedom in their experimental setups as the effects of velocity changes become more predictable. This is useful in the sense that experiments do not necessarily have to be carried out at the expected velocity of the actual impact event.

2.2.3 Fracture Behaviour

The fracture mechanics of composites are examined extensively across all fields where damage occurs in the material. In heterogeneous materials, a multitude of fracture mechanisms and failure modes exist, which may change drastically with only small changes to the material, impact condition or structure. The combined occurrence of some of these fracture mechanisms is the reason why a composite material composed of brittle fibres and a brittle matrix may exhibit relatively tough behaviour when compared to both the constituent materials [31]. Fracture phenomena include, among others, fibre pull-out, fibre-matrix debonding, crack-bridging, matrix plastic deformation or cracking, fibre breakage and delamination [41]. The process of crack propagation and the corresponding failure mechanisms is shown in Figure 2.5. Descriptions of fracture differ accross authors [42], [43], [44] and, while a theoretical framework for the energy dissipation exists, experimentally quantifying individual mechanisms is difficult. The fracture surface is usually examined after testing by using scanning electron or optical microscopy on the failure area. Analysing the imagery identifies the dominant failure mechanisms and yields qualitative information on the effects of parameter modification on material behaviour.

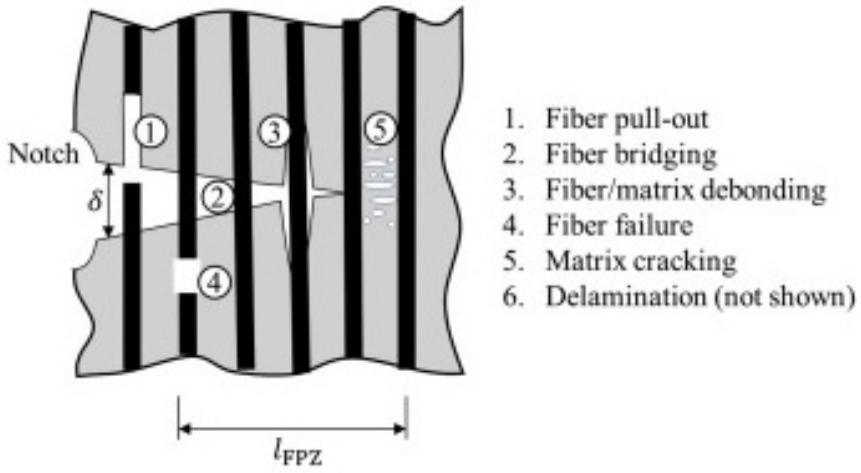

Figure 2.5: Fracture mechanisms in composites [45]

Kim and Mai [41] identify fracture work through pull-out, stress redistribution through fibre bridging and the creation of new surfaces through fibre and matrix damage as the dominant energy absorbing mechanisms, with

$$R_{\text{redistribution}} = \frac{V_{\text{f}}\sigma_{\text{f}}^3 d}{6E_{\text{f}}\tau_{\text{f}}} \tag{2.12}$$

$$R_{\text{pull-out}} = \frac{2V_{\text{f}}\tau_{\text{f}}l_{\text{po}}^2}{d} \tag{2.13}$$

$$R_{\text{surfaces}} = V_{\text{f}}\left(\frac{l_{\text{c}}}{d} - 1\right)R_{\text{m}} \tag{2.14}$$

all defined in terms of the fibre diameter d, the fibre volume fraction V_f, tensile strength σ_f and modulus E_f, the interfacial shear strength (IFSS) τ_f and the matrix toughness R_m. The pull-out length l_{po} and fibre critical transfer length l_c are determined from microscopy imagery.

IFSS is commonly quantitifed by pull-out tests, where a fibre bundle is pulled from the matrix in a tensile test bench. This however requires a specialized specimen to be manufactured so researchers often apply three point bending tests and to obtain a comparable value in the interlaminar shear strength (ILSS). Interlaminar failure occurs either through matrix failure or large scale debonding [46]. When a tough matrix and poorly adhering fibres are used, failure is expected to come from debonding, thereby linking the ILSS to the IFSS. According to the ASTM D-2344 standard [47], the ILSS is calculated by

$$\text{ILSS} = \frac{3P}{4bd} \tag{2.15}$$

where P is the failure load in the three point bending test and b and d the width and thickness of the specimen, respectively.

Measuring the individual contributions of the fracture mechanisms to the fracture energy is possible [7] but not commonly done. Charpy and Izod impact tests return values for the work of fracture which are linked to the critical strain energy release rate G_C denoting the energy absorbed in creating new surfaces in the material [48] through all the combined fracture mechanisms. G_{IC} is derived from the critical stress intensity factor K_{IC}, which is determined in a compact tension tension test with a notched specimen [49]. According to ASTM E-399 standard[50], G_{IC} is then defined as

$$G_{\text{IC}} = \left(\frac{K_{\text{IC}}^2}{2E}\right) \cdot \left(1 - v^2\right) \tag{2.16}$$

where E and ν denote the longitudinal Young's modulus and poisson ration. Arencon and Velasco [48] state that the test has lost popularity in the scientific community due to its limited validity for actual design. Furthermore, Faur-Csukat [13] has compared the work to fracture of various composites in Charpy and drop weight impact but found no meaningful correlation between the twoparameters.

2.3 Manufacturing aramid reinforced thermoplastics

Thermoplastic aramid composite is a widespread material in today's world through its use in ballistic applications. Commodity polymers such as PP, PE and PVB are used as matrix materials as they offer fast processing and improved impact properties over thermoset matrices. Structural aramid fiber reinforced polymers (AFRP) however remain to apply thermoset matrices as research and application of aramid reinforced high performance thermoplastics remains extremely limited. Unlike composites designed purely for impact, structural composites in the aerospace sector require high-performance matrices with high inherent strength, stiffness and thermal stability. Thermosets such as epoxy fulfill this role at a low price compared to the thermoplastic alternatives with comparable properties. While a lot of research has been performed on CF-PEEK and PPS, most research on aramid fibre remains to be conducted with epoxies. High-cost could be one of the main reasons for a limited body of work on aramid reinforced high-performance thermoplastics.

Korbakov et al. [51] have produced aramid fibre reinforced PEEK and conclude that the material has acceptable interface properties, although with limited evidence. Chang and Lees [52]

compared the mechanical properties of some aramid reinforced thermoplastics with E-glass and carbon fibre. The authors were able to produce Kevlar reinforced J-polymer - a polyamide - and Kevlar reinforced polyether ketone ketone (PEKK) Table 2.1. The thermoplastic laminates were compared with Kevlar-"Epon" 828 epoxy and the authors reinforced the same polymers with AS-4 carbon and E-glass fibre. The aramid composites had a stiffer bending response than the glass fibres, presumably due to the higher stiffness of Kevlar, but much lower flexural strength than both glass and carbon. The ILSS, denoted by the authors as short beam shear strength, was exceptionally high for the aramid composites, both in absolute terms as well as compared to the other composites. For comparison, Gupta et al. [53] studied the ILSS of Kevlar 49-PEEK with that of T-300 CF-PEEK and reported 20 MPa and 60 MPa, respectively, with a fibre volume fraction of 40%. Park et al. [54] reported the ILSS of aramid-epoxy to be in the range of 20 to 30 MPa, which appears to be in line with other literature. The comparative validity of Chang and Lees findings therefore has to be viewed critically. Nevertheless, their evaluation suggests that acceptable interfacial adhesion can be obtained with aramid reinforced high-performance thermoplastics. Notably, the polyamide produces a stronger bond than epoxy and appears to be a good matrix matrix material for aramid composites.

Composite (0°)	**Flexural Modulus (GPa)**	**Flexural Strength (MPa)**	**Short Beam Shear Strength (MPa)**
Kevlar /J-polymer	67	707	71
Kevlar /PEKK	68	676	46
Kevlar /"Epon" 828	75	618	62
E-Glass /J-polymer	43	1300	78
E-Glass /PEKK	55	1400	79
E-Glass /"Epon" 828	46	1270	68
AS-4 /J-polymer	-	1450	104
AS-4 /PEKK	-	1620	117
AS-4 /Epoxy	-	1794	121

Table 2.1: Mechanical properties of some high-performance Kevlar, E-glass and AS-4 carbon composites[1][52]

Khondker et al. [2] performed one of few documented studies into the processing of thermoplastic aramid composites at over 200°C. They investigated the influence of the exposure time on tensile strength and modulus at a constant temperature of 290°C. The authors found a rapid drop in tensile strength almost instantly after placing the fibres in the oven, after which the degradation stagnates (see Figure 2.6).

2.4 Composite desgin parameters

2.4.1 Reinforcement

In high-velocity-impact, energy absorption is fibre dominated [55, 56]. Tough fibres like high strength/ high elongation aramid and S2-glass fibres posses these properties, making them popular for ballistic applications. During LVI, the ductility index was observed to decrease with the energy absorbing capability of composites meaning that tougher laminates generally absorb a higher energy fraction before damage initiation [57]. Maximum load and initiation displacement increase with fibre toughness meaning the property is also important for LVI design. This is supported by several other studies from the 1980's and 1990's [7], [41] but less so in more recent literature. Wang et al. [58] for instance determined that the DI is positively coupled to the energy absorption potential.

Authors often attribute aramid fibre to be the best reinforcement option when designing for lightweight, impact resistant structures [4], [7], [58] while its structural properties, notably stiffness,

[1] All composites were unidirectional and contained 60% fibres by volume. The Kevlar was reportedly untreated and the type not specified by the authors. The short beam test was conducted with a span-depth ratio of 4.

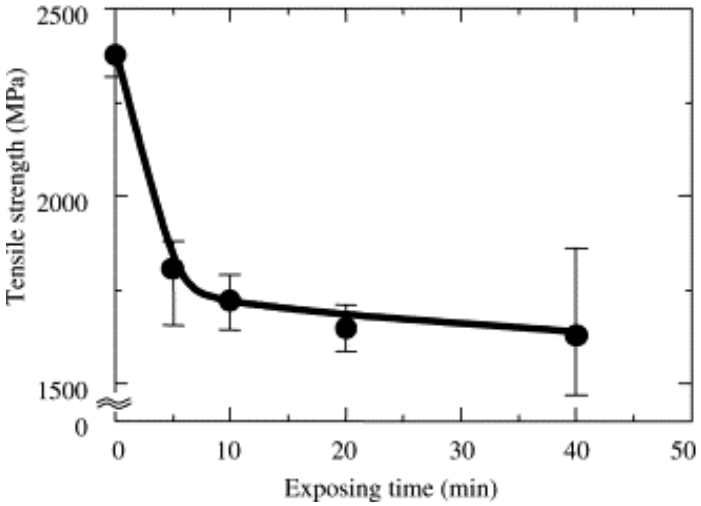

Figure 2.6: Tensile strength retention for Kevlar29 at various exposure times at 290°C [2]

are in between that of carbon and glass fibre. The poor out-of-plane impact performance of CFRP structures is relatively undisputed but studies reach differing conclusions on the performance of glass and basalt fibres, which cannot be clearly categorized in their performance relative to aramid fibre. Figure 2.7 shows the relative differences in energy absorption in out-of-plane impact of various AFRP and other composites. For comparative validity, the energy absorption is normalized with respect to the sample areal density. While this comparison does not produce direct comparative evidence due to the non-standardized tests, it is intended to show possible trends in which reinforcements continuously produce the most impact resistant composites. The graphs show that aramid composites may be both very impact resistant and very poor performers, depending on the fibre grade. Due to the lack of standardisation, experiments continue to produce extremely divided conclusions when comparing the energy absorption potential of aramid with that of competitor fibres. Even in standardized tests, the results vary drastically, presumably due to small differences in the composite.

As seen in the figure, composites of identical reinforcement may produce vastly different results in out-of-plane impact tests. Notably, Park and Jang [59] rate the LVI strength of Kevlar29/VE as more than ten times higher than that of S2-glass/VE, which they attributed to much higher degrees of pull-out and fibre fibrillation in the aramid composite. Faur-Csukat et al. [13] on the other hand investigated drop weight impact and found S2-glass/epoxy to absorb more than 4 times as much energy as Aramid/epoxy, although the type of aramid was not mentioned. This is a common occurrence in research articles and it appears as if aramid is often treated as a uniform material. As seen in Figure 1.2 however, grades of aramid may differ significantly in their properties. Most experiments make use of either Kevlar 49, Twaron 2200 or Kevlar 29, where the former two are high-modulus (HM) yarns and the latter a high-elongation (HE) yarn. Wardle [60] suggested that Kevlar 29, which has approximately the same properties as Twaron 1000, performed better in impact than E-glass fibre, while Kevlar 49 performed worse. Evaluating Figure 2.7 yields a clear distinctive trend between the performance of HE and HM aramid fibre composites as seen in Figure 2.8. The data set suggests that the average perforation energy achieved with HE aramid is more than twice as high than that of HM aramid. Furthermore, HE aramid composites are continuously among the best performers of all the evaluated materials. This suggests the possibilities for optimisation as the incorporation of ballistics grade yarns such as Twaron 2642, Technora or Kevlar KM2 could yet increase the perforation limit by a potentially large amount.

Hybridisation of two or more reinforcements is investigated in numerous studies. The scientific community agrees that hybridising carbon fibre with aramid significantly improves the impact response [3], [61], [62], [63]. Amirian et al. [64] observed that hybridization of Kevlar with Basalt continuously increased the high-velocity impact strength with respect to both pure laminates. The authors briefly attribute this performance increase to the combination of the tensile strength of aramid

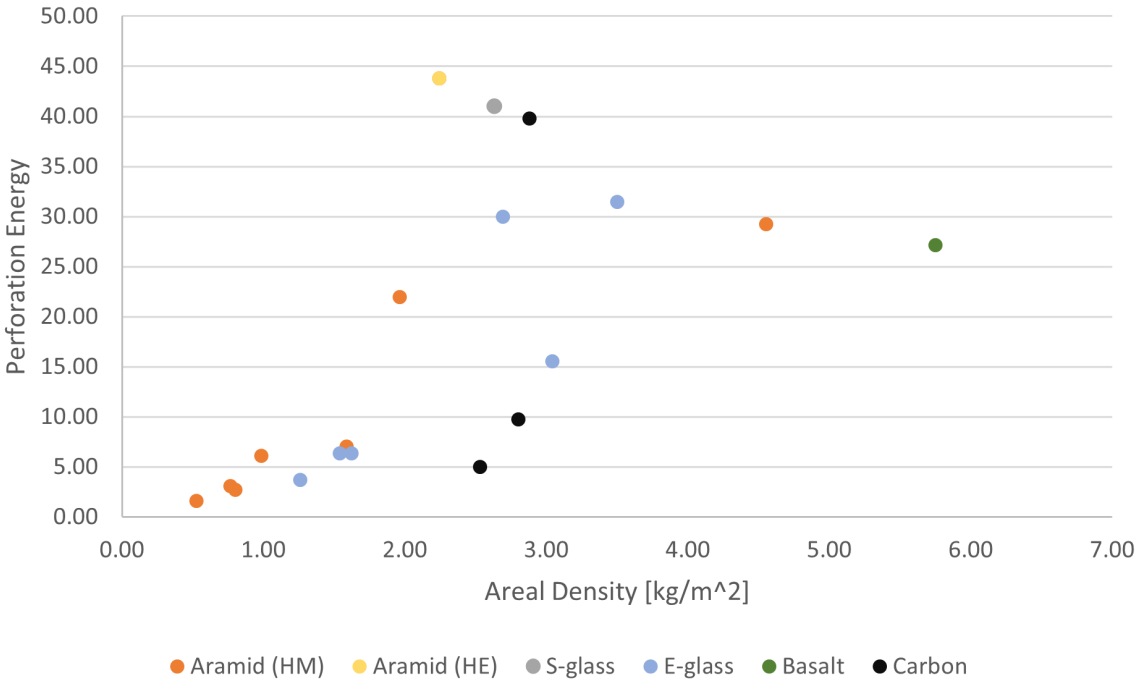

(a) High-velocity impact

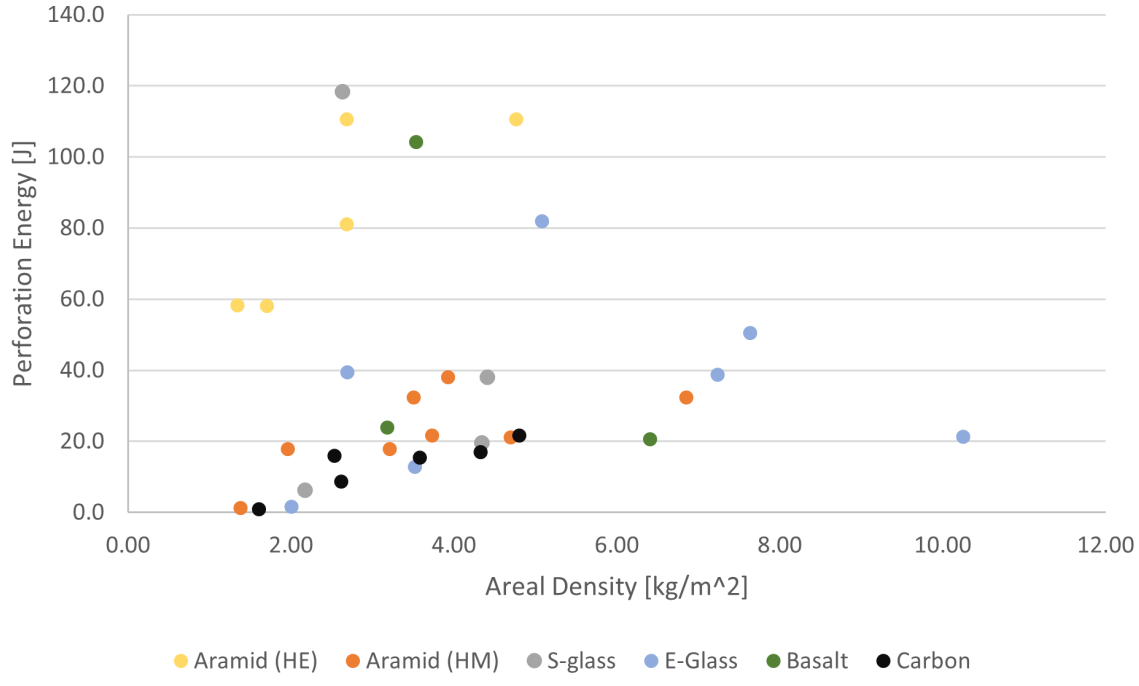

(b) Low-velocity impact

Figure 2.7: Specific LVI and HVI perforation limit of various composites according to research listed in Table A.1

with the elastic properties of basalt but do not investigate the phenomenon thoroughly. Bandaru et al. [65] also found that hybridizing Kevlar 29 and basalt fibre increased the impact performance with respect to both constituents in LVI. This observation is unique as other researchers generally find hybrids to perform below the expected rule of mixtures prediction [57]. Hybrids also suffer from delamination risk due to the stiffness mismatch of the constituents [66] and are very rarely being used in primary or secondary aircraft structures. Sarasini et al. [67] investigated the effects of hybridizing basalt and Twaron 2200 and concluded that the hybrids exhibited similar energy absorption and damage tolerance to the pure Twaron laminate.

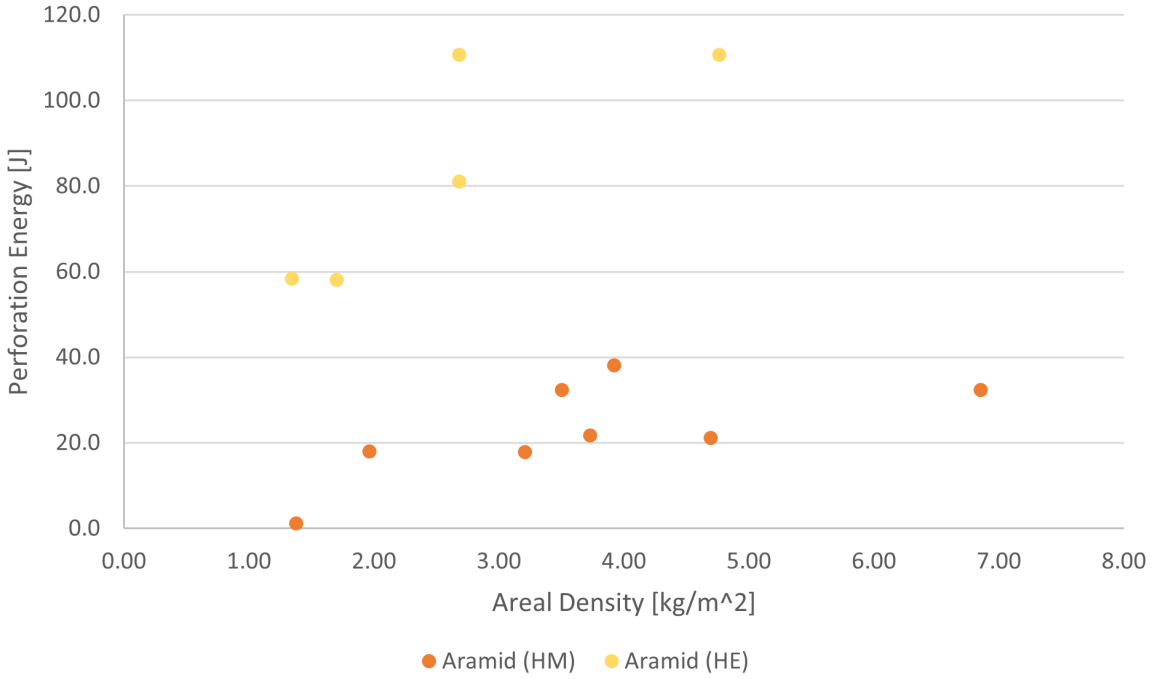

Figure 2.8: Collection of research data on the LVI perforation limit of AFRP, notably Kevlar29 (HE) and Kevlar49 (HM)

It remains unclear whether structural AFRP composites have the potential too produce significantly better impact resistance than optimised S2-glass or basalt fibre based laminates. The studies reveal however that there have been very few attempts to fully optimise AFRP for impact resistance. Consequently, Priyanka et al. [4] have suggested recently that future research should focus on improving the impact resistance of aramid fibre composites without overly compromising the structural integrity.

2.4.2 Matrix material

Thermoplastic matrix materials have seen a recent increase in popularity as they offer better recyclability and repairability, shorter processing times and the option for advanced manufacturing methods. Initially held back by processing complications due to the high melt viscosity, new manufacturing methods such as automated fibre placement allow for in situ consolidation of complex components [3]. Researchers agree that thermoplastic composites in general have a higher toughness than their thermoset counterparts and conclude that the impact behaviour in thermoplastic composites is better due to the ductile matrix behaviour [7], [41], [68].

Ballistic and impact composites with aramid reinforcement widely apply thermoplastic matrices, which are reported to increase the energy absorption capabilities of fabrics [69], [55], [56]. Energy absorbing mechanisms during high-velocity impact are fibre-dominated [55], [56], as suggested by the frequent use of ballistic fabrics without a matrix and extremely high fibre volume fractions of around 90% in ballistic laminates [70]. Often, the matrix serves the main purpose of keeping the fibres

together. Therefore, the properties of the matrix and the interface are not as important as in structural composites. Commodity thermoplastics such as polyamide (PA), polyethylene (PE) and PP are commonly used and numerous studies are available on aramid fibre composites incorporating these polymers as matrices [4], [71], [72].

Thermoplastics also widely outperform thermoset matrices in ballistic applications [73, 74, 75, 71]. Authors report increased and plastic back-face deformation, global damage propagation and higher ballistic limit in the thermoplastic matrix composites. Generally however, ILSS and flexural strength of Epoxy laminates are higher than in those with PP or PVB matrix.

Research of the matrix' role during impact on structural composites is more commonly conducted on glass or carbon fibre composites. As elaborated in subsection 2.4.3, polymer crystallinity affects the interface but has a greater effect on matrix ductility, with amorphous plastics being more ductile then crystalline ones. Both the damage resistance and the damage tolerance were found to be higher for amorphous PEEK composites. Nonetheless, crystalline CF-PEEK was still considerably less brittle than the CF-epoxy [76]. A similar study compared the impact response of carbon fibre-PEEK and polyphenylene sulfide (PPS) composites [77]. Fast cooling rates were used on both materials to increase the ductility but PPS was found to exhibit high crystallinity and brittle behaviour for a thermoplastic. Both materials were tested at different energy levels up to perforation and evaluated for damage resistance, damage tolerance and perforation limit. CF-PEEK exhibited better static properties, higher damage resistance and tolerance and a DI of 0.9 compared to 0.25 for CF-PPS. However, the perforation energy was found to be about 10% higher in PPS. The authors observed the same fracture mechanisms in both materials and explain the higher perforation threshold in the PPS composite with the larger damage area absorbing more energy but resulting in lower post-impact properties. They conclude that CF-PPS is then the better material when designing for energy dissipation and that the ductility index is a flawed parameter, as high DI does not necessarily reflect good impact performance. Rather, the parameter is only effective at comparing the behaviour of other wise similar materials. Vieille et al. [78] compared composites of carbon fibre with PEEK, PPS and epoxy matrices under different energy levels of LVI. They also observed that the damage area was larger in CF-PPS but that the impact stiffness and penetration threshold were very similar to those of the PEEK composite. The epoxy based laminate responded stiffer and had a lower damage initiation and perforation threshold. The authors observed increased fibre bridging in CF-PPS, which they attributed to the poor fibre-matrix adhesion compared to the PEEK composite. As fibre-bridging is a tough fracture mechanism (see subsection 2.2.3), this is a possible explanation for the higher perforation threshold in CF-PPS seen in [77].

While authors researching high-velocity impact universally agree on the notion that increased matrix toughness and weak fibre matrix adhesion improve the energy absorption potential, the findings are more nuanced in low-velocity impact and in structurally loaded composites. In carbon fibre composites, the high degree of fibre-matrix adhesion allows for significant improvements in impact strength through weakening the interfacial bond but the gain potential is much smaller in aramid composites as the interface is already relatively weak. The combined increase in matrix toughness and weakened interface of reducing the polymer crystallinity suggests that impact composites favour amorphous matrix materials.

2.4.3 Interface

The interfacial strength between fibre and matrix has a great effect on both the static and the impact properties of a composite. Structural composites require a high degree of adhesion and a high interfacial shear strength (IFSS) as fibre-matrix debonding may cause delamination and failure of the structure. Optimisation of the interface is less straightforward when designing energy absorbing composites as a strong adhesion counteracts energy absorption through pull-out [41].

Glass and carbon fibres, when treated with a sizing, adhere very well to most matrix materials, making them better suited for structural application than aramid fibre, which remains to have a poor interface with most polymeric matrices due to its chemical inertness and smooth surface. Adhesion may be improved through chemical grafting methods, physically modifying the surface, coating or

sizing methods and the incorporation of nano-structures [12].

The effectiveness of surface modifications is highly co-dependent with both the matrix and fibre material [79]. A study compared the ILSS of treated and untreated aramid fibre in a BMI matrix, where chemical grafting increased the ILSS by 43% [80].

Several studies evaluate the effects of fibre-matrix adhesion on aramid fibre composites [34, 81, 82], [83]. Significant improvements in interfacial strength were achieved through chemical or physical grafting methods. These resulted in higher ILSS and K_{IC} fracture toughness, while the energy absorption was reduced, as the composites failed in a more brittle manner during LVI (see Figure 2.9). The authors reported higher impact stiffness and peak force, while the perforation limit decreased with higher bond strength. Park et al. observed a drastic increase in the static properties due to the improved adhesion and conclude that, for aramid fibre, the benefits of a stronger bond outweigh the penalties in impact performance.

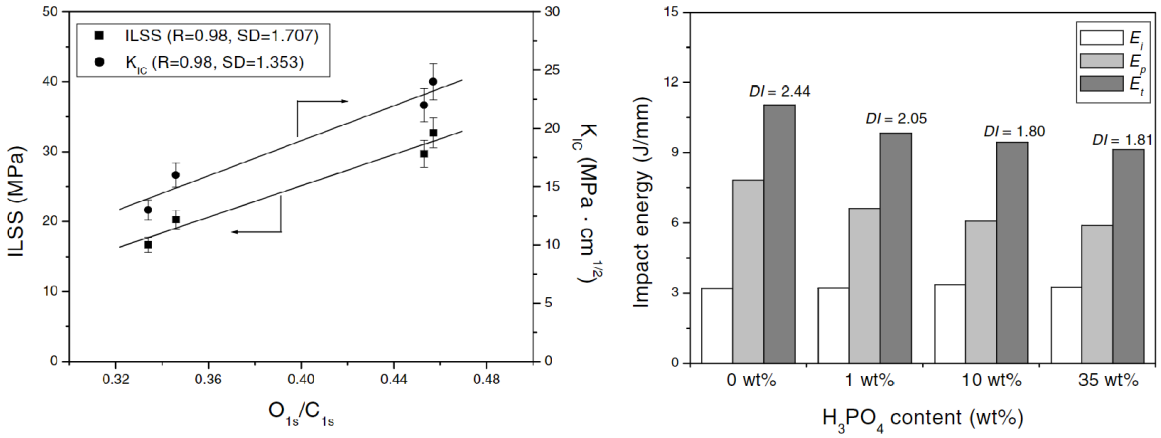

Figure 2.9: ILSS and fracture toughness in terms of chemical bond quantity[2]and the impact energy and ductility index in terms of grafting acid concentration [54]. O_{1_s}/C_{1_s} denotes the ratio of the O_{1_s} and C_{1_s} peak intensities measured by the authors via X-ray photoelectron spectroscopy (XPS) and is an indicator of the bond strength between fibre and matrix. The unit J/mm describes the impact energy normalised by the specimen thickness, eliminating thickness effects. This is comparable to normalising by the areal density

The opposite effect was seen by Bandaru et al. [73, 74], who conducted low- and high-velocity impact tests on aramid-polypropylene (PP) composites. They changed the interfacial adhesion by using two types of PP-matrix and adding various quantities of maleic anhydride grafted (MAg) PP as a coupling agent. A much higher LVI energy absorption was achieved with a higher concentration of MAg, leading the authors to the conclusion that improved adhesion positively affects the impact strength in aramid-PP composites, although they do not quantify the increase in IFSS.

Matrix crystallinity is also found to have a significant effect on interfacial adhesion, although this has not been confirmed for AFRP. In carbon fibre CF-PEEK, pull-out was found to be higher in amorphous samples, indicating poorer adhesion with reduced crystallinity [84]. It was found that the energy required for damage initiation is higher in amorphous CF-PEEK composite. The authors attributed this to the higher toughness of amorphous polymers. They conclude that crystallinity may be used to counterbalance fibre-matrix adhesion and matrix toughness. For carbon fibre composites however, it is suggested that the effects of crystallinity on matrix toughness outweigh the potential gains in interfacial adhesion [76]. It remains unclear whether this applies to aramid fibres, where adhesion is a much larger concern than in carbon fibres.

Generally, the authors agree that a weaker bond increases the energy absorption capability due to reduced impact stiffness and increased fracture energy through the tough pull-out mechanism,

although some exceptions exist. This indicates that if novel matrix materials are to be used, the degree of adhesion should be compared with the impact strength. Better adhesion is universally accepted to improve the static properties. Therefore, compromises between structural and impact performance have to be evaluated when designing the interface.

2.4.4 Fibre Architecture

Modern aerospace structures are often composed of unidirectional plies, which exhibit the highest static properties. However, several studies indicate that woven fabric composites can absorb more energy during impact. Many different weave types are therefore explored by researchers but their findings are limited due to non-standardization and co-dependencies with other parameters. Notably the fibre volume fraction and therefore the laminate thickness and density are highly dependent on the weave type [85]. Naturally, the layup also has to be designed in accordance with the fabric used. The areal density of the weave changes with the linear density of the fibres. Generally, 1D, 2D, and 3D fabric structures are distinguished between. The 1D configuration includes unidirectional weave structures. Conventional fabrics such as plain, twill and satin weaves are two-dimensional. A large number of 3D configurations exist, which in general are preforms that have reinforcements running in all three principal directions. 3D-fabrics include multi-layer weaves incorporating a yarn which is aligned closely with the out-of-plane axis. Non-woven equivalents containing a through-the-thickness reinforcement include non-crimp-fabrics (NCF), which consist of several layers of unidirectional fabrics stitched together by a z-axis reinforcement yarn. A number of other z-reinforcement techniques exist, which include stitched 2D fabrics or z-pins, which are forced through the laminate.

A number of studies compare the energy absorption capacity of unidirectional laminates with that of woven composites. UD laminates have higher flexural and longitudinal properties as fabric crimp reduces tensile strength and stiffness [86, 87]. Woven laminates however are regularly found to have a higher perforation threshold [88, 83, 89].

Sabet et al. [90] conducted HVI tests on E-glass/polyester composites with various fibre architectures, namely chopped strand mat (CSM), plain and satin weave and unidirectional and cross ply laminates. Panels were tested at 3 and 6 mm thickness. Despite using only short fibres, the CSM performed quite well, absorbing only 20% less energy than the best performing continuously reinforced laminates. Likely, this is due to the possibility for extensive pull-out in short fibre composites as suggested by Philips and Tetelmann [42]. The authors did in fact observe significant pull-out during post impact analysis. As expected, the cross ply laminate performed better than the UD as it allows for the loading of additional principal yarns in the 90° direction. Both the UD and CP however were outperformed by the plain weave composite. The authors observed that thicker laminates absorbed significantly more energy per unit weight than thin ones.

3D angle-interlock woven composite was compared with a QI and a NCF laminates [33], the latter two using identical layup structure. Compared to the other specimens, the NCF developed large damage areas in both tests. The energy absorption during HVI was higher than that of the other specimens, but lower in the LVI test, despite exhibiting the highest peak impact load. The authors found the 3D woven fabric to have good post impact strength retention but low energy absorption in all impact conditions, which they explained with the through-the-thickness yarn reducing the ductility index. The UD laminate appeared to be a compromise between the two others. Kang et al. [19] performed a similar study by comparing carbon multiaxial warp-knit (MWK) fabrics with woven and UD laminates in LVI. The MWK clearly exhibited a lower degree of delamination due to the increased interlaminar fracture toughness but overall absorbed more energy than the other configurations as they exhibited more fibre fracture. Francesconi and Aymerich [91] suggested that flexible z-yarns could significantly increase the delamination energy due to bridging between adjacent plies, especially in clustered laminates developing large delamination zones. Consequently, stitching has much less effect on the performance under HVI due to the highly localised damage pattern [92], [93] .

Some common 3D fabric structures are shown in Figure 2.10. Their impact behaviour is examined extensively by numerous studies. Bandaru et al. compared 2D double plain woven Kevlar 29/PP

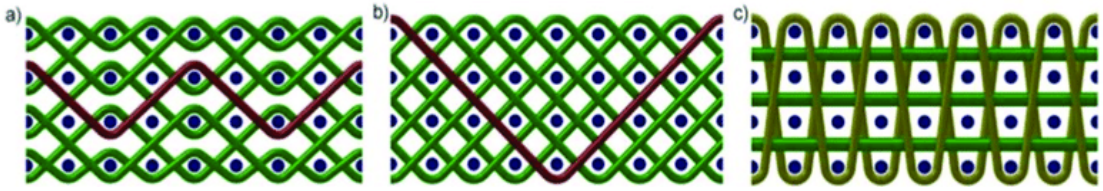

Figure 2.10: (a) layer-to-layer angle interlock, (b) through-the-thickness angle interlock, (c) orthogonal interlock [94]

with the same composite in configuration. Both angle-interlock and orthogonal 3D woven Kevlar composites exhibited higher energy absorption capacity than the 2D sample, with the angle-interlock dissipating 26% more energy [74]. The through-the-thickness yarns were found to transfer stresses through the laminate effectively, as well as maintaining the structural integrity after damage initiation. The authors concluded that fewer layers performed better, suggesting that the z-reinforcement should run through the entire composite. Aktas et al. [95] performed LVI at various energy levels on plain (1D), double plain (2D) and 3D-angle interlock E-glass/epoxy composites of similar areal weight. The perforation limit was found to be 50J in the 1D laminate, while both others failed at 60J, with a significantly higher Ductility Index. Seltzer et al. [96] compared 3D orthogonal and 2D satin weave fabrics of carbon and S2-glass/VE in LVI. The comparative nature of the test has to be viewed critically due to the difference in thickness in the panels but the author found that while the 2D S2-glass laminate absorbed more energy than the 2D carbon samples, it performed similarly to the 3D carbon composite (see Figure 2.11). This suggests that the potential performance gains in the weave are similar to that of the reinforcement selection. The authors found the 3D reinforcements to absorb about twice as much energy as the 2D satin weave, which they attributed to the z-yarns maintaining the structural integrity and promoting energy absorption through fibre splitting and shear plugging. Similar findings were made by Baucom and Zikry [97], who found a 3D orthogonal E-glass/VE composite to absorb about twice as much energy during multiple LVI strikes than an equivalent 2D plain laminate. The authors suggested that the frictional work between broken weft tows and unbroken z-tows contributed significantly to the energy absorption.

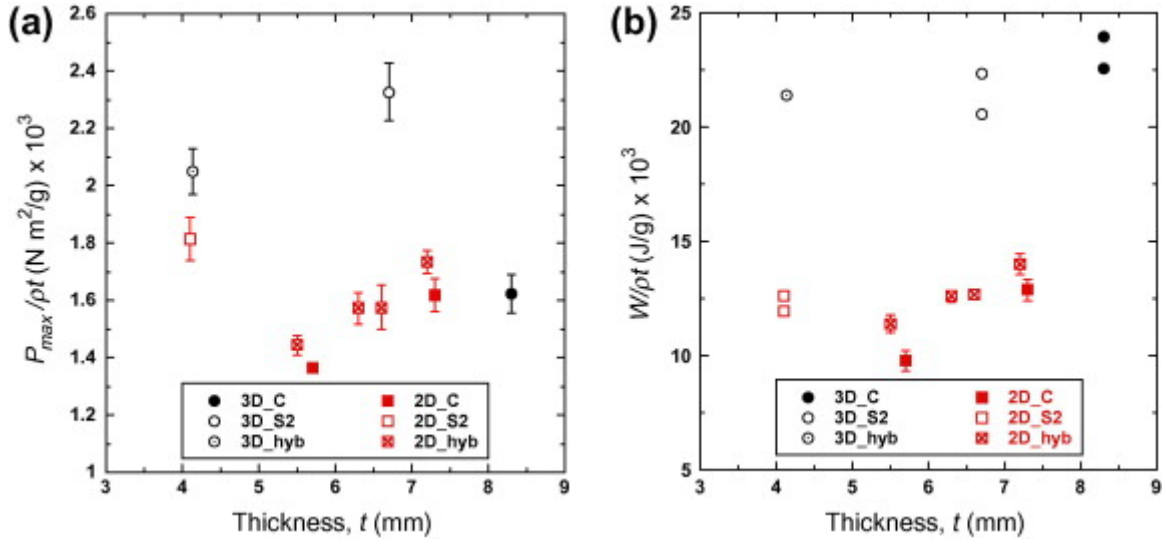

Figure 2.11: (a) Maximum load and (b) energy absorbed, both normalized by the areal density, as a function of the plate thickness [96]

Some researchers deem 3D configurations unsuitable for use in structural laminates due to the high volume of the fabric resulting in resin pockets and low fibre volume fraction [85], however V_f of up to 65% have been achieved using impregnation under high pressures [98].

Authors almost unanimously suggest that the energy absorption capacity is up to two times higher in 3D woven composites compared to 1 and 2D configurations. It is generally suggested that woven fabrics outperform UD laminates although the differences appear to be smaller. The energy absorbtion capacity is also not yet fully understood, as most research focuses on the damage tolerance rather than the energy absorption. There is also evidence that different fibre architectures favour different velocity regimes.

2.4.5 Layup

Researching the effect of the the layup on the impact performance appears to be somewhat more straightforward. Numerous configurations can be evaluated without changing other design parameters. Numerical and experimental studies compare various layups in otherwise identical laminates. unidirectional, quasi-isotropic (QI) and cross-ply (CP) configurations are most commonly evaluated, where CP generally produces the largest damage region and highest perforation limit in both high and low velocity impact[99, 100, 101, 38].Generally, the authors agree that both in LVI and HVI, the cross-ply configuration is capable of absorbing more energy compared QI or angle plies due to their tendency to develop more extensive damage. While the maximum reaction force is lower in the cross-plies, the higher damage degree promotes ductile behaviour and results in a higher total energy absorption capacity This property is detrimental for the structural and post-impact properties but it increases the perforation resistance.

Quaresimin et al. [102] found that the maximum contact load was independent of laminate lay-up, while it depended on laminate thickness and slightly on the impact energy also. The effect of ply-clustering, equivalent to increasing the ply thickness, was investigated by Gonzalez et al. [103]. They observed that clustering drastically increased the delaminated area, while not affecting the impact stiffness. They found that this was detrimental to the damage tolerance but did not make any suggestions regarding the perforation limit. Clustered composites compare to dispersed stacking sequences in a very similar way that CP and QI laminates do, making it likely that thicker plies are detrimental to the structural behaviour but improve the impact response.

Helicoidal layups (see Figure 2.12) are inspired from bio-based impact resistant structures. They are composed of multiple, generally UD layers, with small angles between adjacent plies. Grün-

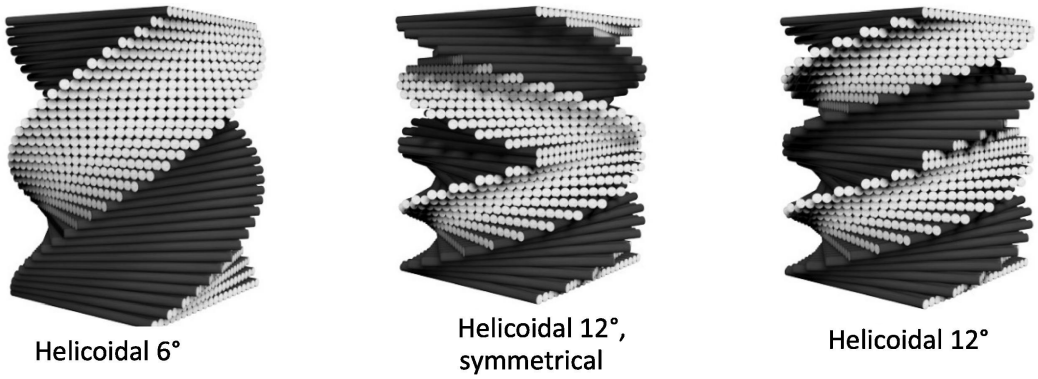

Figure 2.12: Various helicoidal layup configurations [104]

felder et al. [101] evaluated the damage resistance of helicoidal layups with different interply angles. They found the residual strength to be higher in a large angle helicoid compared to a QI layup, which they attributed to a lower degree of damage propagation through the thickness of the laminate. This was also seen by Ginzburg et al. [104], who simulated the LVI response and post-damage performance of various helicoidal layups. Their post impact behaviour was deemed poorer than that of QI and CP laminates due to the poor structural properties and the tendency to extensive delamination. However, the authors concluded that the impact strength of helicoids is larger due to being able of spreading damage in-plane, increasing the ductile response.

Lopes et al. [105] attempted to produce a dispersed stacking sequence somewhat similar to a helicoidal layup but with improved structural performance. The authors suggested that configurations such as $[\pm 45/0/70/-70/0/15/10/-10/-15/15/-15]_s$ could present a good trade-off between structural and static properties.

Virtually all studies give similar suggestions regarding energy absorbing layups. The authors agree that the stacking sequence may be taylored to incite damage and therefore the ductile response of the composite. Results also appear to overlap between low and high-velocity impact. Therefore, it is almost unanimously suggested that cross-ply composites absorb more energy than quasi-isotropic ones. Helicoidal layups are also often found to outperform QI-configurations, although further research is required. Generally, the gains in energy absorption appear to be quite small between layups and improvements of more than 50% are very rarely seen.

2.5 Conclusion

The characterisation approaches for impact performance were presented. The out-of plane perforation energy normalized by the areal density was used as a general comparative measure accross studies. Many studies evaluate the damage resistance and damage tolerance of materials and do not give values for the perforation energy. Nevertheless, these studies can be used to compare the energy absorption capacity of two similar materials through evaluation of the ductility index. This parameter returns the fraction of the energy dissipated through damage.

The effects of parameter modifications on the energy absorption capacity of structural composites were evaluated through literature findings. While there are some general design guidelines to be universally accepted by authors, many findings contradict with those of other researchers. Especially conclusions regarding the optimum reinforcement for impact remain to be extremely varied. A sweep study was conducted to collect research from numerous sources comparing the energy absorption of the reinforcement options. It showed a large spread in all materials but high-elongation aramid fibre was found to continuously produce among the most energy absorbing composites, while high-modulus aramid often performed poorly. Generally, it appears that low material densities are beneficial to the impact behaviour, especially with high incipient velocities due to the positive increase in specific energy absorption capacity with thickness. Aramid is the lightest of the high performance technical fibres currently used in structural composites.

The characteristics of aramid make it best suited to be used in structures experiencing light to medium service loads, and where resistance to impact is the limiting factor rather than structural strength or stiffness, for example the leading edges of an aircraft. Research should aim to optimise for such an application by designing the entire composite around the incorporation of aramid fibres, rather than to use them as a substitute reinforcement. Thermoplastic composites were generally seen to have better impact properties than thermoset composites, however the commodity thermoplastics currently used with ballistic aramid composites cannot provide the properties required for structural application. High-performance thermosets combine both high stiffness and high toughness but have thus far not successfully processed with aramid reinforcement. Future efforts should therefore focus on manufacturing such a material with adequate properties for use in laminates with combined impact and structural loading.

Chapter 3

Research

As shown in section 2.3, the concept of aramid fibre reinforced thermoplastic (AFRT) is virtually unexplored, both in the aspect of manufacturing and its properties. Kevlar and Twaron are known to degrade under heat exposure, making the feasibility of processing with high melting point-polymers questionable. The primary objective of this master's thesis work will therefore be attempting to demonstrate to which extent the processing of AFRT is possible in view of fibre degradation and interfacial interaction.

"How can Twaron and Technora fibre reinforced polymers be processed under high temperatures?"

"What are the effects of exposing Twaron and Technora fibre to the conditions required to process high-performance thermoplastics?"

"Which mechanisms cause thermal degradation during processing of aramid fibre reinforced high-performance thermoplastics?"

High energy absorption is expected to be the main strong-point of the new material. Long term feasibility will to a large part depend on the impact strength exceeding that of competitor materials such as aramid fibre reinforced epoxies and vinyl esters, as well as GFRP.

The second objective of the thesis work will focus on characterising the energy absorbing potential of the newly developed material with respect to other energy absorbing composites. A simple evaluation of the energy absorption is inconclusive due to the influences of other design and impact parameters. Therefore, the effects of matrix material and fibre matrix interface on the impact strength will be addressed.

"How does the impact performance of aramid fibre reinforced high-performance thermoplastics compare to that of other structural aramid fibre composites?"

"How is the low-velocity impact behaviour of ARRET influenced by the type of thermoplastic matrix and the fibre-matrix adhesion?"

While changing the matrix material is relatively straightforward, no sizing options for the specific application have been developed. The effectiveness of conventional sizings must then be evaluated.

If sufficient performance gains are made, the material could accelerate the replacement of metals by composites in aircraft. The high price of aramid will limit the use towards high-performance

applications but the use in other sectors is possible. With recent improvements in the recyclability of thermoplastic composites, the material could also contribute to more sustainable aircraft structures, although the production of aramid remains an energy intensive process.

Research will be conducted experimentally due to the novelty of AFRT and the limited available information. With the added complexity of impact, accurate modelling is deemed unfeasible at this point in time. The thermoplastic specimens are produced through film stacking. Vacuum infusion processing is used for epoxy reference samples. Processing quality is assessed using C-scan, microscopy and thickness measurement. Tensile strength retention after heat exposure will be tested on both composite and yarn level, with the latter serving as a simpler and more versatile means of producing tensile specimens. Impact characterisation is done at both low and high velocity, using a drop tower and gas gun, respectively.

Part I

Manufacturing

Chapter 4

Experimental Approach

This chapter presents the materials and the manufacturing processes used to produce the test composites. The specimens and their use in the various experiments are listed. Finally, the characterisation techniques are elaborated.

4.1 Materials

The reinforcement and matrix materials used in the manufacturing process of the composite test specimens are listed in Table 4.1 and Table 4.2. The reinforcement yarn and fabrics were provided by Teijin Aramid, while polyether imide (PEI) and polyphenylene sulfide (PPS) sheets were available at TU Delft. It was decided not to purchase other polymer films as PPS and PEI differ greatly in their processing conditions, mechanical and impact properties, making them suitable for comparison.

	Matrix		
Material	PPS	PEI	Epoxy
Supplier	TenCate	TenCate	Hexion
Description	Rayotec S080 PPS I0827C film	Rayotec S060 PEI 4322D film	EPIKOTE^{TM}/ EPIKURE^{TM} 04908
Film Thickness [mm]	0.08	0.06	-
Density [kg/m^3]	1350	1270	1150
Area Density [kg/m^2]	0.108	0.076	-
Tg [°C]	90	217	82
Melt Temperature [°C]	280	-	-
Tensile Strength [MPa]	90.3	105	74
Tensile Modulus [GPa]	3.80	3.28	2.90
Tensile Strain [-]	0.15	0.19	0.09

Table 4.1: Matrix properties[1]

Twaron and Technora (see section 1.1) were used as reinforcement materials. For all composite panels, 2000 filament yarn was used. Note the much higher modulus of Twaron 2200 over Technora T200, where low modulus, high elongation aramids are preferred over higher stiffness yarns due to their supposedly higher energy absorption capacity. The other grades listed in Table 4.2, notably the high stiffness Twaron 2200 and 1000 filament Technora T200 yarn were used only in individual tensile tests on raw fibres. As standard, the yarns were treated with a spin finish to protect and coalesce

[1]Tensile strain data for PPS and PEI was taken from https://matweb.com. All other data was provided by the respective supplier.

the filaments. The listed Twaron 1015 yarn uses a different, epoxy based sizing designed to improve adhesion to various polymer matrix materials. Otherwise, the grade is identical to Twaron 1000.

Reinforcement Yarns used in the project

Type	Twaron 1000	Twaron 1015	Twaron 2200	Technora T200
Sizing	Standard	Epoxy	None/ Std	Standard
Density [kg/m^3]	1445	1445	1445	1390
Filaments	2000	2000	1000/ 2000	1000/ 2000
Linear Density [dtex]	3360	3360	1610/ 3220	1670/ 3300
Tensile Strength [N]	688	688	365/ 695	409/ 818
Tensile Modulus [GPa]	67	67	105/ 102	73
Elongation at Break [-]	0.037	0.037	0.028	0.045

Table 4.2: Yarn type properties as provided by Teijin Aramid

The fabrics used during the project are listed in Table 4.3. The Twaron 2200 based interwoven double plain MLF21 weave was selected as the base fabric for the optimisation of the manufacturing process. It was designed for use in composites and readily available at the Teijin Aramid facility. An identical MLF21 fabric from Technora T200 yarn was later produced by Teijin as a means of comparison between the Twaron and Technora reinforcements. Note that the difference in surface density of the two MLF21 weaves is due to the slightly lower density of Technora. The listed T741 and T736 AA fabrics are configured in the exact same one dimensional plain weave structures and differ only in the spin finish type of the Twaron 1000 reinforcement. These fabrics are used in hard ballistics applications and were brought in with the intent of studying the influence of fibre matrix adhesion on impact performance.

Fabric Reinforcement

Fabric Type	TW MLF21	TN MLF21	T741	T736 AA
Yarn Type	Twaron 2200 (2000f)	Technora T200 (2000f)	Twaron 1000	Twaron 1015
Weave Type	3D plain	3D plain	2D plain	2D plain
Area Density [kg/m^2]	0.468	0.450	0.410	0.410

Table 4.3: Fabric type properties as provided by Teijin Aramid

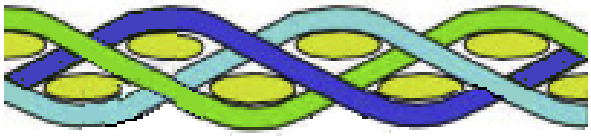

Figure 4.1: 3D double plain weave fabric structure of MLF21

4.2 Manufacturing Methods

As both thermoplastic and thermoset composites are used in testing, two different manufacturing approaches were required. Film stacking was used to process the thermoplastics and vacuum infusion processing for the thermosets.

4.2.1 Film stacking

Processing the composite panels was done at the TU Delft facility through film-stacking, where plies of fabric are layered alternately with a number of thermoplastic polymer sheets and consolidated in a hot press under application of heat and pressure. The polymer film was cut to 580x580 mm sheets

from its roll using an automatic Gerber cutting machine, while the aramid was hand cut to the same dimensions due to the machine being unable to lacerate the fabrics. In the layup, the film sheets were distributed inbetween the fabric plies as evenly as possible, after which the stack was placed between two thin steel plates which had been cleaned with acetone and then treated with a Marbocote release agent. Finally, the edges of the laminate were wrapped in aluminium foil to contain the squeeze-out, as well as to avoid spilling of molten polymer into the press. Processing was done in a Joos LAP 100 press with controlled heating and cooling and 1000 kN pressing capacity. The process cycle consisted of a heating step, a dwell stage to ensure full heating of the composite, the consolidation phase and finally cooling (see Figure 4.2). The standard processing temperatures commonly used in the Joos press are 320°C for PPS and 380°C for PEI, at 10 bar consolidation pressure and 20min dwell time. Changes to the cycle were made in an attempt to reduce the high-temperature exposure time of the aramid reinforcement. The heating rate was generally set at 8 °C/min due to being commonly used in previous consolidation cycles. A cooling rate of 10 °C/min was used for the amorphous PEI, whereas

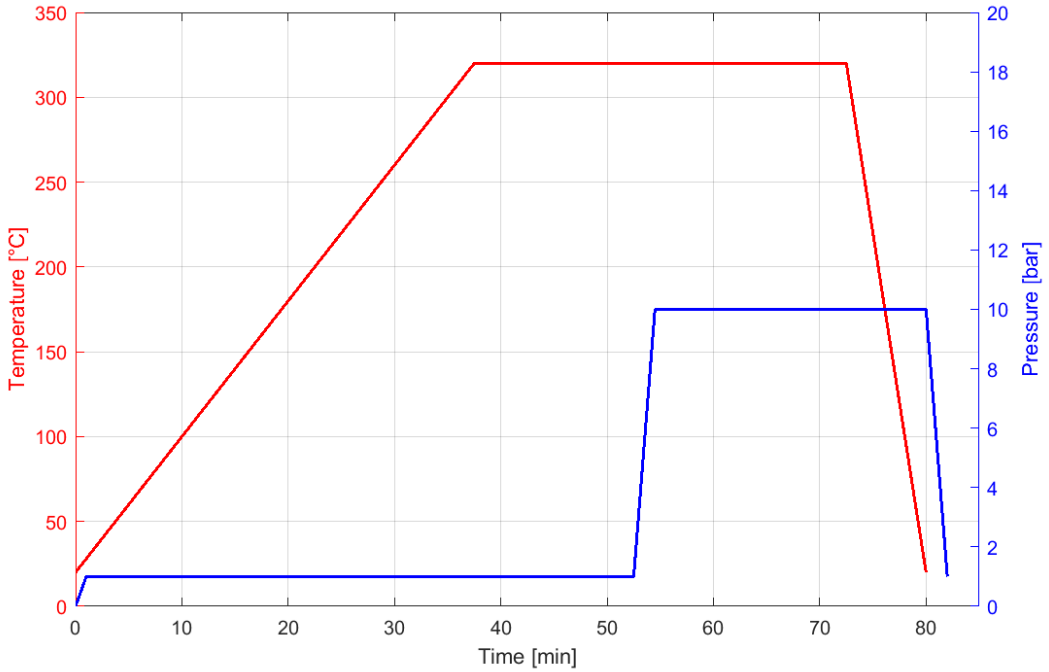

Figure 4.2: Consolidation cycle used for PPS matrix composites

fast cooling of 50 °C/min was used for PPS in order to minimize crystallisation. Slow cooling rates are meant to reduce warping in the panel. Note that the fast cooling cooling rates could only be achieved by the press at higher temperatures. A consolidation pressure of 10 bars was applied after the dwell stage to allow the polymer to fully wet out the fibres. The pressure was maintained until the cooling step was finished. After consolidation, the edges of the panels were trimmed off using a sheet metal cutting machine.

Later panels were manufactured under vacuum as a means to prevent air exposure during processing in the Joos press. This was achieved by means of encapsulating the panel in thick (0.125 mm) Kapton polyimide film and sealing the edges with heat resistant tacky tape (see Figure 4.3). Prior to use, the films were cleaned with isopropanol and coated with Marbocote release film. After layup, the stack was placed inbetween the steel plates and then encapsulated in the vacuum bag. A breather sheet was placed on top of the upper steel plate to ensure full distribution of the vacuum. Glass fabric was used as a breather layer initially but in later panels was replaced with a sheet of aramid, which had a much lower tendency of adhering to the Kapton film. This approach had the added benefit of providing yarn samples to compare the effects of the processing cycle on both composite and fibre. The aramid breather would also indicate failure of the vacuum bag as aeration

would cause discolouration through oxidation. The connection to the pump consisted of a flattened aluminium pipe serving as a connecting piece. It was embedded in the tacky tape seal and connected with the pump through a silicone tube. Before processing, the vacuum was tested for large leaks. The pump was kept running for the entire process. After completion of the processing cycle, the vacuum was checked again to indicate if leaks had occurred during manufacturing. The encapsulated stack, as shown in Figure B.1(b) was placed in the press and processed similarly to the panels which did not use vacuum. It was deemed possible that the vacuum bag and aramid breather layer would serve as insulators and lower the temperature in the stack, however no differences in consolidation quality could be observed between regular and vacuum processed specimens.

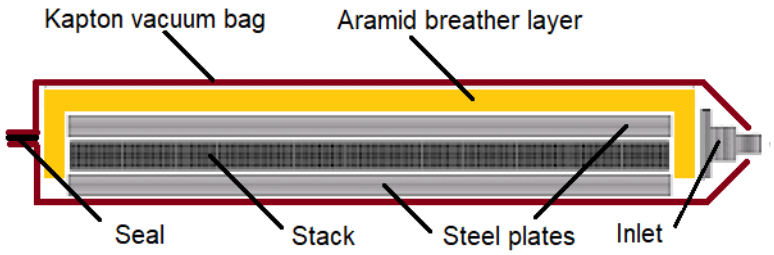

Figure 4.3: Vacuum bag processing setup

Due to the high price and energy uptake of Kapton, it was attempted to reuse the vacuum bag multiple times. This was possible but only if no or only small amounts of resin would leak from the panel, as the polyimide would embrittle after heat exposure and rip where the panel adhered to the leaked polymer.

4.2.2 Vacuum infusion

Vacuum infusion processing (VIP) was used to manufacture the epoxy matrix specimens used as a reference or comparison for the thermoplastic panels. This method was selected due to its availability at TU Delft and its high versatility for low volume components.

A roughly 5 mm thick, square aluminium plate formed the base of the setup and the hard section of the mould. Its dimensions were 750x750 mm to accommodate the 600 x 600 mm composite plates. The epoxy resin system used was Epikote 04908 resin and Epikure 04908 hardener. The resin was degassed before adding the hardener and again after mixing, each for 20 min at 10 mbar. Mould preparation included cleaning with acetone, applying the Marbocote release agent and covering the edges with tacky tape. The same [0°,0°]-layup as in the thermoplastic samples was used. After placing the reinforcements on the pre-treated mould, peel ply, a perforated separator film and a flow mesh were added on top of the stack in the respective order. Before applying the vacuum bag, the in- and outlets of the mould were prepared, connecting the resin reservoir and the vacuum pump with the mould in between. The appropriate amount of matrix material was prepared based on the laminate to be injected. Some additional amount of resin was added to fill the inlet tube, the in- and outlet and the flow mesh, as well as to have a remainder in the reservoir. After mixing and degassing the resin, the vacuum pump was reattached to the outlet while the inlet was placed into the resin reservoir, forcing the resin through the plate. After impregnation, the inlet and outlet were clamped shut and the plate was left to cure for at least 48h before removing the moulding components.

4.3 Specimens

The panels produced to optimise the manufacturing process are listed in Table 4.4, along with their processing conditions, thickness (after processing) d and fibre volume fraction V_f. The materials were designated according to their constituents and the processing temperature. Initial panels which were processed under aerated atmosphere are marked as such.

All specimens used two sheets of fabric, stacked in a [0°,0°]-configuration. A fibre volume fraction of around 0.6 was targeted initially, requiring 5 sheets of PPS or 7 sheets of PEI (specifications listed in Table 4.1). This configuration appeared to result in slight resin poverty with the MLF21 fabrics, therefore later specimens used 6 and 8 sheets, respectively. The thickness reported in the table was measured from the composite tensile specimens using a micrometer in 8 different locations in the panel. Based on the thickness measurement, the fibre volume fraction $V_{f,measured}$ was calculated as

$$V_{f,measured} = \frac{n_f \rho_{A,f}}{\rho_f d} \tag{4.1}$$

With n_f the number of fabric plies and $\rho_{A,f}$ and ρ_f their individual areal density and density. The measured value was compared with the target fibre volume fraction $V_{f,target}$, which was calculated as

$$V_{f,target} = \left(1 + \frac{n_m \rho_{A,m} \rho_f}{n_f \rho_{A,f} \rho_m}\right)^{-1} \tag{4.2}$$

With n_m the number of matrix sheets and $\rho_{A,m}$ $\rho_{A,m}$ their areal density and density. Comparing the predicted and real fibre volume fraction appeared to give a good indication of the quality of consolidation. If the measured value was lower than predicted, voids were inevitably present, whereas a higher value than predicted indicated squeeze-out and presumably good consolidation.

	Processing Conditions				Properties	
Specimen	T [°C]	p [bar]	t [min]	Cooling rate [°C/min]	thickness (std) [mm]	V_f target/ measured
TW-MLF21-PEI-380-air	380	10	20	10	1.02 (0.01)	0.61/ 0.64
TW-MLF21-PEI 320-air	320	10	20	10	1.40 (0.04)	0.61/ 0.46
TW-MLF21-PPS-320-air	320	20	10	50	1.19 (0.02)	0.62/ 0.54
TW-MLF21-PPS-320	320	10	20	50	1.08 (0.03)	0.57/ 0.6
TW-MLF21-PPS 300	300	10	40	50	1.14 (0.02)	0.57/ 0.57
TW-MLF21-PPS-320 (dried fabric)	320	10	20	50	1.08 (0.00)	0.57/ 0.6
TW-MLF21-Epoxy	-	-	-	-	1.39 (0.03)	- / 0.47
TN-MLF21-PPS-320	320	10	20	50	1.18 (0.00)	0.57/ 0.55
TN-MLF21-Epoxy	-	-	-	-	1.88 (0.03)	- / 0.34
TW-T741-PEI-380	380	10	10	10	1.19 (0.02)	0.51/ 0.49
TW-T741-PPS-320	320	10	20	50	0.86 (0.03)	0.54/ 0.67
TW-T741-Epoxy	-	-	-	-	1.19 (0.02)	- /0.48

Table 4.4: Panel Specimens for process optimisation

4.3.1 Designation

A universal naming designation for specimens is used across the document. The convention as used to describe the panel specimens listed in Table 4.4 distinguishes the following material and processing parameters: Yarn type, fabric type, matrix material and processing temperature. The added suffix -air is used for the initial panels which were processed under plain air rather than vacuum. TW-MLF21-PPS-320-air then describes a panel composed of Twaron MLF21 fabric and PPS matrix, which was processed at 380°C without vacuum bag. Epoxy composites do not have the temperature mark as they underwent no high processing temperatures.

4.4 Methodology

The manufacturing stage of the project was aimed at producing a well consolidated composite, while simultaneously minimizing the exposure of the aramid reinforcements to the extreme conditions in

the press, notably the processing temperature and exposure time. Increasing the processing pressure was evaluated as a means to reduce exposure time and temperature. Other concepts focused on directly reducing the processing temperature and exposure time. Finally, it was tested if the Kapton vacuum bag, forming an insulator between the panel and the press plates, would have an effect on the degree of consolidation. Table 4.5 shows the testing approach and the panel specimens used in the characterisation.

Varying Parameter	Value	Panel	Concept
Pressure/ time	10 bar, 20 min	TW-MLF21-PEI-380-air	Reducing exposure time
	10 bar, 10 min	TW-T741-PEI-380	
	10 bar, 20 min	TW-T741-PPS-320	Reducing exposure time
	20 bar, 10 min	TW-MLF21-PPS-320-air	while increasing pressure
Temperature	320°C	TW-T741-PPS-320	
	300°C	TW-MLF21-PPS-300	Decreasing processing
	380°C	TW-MLF21-PEI-380-air	temperature
	320°C	TW-MLF21-PEI-320-air	

Table 4.5: Testing methodology for consolidation quality evaluation

The quantification of strength retention under processing required numerous data points in order to model the behaviour. Due to the limited availability of composite tensile specimens, yarn tensile testing were used to generate complementary data. The main focus point of the tensile test was strength retention under exposure to heat. Strength retention was quantified in terms of a reference which had undergone no notable heat treatment. For the yarn test, untreated fibres were used while epoxy composites formed the reference on composite level. Fibre volume fractions were lower in the epoxy laminates but under the assumption of fibre dominant behaviour, this was ignored. These were exposed only to the heat of the exothermic curing reaction, which was assumed to have no effect on the fibre strength.

Oven treated yarn was used to evaluate degradation in terms of temperature, exposure time and atmosphere, as listed in Table 4.6. In-house data was available on temperature and time dependent strength loss of Twaron yarn in air and nitrogen atmosphere. Additional data was to be generated on Technora, as well as for heating under vacuum. Temperature effects were evaluated at 300°C and 400°C, as these form the range between which high-performance thermoplastics are processed. Strength retention was assessed on Twaron and Technora for 15 and 60 min exposure in a vacuum oven at 300°C. These duration were estimated as the lower and upper bounds of the dwell time. Note that the processing temperature is maintained as standard for 15 min to fully melt the polymer, followed by 20 min dwell time, or 35 min in total. The total time at elevated temperature is somewhat higher due to heating and cooling.

Finally, tensile tests were conducted on yarn taken from the aramid breather sheet used while processing a PPS based composite (see Figure 4.3). This test served as a bridge between tensile tests on yarn and composite level, as the breather sheet had undergone the exact same treatment as the composite it was used on.

Composite tensile tests assessed the feasibility of exposing the two available aramid types to the conditions required to process the PPS and PEI matrix materials. The processing pressure was hypothesised to have no effect on the fibre condition [106], which was tested swiftly by comparing identical composites processed 10 and 20 bar respectively. Processing temperature was expected to be the main driver of degradation. Both Twaron and Technora reinforced PEI (380°C) and PPS (320°C) composites which were processed under vacuum at the standard processing conditions were compared to epoxy based laminates. The press atmosphere was changed from aerated to vacuum in order to study degradation under the presence of oxygen. Lastly, hydrolytic effects were assessed by comparing the tensile strength in a standard-processed composite with on where the reinforcement

Varying Parameter	Value	Fixed parameters	Yarn Type
Time	15 min 60 min	300°C, vacuum	Twaron 2200 (1000f)
	15 min 16 min		Technora T200 (1000f)
Temperature	300°C 400°C	vacuum, 60 min	Twaron 2200 (1000f)
	300°C 400°C		Technora T200 (1000f)
Atmosphere	Air N2	300°C, 15 min	Twaron 2200 (2000f)
	Vacuum		Twaron 2200 (1000f)
Environment	Oven	300°C vacuum, 60 min 400°C vacuum , 60 min	Twaron 2200 (1000f)
	Press (PPS cycle)	320°C vacuum, 10 bar, 35 min	Twaron 1000

Table 4.6: Testing methodology for yarn strenght retention evaluation

and matrix material had been dried before in an oven at 95°C before pressing.

Varying Parameter	Value	Panel	Reference
Pressure	10 bar	TW-MLF21-PEI-320-air	TW-MLF21-Epoxy
	20 bar	TW-MLF21-PPS-320-air	
Temperature	-	TW-T741-Epoxy	TW-T741-Epoxy
	300°C	TW-MLF21-PPS-300	TW-MLF21-Epoxy
	320°C	TW-T741-PPS-320	TW-T741-Epoxy
	380°C	TW-T741-PEI-380	
	-	TN-MLF21-Epoxy	TN-MLF21-Epoxy
	320°C	TN-MLF21-PPS-320	
	380°C	TN-MLF21-PEI	
Atmosphere	320°C air	TW-MLF21-PEI-320-air	TW-MLF21-Epoxy
	380°C air	TW-MLF21-PEI-380-air	
	320°C vacuum	TW-T741-PPS-320	TW-T741-Epoxy
	380°C vacuum	TW-T741-PEI-380	
Water content	No drying	TW-MLF21-PPS-320	TW-MLF21-Epoxy
	Dried 3h @ 95°C	TW-MLF21-PPS-320 (dried fabric)	

Table 4.7: Testing methodology for composite strenght retention evaluation

4.5 Characterisation Techniques

C-scan and microscopy were used to evaluate the processing quality on the aramid composites.

4.5.1 C-scan

A C-scan was used in the initial optimisation of the processing cycle as a quick measure to evaluate the consolidation quality. The setup consisted of a transmitter on one and a receiver probe on the opposite side of the specimen, returning the attenuation level accross the panel. High signal attenuation is an

indicator of voids [107] or damage due to the entrapped air serving as a dampening medium. This property of air required the sample to be submerged in water, serving as a transmitter medium. The setup is shown in Figure B.2(c). The resolution of the scan could be specified by setting the number of probing iterations in the width and length direction of the panel. Dedicated C-scan samples were cut from the panel to avoid submerging the entire plate. This was done to avoid possible alteration of the properties as both aramid and PEI are known to absorb water. While the setup contained its own programme for graphical data analysis, the data was exported and processed using MATLAB, which allowed changing the colour map and removal of unessential parts of the images.

4.5.2 Cross-sectional Microscopy

Optical microscopy was used as a means to observe consolidation quality and fibre bundle wetting. The Keyence VK-X1000 (Figure B.2(e)) provided tools to determine void content and surface roughness through laser scanning, while the high magnification of the VH-Z1000UR (Figure B.2(f)) could be used to observe individual filaments and resin penetration into the fibre bundle. To obtain a clean, even surface, the specimens were machine cut to size, cleaned with ethanol and embedded in resin. After curing, the microscopic samples were first sanded with increasing grit size and then polished to obtaine a flat, screatch-free surface.

Two separate microscopic samples were produced, containing three specimens of the initial panels each. TW-MLF21-PEI-380-air, TW-MLF21-PEI-320-air and TW-MLF21-PPS-320-air were contained in Sample 1. The second sample contained specimens TW-T741-PPS-320, TW-T741-PEI-380 and TW-T741-Epoxy.

4.6 Mechanical Testing

Tensile testing on yarn and composite level was used to determine thermal degradation effects on the aramid reinforcement.

4.6.1 Fibre tensile testing

Yarns were tested in tension as a simple means to evaluate thermal degradation. This method was more versatile than testing composite samples, which had to be processed and cut to size before testing. Furthermore, comparing composite samples was deemed less accurate due to the added influences of the resin and fibre-matrix adhesion. Degradation in the yarn was evaluated as the strength ratio between heat treated yarn and identical, untreated yarn. Setups in both Delft and Arnhem were used, as some types of fibres were available in only one of the locations. The use of different test standards was deemed unproblematic as comparisons were made only on the basis of strength retention ratios. 5 specimens each were tested for statistical significance.

As only woven aramid was available at TU Delft, yarns were obtained by pulling them from the fabric weft. Heat treatments were conducted in a Nabertherm LV 5/B180 burn-off furnace, which could be placed under Nitrogen atmosphere. A container made of aluminium foil was used to avoid direct contact with the oven. The fibres were then tested to break in a 20 kN Zwick Roell test bench with 1 kN load-cell. A dedicated clamp was used to fixate the yarn (see Figure B.2(b)) in order to avoid failure near the clamp.

Tensile testing at the Teijin aramid facility was done according to the ASTM D7269 standard [108], which is specifically tailored towards aramid yarns. The method prescribes the use of a simple hydraulic clamp Figure B.2(a) and specifies the twists per meter (tpm) according to the yarn's linear density. For the 1680 dtex yarn used, 80 tpm were applied. Tests were carried out with an Instron testing machine and 2 kN load cell. Heat treatments at the Arnhem facility were carried out in a vacuum oven.

4.6.2 Composite tensile testing

A composite specimen tensile test was taken as the primary indicator of strength degradation due to the processing cycles. Specimens taken from all panels were compared to quantify thermal ageing to the fibres. Testing was carried out in accordance with the ASTM D3039-08 standard [109], using the Zwick Roell 20 kN test bench from the fibre tensile test. A self tightening wedge grip was used as the fixture, along with a 20 kN load cell to allow for specimen break Figure B.2(d). Along with the failure strength, the strain was recorded using an extensometer, in order to maintain a means of determining the tensile stiffness. All panels were tested with at least 5 tensile specimens of dimensions 25.4x200 mm. Paper was glued onto the ends of the specimen to avoid slipping of the wedge clamps. The samples were cut from each panel using a sheet metal cutting machine and then lathed to their exact dimensions. All specimens were tested along the 0° fibre direction, amounting to half of the reinforcement being loaded with the other half pointing in the transverse direction.

The composites were compared based on the failure load in Newtons. This approach was chosen as the panel thicknesses differed and therefore the stress would not be dependent only on the fibre's constitution. As all the composites used two identically oriented plies of reinforcement, it was assumed that their failure load would depend only on the constitution of the reinforcement. This approach required the width of the panels to be identical, which was tested using calipers. Before testing, the thickness of each sample was measured in the center using a micrometer.

Chapter 5

Results and Discussion

This section evaluates the effects of the processing parameters on processing quality and strength retention through C-scan, cross-sectional microscopy and tensile behaviour. The balance between adequate consolidation and strength retention is discussed.

5.1 Consolidation quality

The consolidation quality depends on the effectiveness of the processing conditions. Good consolidation encompasses low void content, absence of matrix rich regions and full wet-out of the fibres. In the following, the

C-scan images are shown for panels which differ in their processing parameters, denoting regions of high attenuation likely to contain voids in blue. For all panels, the discrepancy between regions of low and high attenuation is very large with no intermediate state (yellow or green regions) present, suggesting that any amount of voids would generally result in high dampening. The attenuating region seen in the upper left of all C-scan images reflects the sample fixture. A C-scan image taken from a Twaron-Epoxy composite sample was taken as the reference. As seen in Figure 5.1, the entire panel is red coloured red, denoting low attenuation in the absence of voids.

Microscopic images of samples of the composites processed under plain air, TW-MLF21-PEI-380-air, TW-MLF21-PEI-320-air and TW-MLF21-PPS-320-air (see Figure 5.5(b)). Figure 5.5(a) shows the two thermoplastic TW-T741 fabric composites, as well as TW-MLF21-PPS-320, all of which were processed under vacuum. A microscopic sample containing all the laminates from the process optimisation stage is included in Figure F.1.

Figure 5.4 compares the load displacement curves of variously processed thermoplastic composites with their respective epoxy reference samples.

5.1.1 Dwell time

The effect of shorter dwell time on consolidation quality is clearly shown when comparing TW-MLF21-PEI-380-air and TW-T741-PEI-380, which were processed for 20 and 10 min respectively. Clear differences are found under C-scan observation (Figure 5.2 and Figure 5.3). The continuously blue region in TW-T741-PEI-380 indicates voids throughout the entire composite, while the longer dwell time results in part in a red region, indicative of low attenuation and therefore absence of air inclusions. These same findings are observed under cross sectional microscopy in subsection 4.5.2, where the short-processed TW-T741-PEI-380 shows vast areas of matrix rich regions, which are absent in TW-MLF21-PEI-380-air. Lastly, evaluation of the fibre volume fraction shows higher-than-anticipated V_f for the 20 min dwell time and the opposite for 10 min treatment (see Table 4.4).

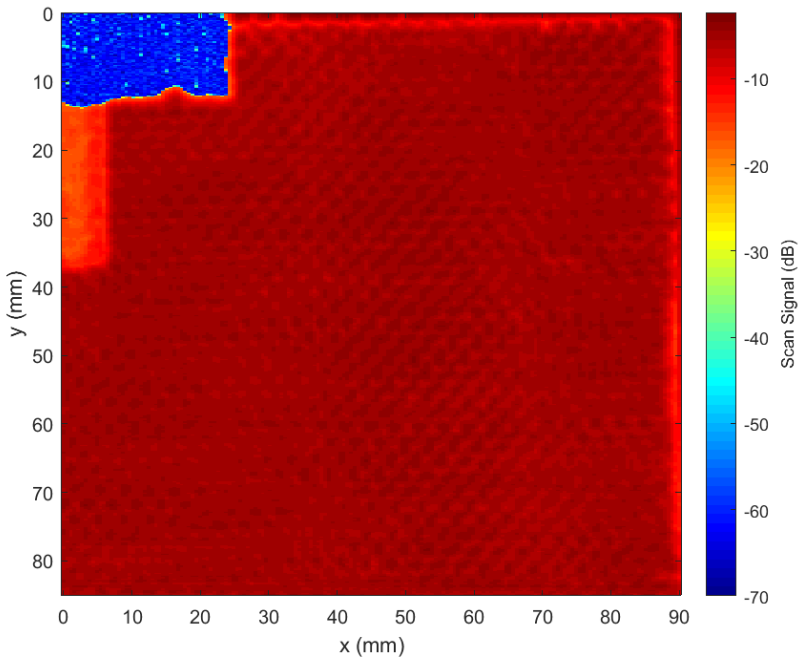

Figure 5.1: C-scan of a Twaron-Epoxy composite (TW-T741-Epoxy)

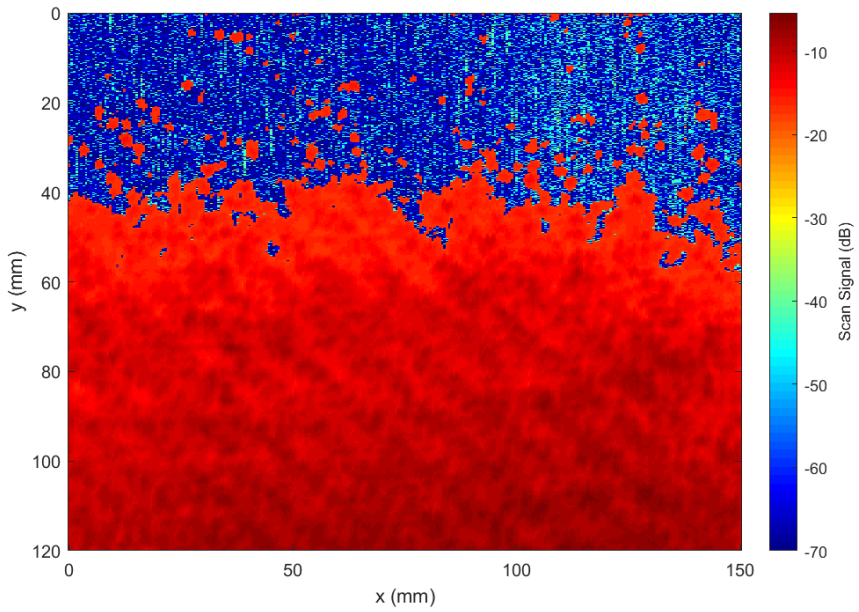

Figure 5.2: C-scan of TW-MLF21-PEI-380-air consolidated at the standard conditions of PEI

The degree of consolidation can also be observed in the tensile behaviour of the laminates. Figure 5.4 shows the median tensile curves of some Twaron MLF21 and T741 composites. Among all the composites, there is a general trend of composites with better consolidation having a stiffer response. Between the two thermoplastic composites shown in Figure 5.4(a), the PPS composite, using a 20 min dwell time, produces a stiffer response than the PEI composite consolidated for 10 min only.

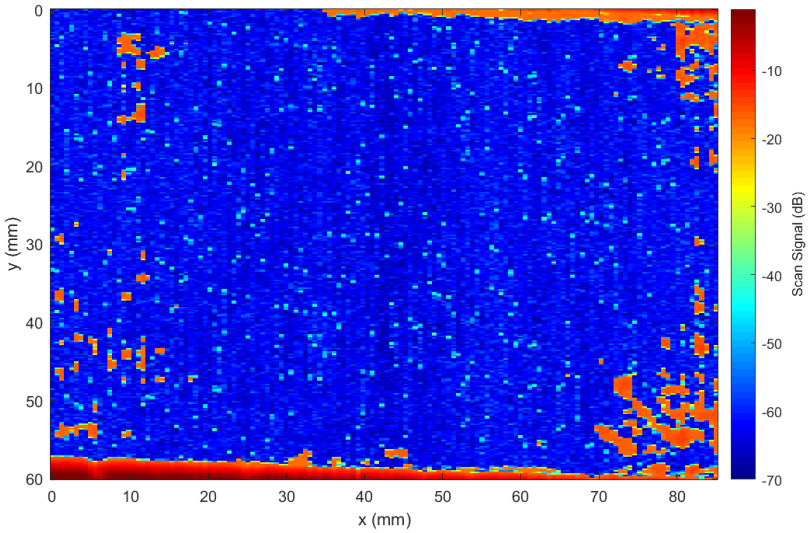

Figure 5.3: C-scan of TW-T741-PEI-380, using a shortened dwell time

The observations clearly indicate that substantial reductions in dwell time are unfeasible under otherwise standard processing conditions.

5.1.2 Pressure

TW-MLF21-PPS-320-air, which was processed under shortened dwell time but increased pressure, is observed under cross-sectional microscopy in Figure 5.5(b). Comparing to TW-MLF21-PPS-320 (Figure 5.5(a)), which used the standard cycle, the composite quality appears somewhat poorer. Some matrix rich zones are present, as well as some non-embedded fibre bundles sticking out from the composite's surface.

The pressure increase appears insufficient in counteracting the shortened processing time, however the degree of consolidation appears to produce better than in TW-T741-PEI-380, where the dwell time was decreased without countermeasures. With further pressure increases, good consolidation could be achieved. The concept is however abandoned due to the findings of Khondker et al. [2], who established that reduced exposure time would only yield minor improvements in strength retention.

5.1.3 Temperature

The effect of lowering the processing temperature on PEI based composite is shown through cross-section microscopy in Figure 5.5(b). The uppermost sample, TW-MLF21-PEI-380-air was processed at 380°C, as recommended by the supplier, whereas 320°C were applied on TW-MLF21-PEI-320-air. The latter sample exhibits large resin rich zones and is noticeably thicker. The higher thickness is reflected in the fibre volume fraction, which is 0.46 vs the anticipated 0.61. Comparison in Figure 5.4(b) also shows a much stiffer tensile response of TW-MLF21-PEI-380-air over TW-MLF21-PEI-320-air, denoted by the red and purple lines, respectively. The observations clearly show that extensively lowering the processing temperature is impossible. However, as shown in Figure 5.2, even at a temperature setting of 380°C, poorly consolidated regions are formed near the cooler edges of the press.

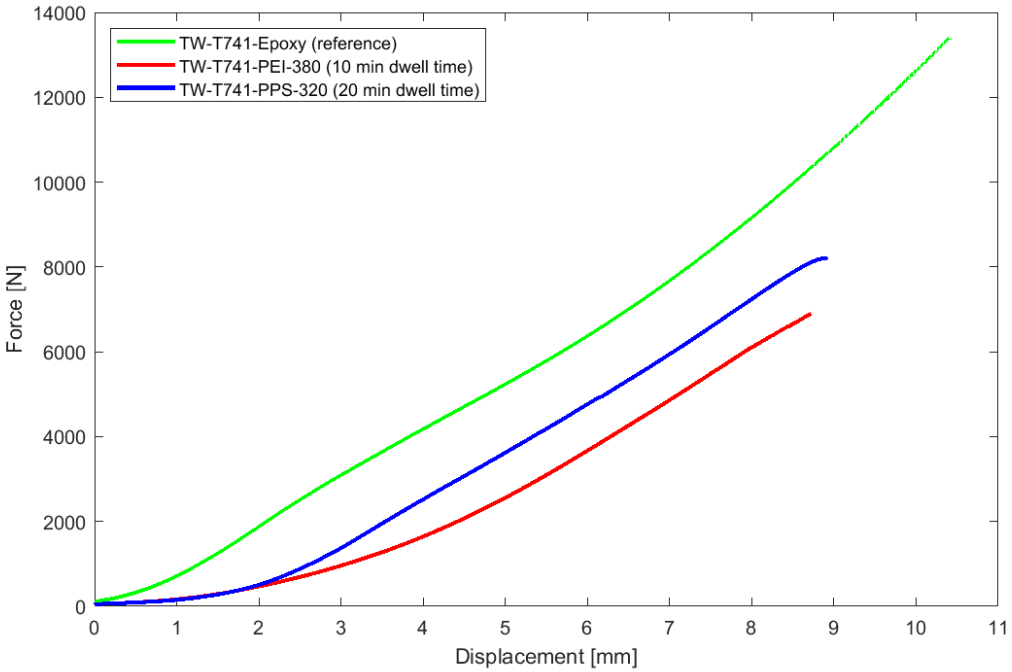

(a) Tensile strength of variously processed TW-T741 composites

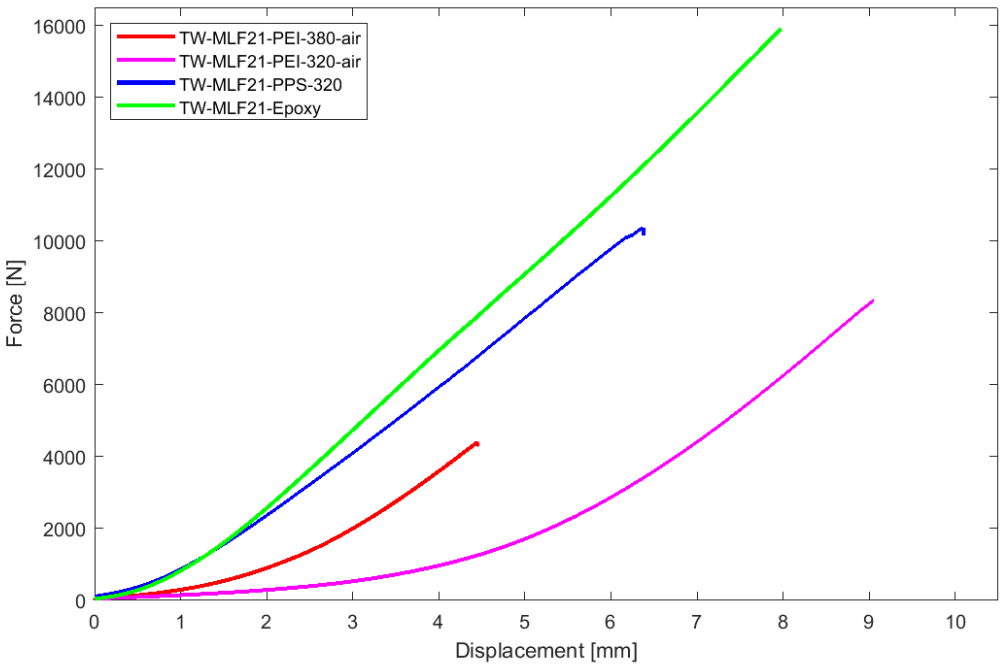

(b) Tensile strength of variously processed TW-MLF21 composites

Figure 5.4: Tensile strength of variously processed Twaron composites

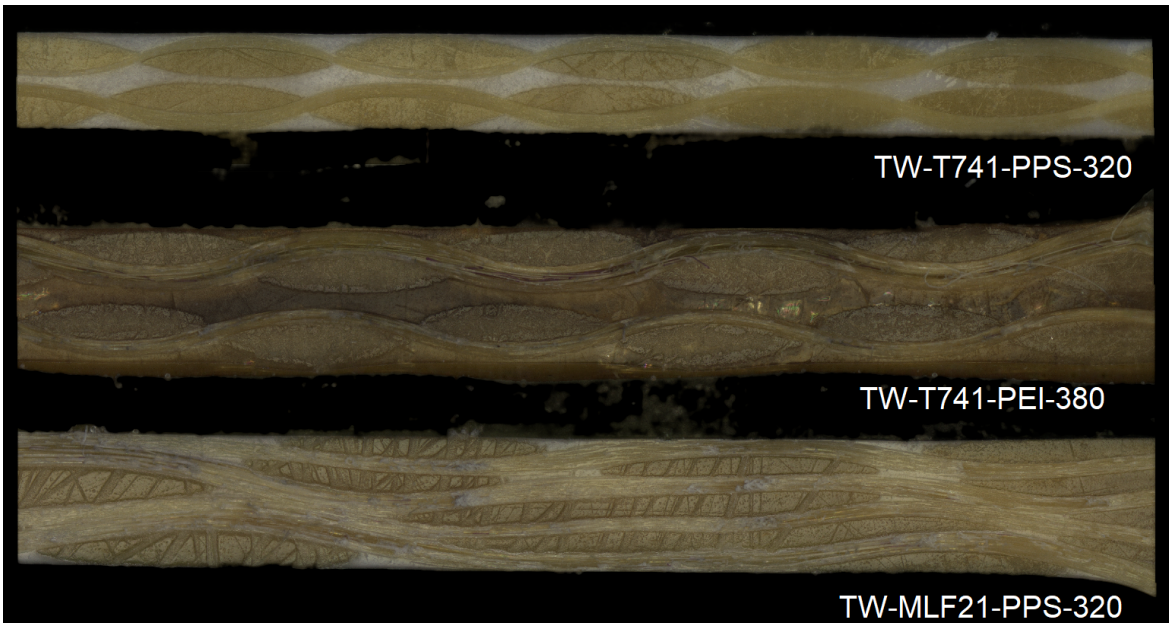

(a)

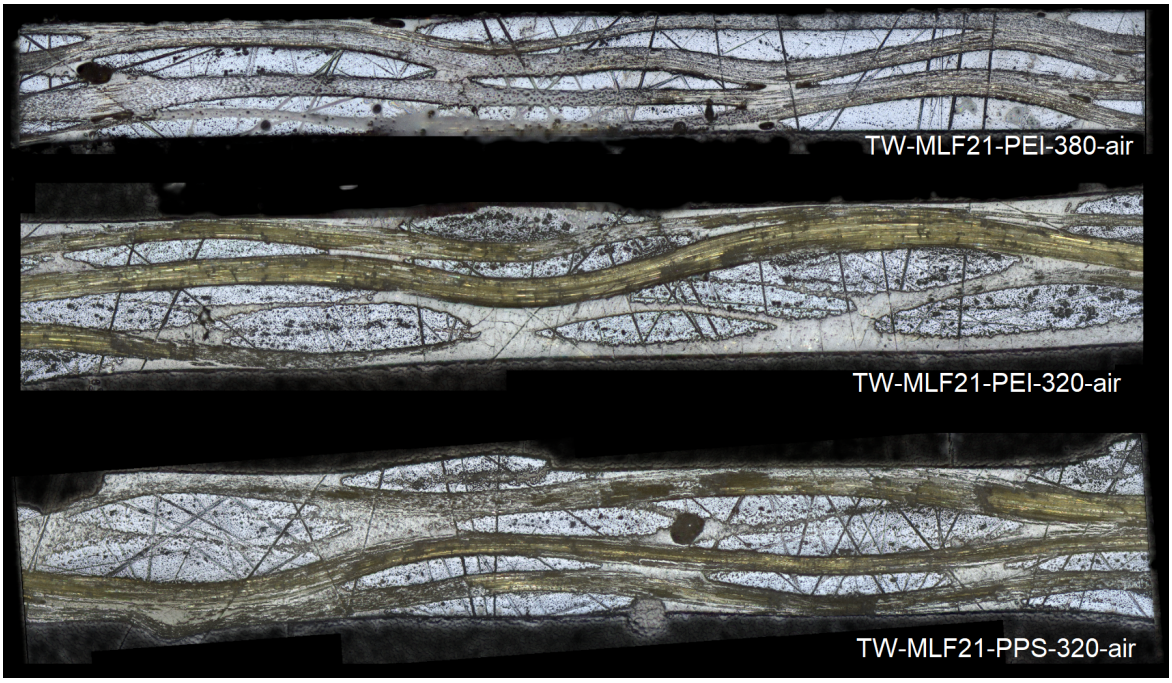

(b)

Figure 5.5: Microscopic images of selected composite samples

Somewhat similar observations are made for the PPS based laminates. Figure 5.6 shows a C-scan image of a section of TW-MLF21-PPS-320, which used the standard processing cycle. As with the PEI composite shown in Figure 5.2, the section stemming from the panel center appears well consolidated, whereas the right side has some attenuating regions, indicative of voids. The transition is not as sharp as in Figure 5.2, presumably due to the lower temperatures used for processing PPS, resulting in a smaller temperature gradient between centre and edges of the press.

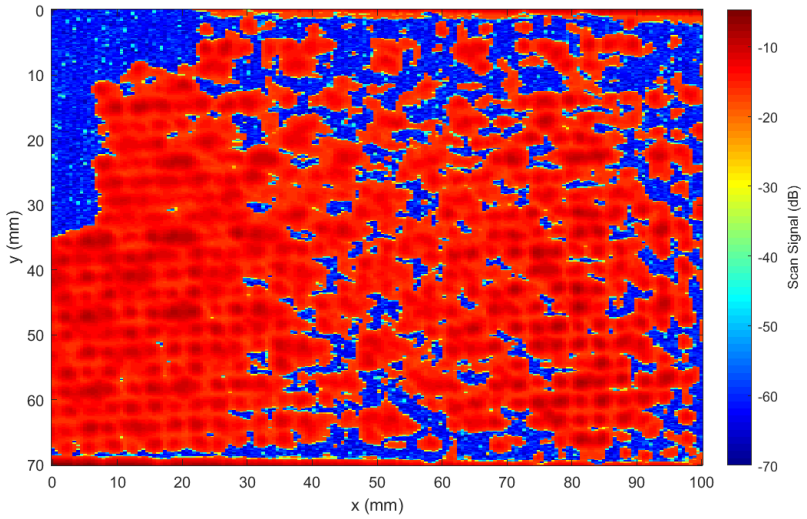

Figure 5.6: C-scan of TW-MLF21-PPS-320, using the standard processing cycle

TW-MLF21-PPS-300, where the dwell time was doubled to 40 min in order to counteract the reduced processing temperature, exhibits a fibre-volume fraction as anticipated, at 0.57. This is deemed promising but lower than the 0.6 V_f of TW-MLF21-PPS-320, which nonetheless exhibited imperfections. Between the two materials, TW-MLF21-PPS-300 indeed contains more matrix-rich zones and is thicker as seen in Figure F.1.

Lowering the processing temperatures below the recommended setting then always results in poor consolidation, even when increasing the dwell time. In fact, even the recommended temperature setting is insufficient in creating uniformly processed composites, with all panels exhibiting voids at the edges due to cooler temperatures in the press. The findings indicate that lowering the processing temperature is problematic, most likely requiring massive increments in time and pressure to counteract the higher melt viscosity. For uniformity, some insulation around the press should be implemented.

Due to the anticipated insulating effects of the Kapton vacuum bag, potential changes in consolidation between vacuum and air processed laminates were monitored. A C-scan image of TW-T741-PPS-320, which was produced using the standard processing conditions and under the Kapton vacuum bag, is shown in Figure 5.7. No voids are found in the specimen and it is concluded that use of the vacuum bag does not require the processing conditions to be changed.

The results indicate that even with the recommended processing conditions, achieving good consolidation with the thermoplastic laminates is difficult. Compared to the epoxy reference samples, most of the composites appear to have some deficiencies, manifested through voids in the C-scan, matrix rich zones seen under the microscope and reduced stiffness under tensile loading. Favorable results are achieved only with PPS composites produced at the standard settings. TW-T741-PPS-320 shows no voids under C-scan (Figure 5.7) and microscope (Figure 5.5(a)). Good wetting is achieved in TW-MLF21-PPS-320, as seen in Figure 5.5(a) and the laminate produces a tensile response close to that of TW-MLF21-Epoxy, as seen in Figure 5.4(b). Furthermore, these laminates were the only ones to produce the same, brittle fracture mode as seen in the epoxy based composites, which was assumed to be a result of the high degree of consolidation.

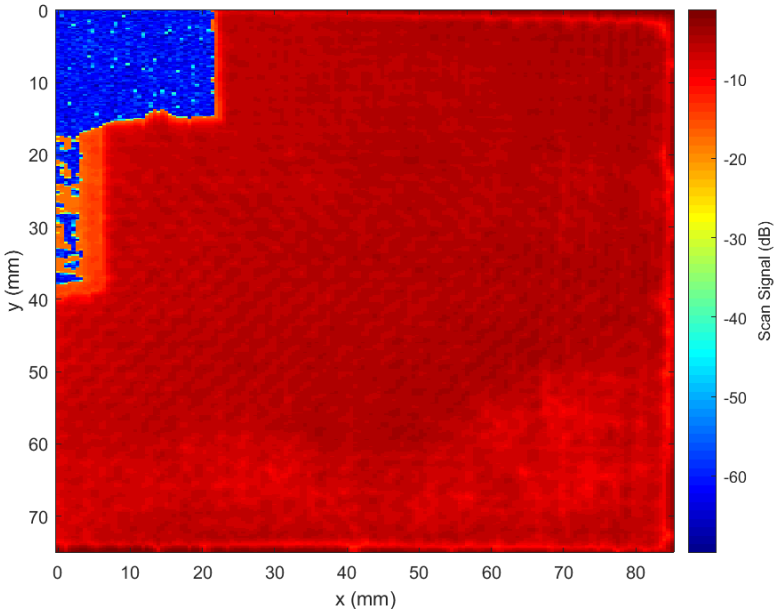

Figure 5.7: C-scan of TW-T741-PPS-320, using the standard processing cycle

Similarly, research by NLR [110] found notorious difficulties with the processing of aramid reinforced PEEK, where re-consolidation of Twaron-PEEK was required in order to eliminate voids. The prospects of achieving good results with a lowered processing temperature are then very small and would certainly require massive increments in dwell time and pressure.

Even with well-consolidated composites, there are indicators that interfacial adhesion between the aramid and thermoplastic matrix is worse than in epoxy laminates. Even in the well consolidated aramid-PPS composites, delaminations could be induced by bending by hand, while this was impossible with the epoxy matrix samples.

5.2 Strength retention

Degradation during processing is evaluated through measuring the strength retention of heat treated yarns and composites. Strength retention is defined as the tensile strength of exposed yarn with respect to untreated yarn or that of composites processed under high heat with respect to epoxy matrix composites of the same composition. Degradation is evaluated based on the processing parameters dwell time, pressure and temperature, as well as the heating environment.

Tensile test results from the oven and press treated yarn are listed in Appendix D. All oven treated fibres displayed some degree of discolouration, even when heat treated under vacuum. Tensile loading was characterised initially by alignment and later breakage of some outer filaments well before sudden failure of the entire yarn.

Comparison of yarn and composite behaviour is shown in Figure 5.11 and the strength retention for the variously processed composites is logged in Figure 5.10. Composite tensile loading was characterised by an onset of acoustic emmissions well before final fracture. The epoxy matrix composites fractures transversely to the tensile axis in a brittle manner, while most of the thermoplastic composites showed a diagonal, ductile break (see Appendix E. Only TW-PPS and TN-PPS using the standard processing cycle exhibited the brittle fracture mode.

5.2.1 Time

Time effects on strength retention in air and nitrogen atmosphere are shown in Figure 5.8. 15 min exposure shows relatively little difference between air and nitrogen, while 60 min treatment results in much faster decay in the aerated atmosphere. At higher temperatures, the exposure has a much bigger impact, with a much steeper decline in strength for the 60 min exposure. Clearly, time effects are highly co-dependent with environment and temperature.

On composite level, small improvements in strength retention are seen for decreases in exposure time. TW-MLF21-PPS-320-air, compared to TW-MLF21-PEI-320-air had a reduced dwell time from the standard 20 min setting to 10 min, resulting in 9.25 kN failure strength compared to 8.51 kN, a 9% improvement. Note that this is observed in composites processed under plain air. Figure 5.8 shows the impact of time on degradation to decrease when processing without air exposure, meaning the difference will likely be smaller in composites processed under vacuum. In TW-MLF21-PPS-300, the dwell time was increased to 40 min, while the temperature was reduced from 320 to 300°C. Compared to TW-MLF21-PPS-320, which used the standard setting, the strength increased from 10.4 to 12.1 kN, or by 16%.

As elaborated in section 2.3, Khondker et al. [2] described strength retention in terms of time with bi-linear behaviour, finding steep decline within the first 10 min of exposure and shallow decline afterwards. As observed by Teijin time dependent degradation behaviour is described by power law [111]. Both sources then agree that the effects of time are of less importance within the range of thermoplastic composite processing. With some time required to fully melt the polymer before dwell time initiation, exposure times during processing appear to be limited to no less than 25 min. Note that the duration of heat exposure is even longer when taking into account heating and cooling times.

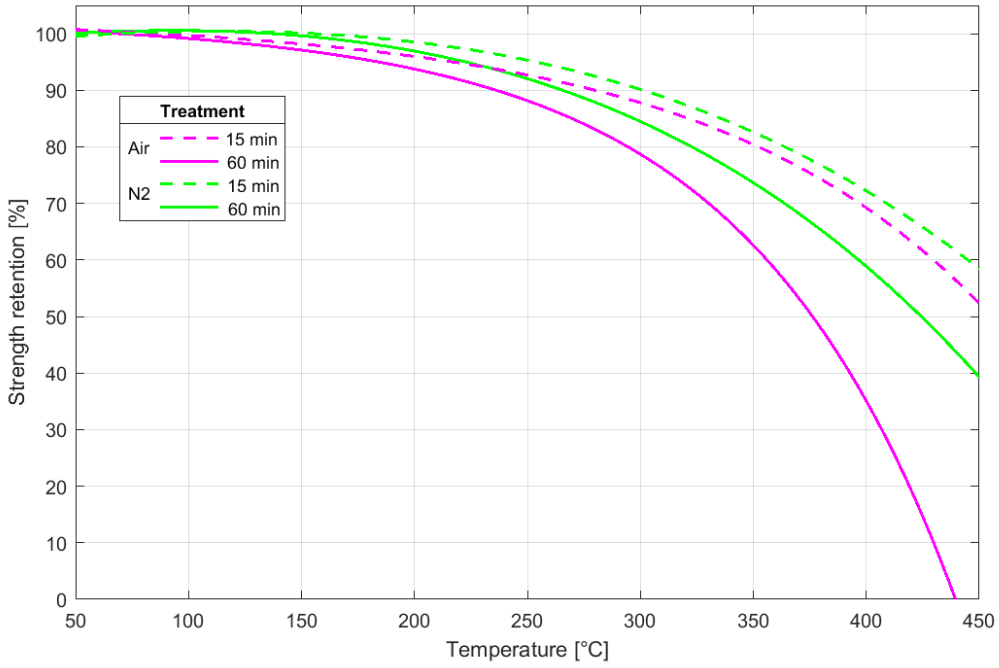

Figure 5.8: Strength retention in Twaron yarn for 15 and 60 min exposure times in air and N2[1]

Shortening the dwell time to less than 10 min is deemed unfeasible. Therefore, the potential for strength improvements is somewhat limited. Considering that time dependent degradation stagnates at prolonged exposure, it appears preferable to attempt decreasing the processing temperature, even

[1]The data for air and N2 was made available by Teijin and the data under vacuum was generated in a tensile test at the Teijin facility

when this necessitates a longer dwell time.

5.2.2 Pressure

Compared to the 10 bar processing pressure used as the standard setting for processing high-performance thermoplastics, ballistic composites are commonly processed at more than 100 bar [106]. It is then assumed that the processing pressure does not have a degrading effect on the fibres. Comparison between panels TW-MLF21-PEI-320-air (processed at 10 bar for 20 min) and TW-MLF21-PPS-320-air (processed at 20 bar for 10 min) supports this hypothesis. The composite processed at elevated pressure sustains 9.25 kN, versus 8.51 kN for the composite processed at standard pressure, amounting to a strength loss of 40 and 45%, respectively. As exposure duration is found to have some impact on the performance, the reduced dwell time is thought to be the reason behind the slight improvement in strength retention. In any case, the increased processing pressure does not appear to produce an adverse effect.

This makes the processing pressure an attractive parameter to maximise in order to reach good consolidation with reduced temperature or dwell time. Future research could focus on the effects of much higher pressures and to what extent this can counterbalance the other processing parameters.

5.2.3 Atmosphere

Figure 5.9 compares strength retention in Twaron and Technora for heating under air and nitrogen atmosphere, as well as under vacuum. Heating for both 15 min and 60 min shows a similar trend. Exposure in plain air causes the highest degree of strength loss, followed by the nitrogen atmosphere with vacuum producing the best results. While the differences between atmospheres are somewhat small when heat treating for 15 min duration, the benefits of oxygen deprivation become more apparent under 60 min exposure. This trend is readily observable in Figure 5.8, where the gains of the nitrogen over the air treated sample increase exponentially with temperature.

Similarly, the environment plays a large role on composite strength degradation. Figure 5.10 compares Twaron laminates pressed under plain air with vacuum-processed samples. Clearly, aeration reduces strength retention, with the effect being much more pronounced at higher temperatures.

The effect of the atmosphere could also be observed visually. The sample seen in Figure 6.1 (TW-MLF21-PEI-380-air) has distinctly browned compared to the natural yellow colour of aramid. A colour gradient is seen across the panel, with darker fibres in the center area of the panel, where the heat was presumably higher than at the edges. Similarly, fibres tested in plain air would become distinctly brown. Furthermore, the filaments were seen to let go of each other after the heat treatment. Heating under nitrogen atmosphere drastically reduces the discolouration but the fibres still appeared somewhat darker than untreated ones. Fibrillation also appeared to be reduced under the nitrogen atmosphere. Interestingly, the composites processed at 320°C (TW-MLF21-PEI-320-air, see Figure C.2) show a lesser degree of browning than the fibres exposed to 300°C in air. In Technora, browning was less readily observable due to the naturally brown colour of the material. The fibrillation effect however was seen to a similar degree as with Twaron.

The discolouration and sharp reduction in tensile strength under aerated atmosphere strongly hint towards oxidation as the degradation mechanism. Oxidation is a commonly known problem with aramid fibre [112], occurring under heat application or in the presence of uv-light. The observation of lesser discolouration on composite level could be a result of reduced oxygen flow inside the press, especially after wetting through the matrix. Nonetheless, these composites still exhibit dramatic strength loss compared to similar composites processed under vacuum, highlighting the absolute necessity for processing in the absence of oxygen.

Technora fibres were only evaluated under vacuum atmosphere, However, Curosu et el. [113] observed degradation in Technora under plain air from 200° onward, showing that it too suffers from

[2]The data for air and N2 was made available by Teijin and the data under vacuum was generated in a tensile test at the Teijin facility

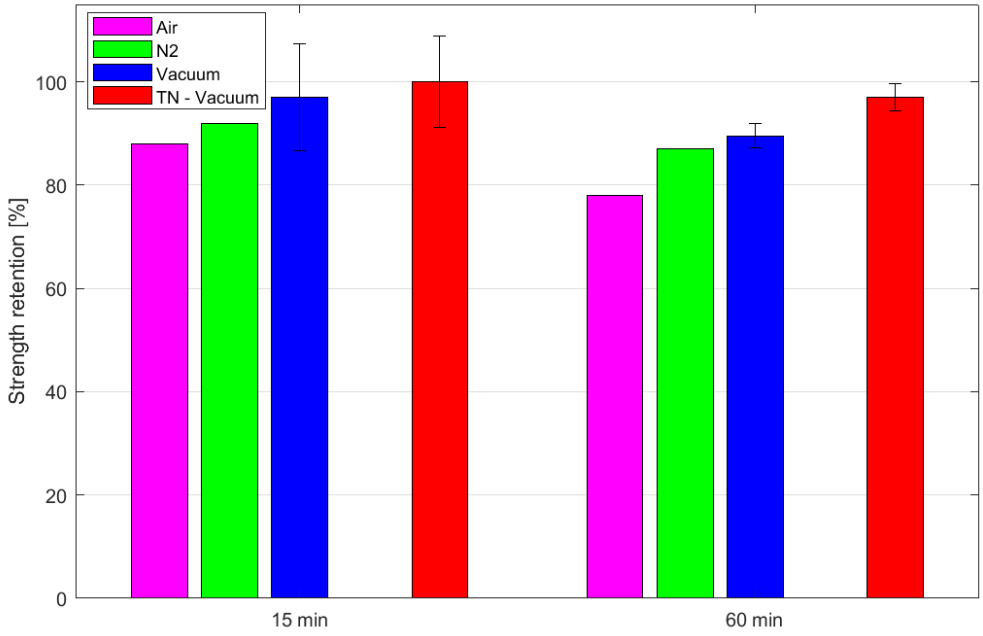

Figure 5.9: Strength retention in Twaron and Technora yarn under various environments[2]

oxidation. For this reason, it is decided not to attempt processing the TN-composites without vacuum bag.

5.2.4 Environment

Figure 5.11 compares heat induced strength loss on yarn and composite level. Remarkably, strength retention in yarn is different from that in composites by some margin, despite using the same atmospheres. The dotted lines represent the behaviour of Twaron and Technora yarn, while the individual data points show strength loss in terms of temperature for the various composites.

As the heating conditions and atmospheres are similar in the press and the oven, one would expect the same behaviour on yarn and laminate level. Comparison however shows that degradation in the composites is generally more severe than when conducting the same treatment on fibre level. Both the vacuum and air processed laminates see higher strength losses than their respective N2 and air heat-treated yarn counterparts denoted by the same colours. Note that this is despite the fibres having undergone somewhat longer heat treatments[3]. Only when pre-drying fibre and matrix material before pressing are similar levels of performance achieved, with the dried fabric composites coinciding well with the behaviour of the yarn heated under nitrogen. The differences between Technora yarn and composites are less apparent than those seen in Twaron. At 380°C, the laminate deteriorates more extensively, while at 320°C, thermal degradation overlaps well with that of the dry fibres, despite the stack not having been dried. Generally, the differences between yarn and composite are much smaller than with Twaron.

The phenomenon is not limited to composites treated in the press. Dry fibres taken from the exposed aramid breather sheet (see subsection 4.2.1) are also seen to experience a higher degree of degradation than oven treated fibres. While the data in Figure 5.11 indicates around 20% strength loss for yarn exposed to 320°C for 1h, only 35 min at the same temperature resulted in 30% strength loss in the press treated fibres. Interestingly, this value coincides very well with the 32% strength loss seen in the composites processed under theses conditions.

[3]Recall that the composites were commonly processed for 35 min, whereas the yarns were exposed for 60 min

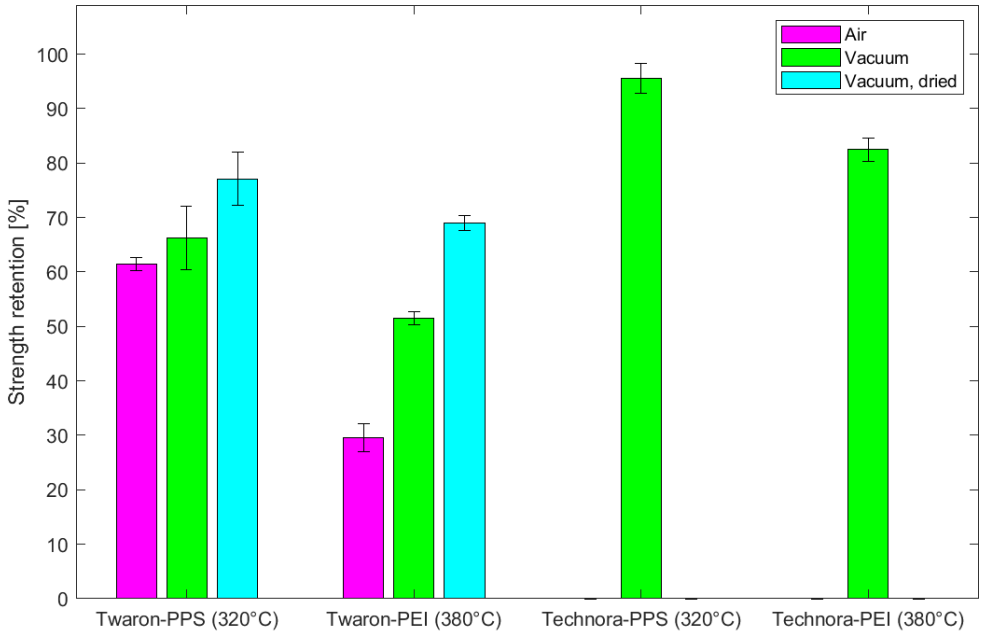

Figure 5.10: Strength retention in Twaron and Technora composites under various environments

In summary, heat exposure inside the press results in a higher degree of degradation than anticipated from the data on oven treated yarn. Drying the aramid appears to mitigate this issue. This suggests that the phenomenon is caused by hydrolysis, a common degradation mechanism of aramid. Exposure to moisture under elevated temperatures may cause drastic strength loss through shortening of the molecular chains [114], whilst not affecting the fibre stiffness. Heating causes the natural 5% by mass water content in the fibres to evaporate. While the vapour can leave the fibres inside an oven, this is prevented by the close packing inside the press, thereby aggravating the mechanism. As seen with oxidation, the mechanism becomes more prevalent at higher temperatures.

The observations on Technora indicate that the material is less affected by hydrolysis. Not only is the resulting strength loss much smaller, it also appears to occur at higher temperatures only, as evident by the composite processed at 320°C. Technora, which has more flexible molecular chains than Twaron, undergoes a higher heat treatment during the spin process. The reason for the reduced hydrolytic effects could be due to the lower natural water content of Technora of 2% compared to 5% in Twaron [114]. Nonetheless, hydrolysis remains to affect the materials and it is advisable to dry fibre and matrix material before processing [113].

Hydrolysis is also thought to be the reason behind the differences between vacuum and nitrogen atmosphere seen in Figure 5.9. Even though both environments are expected to mitigate oxidation, heating under vacuum appears to bring slight improvements in strength retention over nitrogen atmosphere. This is thought to be due to the osmotic potential created by the vacuum resulting in faster evaporation of the fibre's natural water content, reducing the effects of hydrolysis.

5.2.5 Temperature

Heat effects manifest themselves visually, when exposure occurs under plain air. The transparency of PEI shows the discolouration in the fibres between processing at 320 and 380°C (see upper row of Figure C.2). Browning is also seen to increase with temperature on the oven treated yarns.

[4]The trend-lines for Twaron yarn were generated from in-house data, while the behaviour for Technora yarn was estimated from measurements at 300 and 400°C and the exponential behaviour seen in Twaron

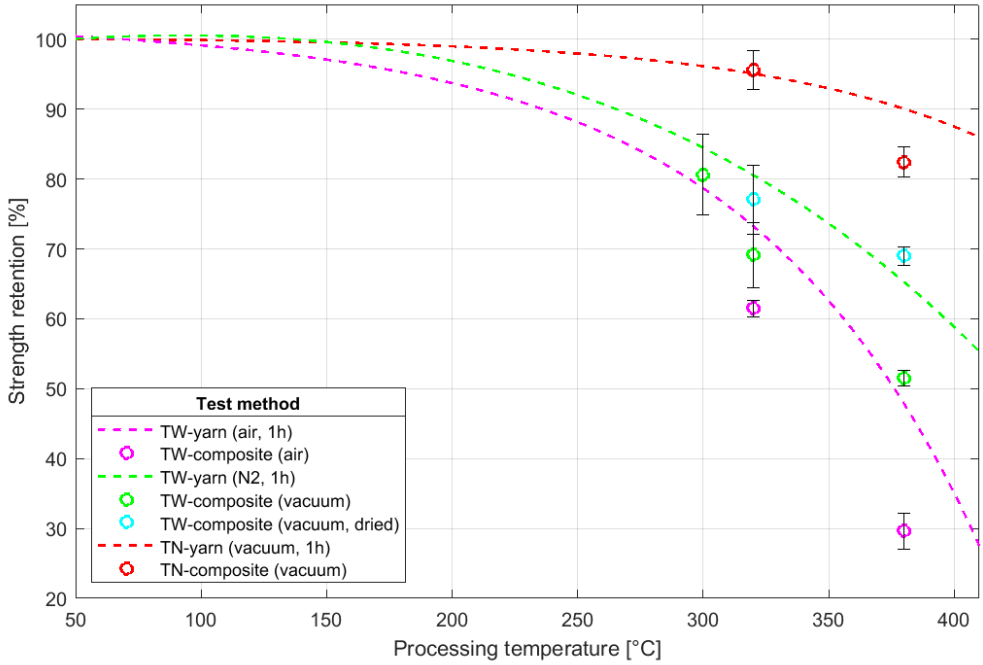

Figure 5.11: Comparison of strength retention in oven (yarn) and press (composite) environments [4]

Observation of the figures in the present chapter shows that all degradation mechanisms are ultimately temperature driven. In Figure 5.8, strength loss is seen to increase exponentially with temperature at both exposure times. Similarly, oxidative and hydrolytic degradation increases rapidly with higher heat exposure, as seen in Figure 5.11. In fact, thermal degradation follows exponential behaviour, irrespective of the fibre material and the countermeasures taken.

Between the two reinforcements, Technora fibre universally exhibits better heat tolerance than Twaron. Apart from hydrolysis, the fibre also suffers less from purely heat induced degradation. Both on yarn and composite level, it is shown to retain 95% of its original strength well into the processing range of high-performance thermoplastics. Figure 5.11 shows the estimated strength retention in Technora in terms of temperature, suggesting that processing at 380°C can be done at the cost of 10% strength loss. Twaron, even when mitigating hydrolysis and oxidation suffers much higher deterioration, where processing beyond 300°C will almost certainly cause more than 10% reduction in strength.

Chapter 6

Conclusion

The requirements for manufacturing AFRTP composites were researched. The goal of the investigation is to find the appropriate processing conditions to produce such a material with acceptable properties for semi-structural applications exposed to high-energy impact. The research reveals that the main challenge lies in solving the trade-off between consolidation quality and retention of the fibre's tensile strength. While lower processing temperatures reduce fibre degradation, the increased viscosity of the polymer melt results in poor impregnation and wetting of the fabric.

Thermoplastic composite specimens are manufactured through film stacking under application of heat and pressure for some dwell time. These parameters were varied to determine their optimal setting with regard to degradation and fabric impregnation. PEI and PPS were used as matrix materials while Twaron and Technora fabrics were provided by Teijin Aramid. Epoxy composites were produced as reference samples through vacuum infusion.

The consolidation quality is investigated using C-scanning, microscopy and thickness measurements. Impregnation is also assessed in tensile testing, through force displacement behaviour and the nature of the fracture area. Sufficient impregnation is deemed a requirement for structural application. The processing parameters are selected based on the findings on the consolidation quality. Visual inspection and tensile tests on both yarn and composite level are used to quantify the degree of fibre degradation. The strength of the dry yarn after heat exposure is taken as a quick means of determining the effects of temperature and exposure time on the fibre strength.

C-scanning indicates good consolidation quality with both PPS and PEI composites, however many panels contain some voids due to local temperature differences in the hot press. Retroactively, slightly higher processing temperatures than the 320°C used for PPS are advisable. Even with signs of good consolidation, many of the laminates show signs of very poor fibre-matrix interaction. The Epoxy composites appeared to outperform the thermoplastic composites in this aspect.

The consolidation pressure is found to have no effect on fibre degradation. Time dependency follows power law behaviour, where the strength decreases rapidly in the first few minutes of heat exposure and then stagnates. Therefore, the setting of the time and pressure is deemed of importance only to the consolidation quality. However, it remains questionable whether a decrease in temperature can be realised by increased time and pressure setting.

Oxidation and hydrolysis are identified as the two major degradation mechanisms affecting the tensile strength in Twaron and Technora. Both become more severe with increasing heat but can largely be counteracted by processing the composite under a Kapton vacuum bag, as well as by drying fabric and matrix material in an oven before hot pressing. Nonetheless, strength loss continues to occur after mitigating these processes and a purely thermal component is identified as a third degradation mechanism. Twaron is shown to be much more susceptible to hydrolysis and thermal degradation than Technora. Even under ideal circumstances, strength losses in excess of 10% are projected when processing Twaron reinforced high-performance thermoplastics, leading to

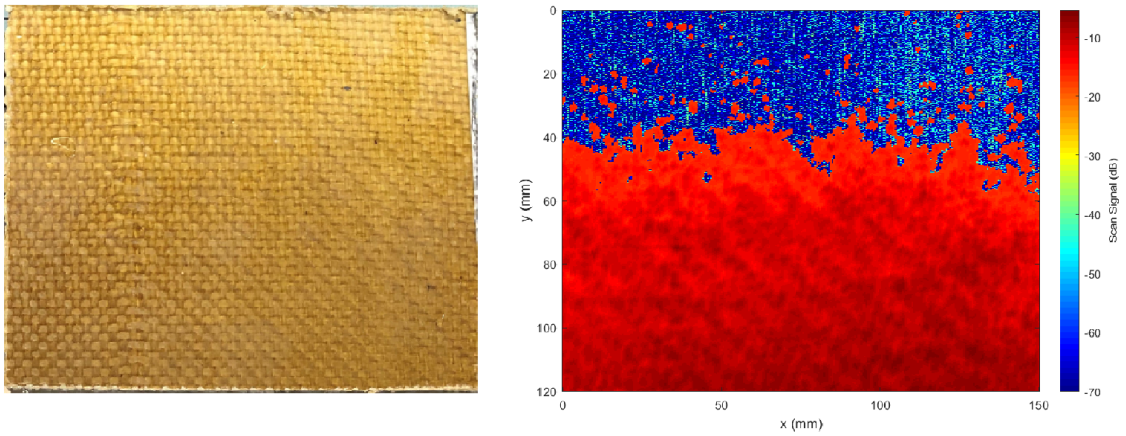

Figure 6.1: Optical and C-scan image of TW-MLF21-PEI-380-air

the conclusion that processing homoplymeric para-aramids beyond 250°C is unfeasible for composite use. Technora composites are shown to retains their tensile strength beyond processing temperatures of 320°C, even without drying. This makes the material a viable aramid reinforcement material for high-performance thermoplastics.

The trade-off between consolidation quality and fibre constitution is illustrated in Figure 6.1. While the C-scan indicates voids due to the cooler temperatures at the edge of the press, the fibres exhibit less browning due to reduced oxidation in this region.

Part II

Impact

Chapter 7

Experimental Approach

This chapter lists the specimens used for the impact characterisation and test equipment and elaborates the how impact data is interpreted. Impact tests were conducted to evaluate the effects of matrix material and fibre-matrix adhesion on the impact performance, as well as to give a general indication towards the performance of the newly developed composite class.

7.1 Specimens

The effect of the fibre matrix adhesion was investigated with TW-T741-PPS and TW-T736-PPS. The T741 and T736 fabrics were identical with the exception of the fibre sizing, where T741 uses a standard sizing while T736 incorporated adhesion activated yarn, whose epoxy sizing is known to increase the bond strength with epoxy and nylon matrices. Two composites were processed under the same conditions with the aim of creating two composites varying only in their fibre-matrix adhesion. Due to thermal degradation effects on Twaron, these panels were expected to perform poorly in impact. However, the test was aimed only at evaluating the interface effects on impact performance. Due to the novelty of AFRTP, it was unknown whether the adhesion activated yarn would bond well to the PPS matrix. The main concern was that the high processing temperature would cause the fabric to burn-off. Thermogravimetric analysis (TGA) was conducted on a yarn sample taken from the T736 fabric in order to find the decomposition temperature of the sizing.

Other impact used the Technora MLF21 fabric as this was expected to retain its strength and produce good impact performance, making comparisons with other materials possible. These composites compared the effects of the matrix material on impact behaviour. Crystalline and amorphous PPS were to be compared with naturally amorphous PEI. THe crystallinity of PPS was to be modified using the cooling rate in the press. TN-MLF21-PPS-c was aimed to have a highly crystalline matrix, therefore using a slow cooling rate of 1°C/min. TN-MLF21-PPS-a was cooled at 100°C/min, aiming for amorphous PPS structure. Lastly, a TN-MLF21-PEI composite was produced to compare the PEI and PPS matrices on otherwise identical composites. As the effects of the extreme processing conditions of PEI on Technora had not been evaluated at the time, tensile tests were carried out on this laminate to obtain an indicator.

The specimens used for the impact characterisation were produced with the processing cycles derived in Part I and the same matrix and reinforcements materials were carried over. Compared to the processing optimisation specimens, the panel thickness was increased to avoid slipping at the clamp of the impact set-up and at the same time be compliant with ILSS, in-plane-shear (IPS) or three-point-bending test standards. All panels retained the $[0°]_n$-layup configuration. Their thickness and V_f-properties are listed in Table 7.1.

The naming convention from Part I is carried over but the suffixes for temperature and processing atmosphere are omitted as these parameters were standardized for each of the specimens.

The slow- and fast-cooled TN-MLF21-PPS specimens are denoted by -c and -a, respectively, hinting at the targeted crystalline and amorphous matrix structures.

Table 7.1: Panel Specimens for impact characterisation

	Processing Conditions				Properties	
Specimen	T [°C]	p [bar]	t [min]	Cooling rate [°C/min]	thickness (std) [mm]	V_f target/ measured
TW-T741-PPS	320	10	25	50	2.11 (0.04)	0.58/ 0.67
TW-T736-PPS	320	10	25	50	2.42 (0.06)	0.58/ 0.59
TN-MLF21-PPS-c	320	10	25	**1**	2.20 (0.04)	0.6/ 0.59
TN-MLF21-PPS-a	320	10	25	**100**	2.16 (0.02)	0.6/ 0.6
TN-MLF21-PEI	380	10	20	50	2.07 (0.03)	0.59/ 0.62

7.2 Low-velocity test setup

Low-velocity impact was selected as the characterisation technique due to the ability to generate large amounts of data, describing the entire impact event. The setup can record reaction force and displacement data in terms of time. While the targeted regime falls under medium or high-velocity impact, these generally record the absorbed energy only, requiring more test specimens while returning less information. Furthermore, the medium velocity test setup in Delft is used for non-destructive testing and did not have the required sensor to record the post-perforation velocity at the time. High-velocity impact testing at the Arnhem facility was planned initially but could not be carried out as the setup was not operational. However, as observed in section 2.2, there is a general correlation between performance in the low- and high-velocity regimes, meaning the results are expected to be somewhat translatable.

Drop weight impact was carried out at TU Delft according to the ASTM D7136 methodology [115]. The drop tower setup is depicted Figure 7.1. It consisted of a rail mounted sledge, which could be raised to a specified height through a pulley system. The impacter was connected to the sledge via a steel guide rod, which also housed the load cell and a mount for added mass. A conical, round-nose tup was used, emulating blunt impact. Samples with dimensions 150x120 mm were secured on the support fixture with four toggle clamps, ideally resulting in clamped boundary conditions. All thin samples had a strong tendency to globally yield to the impacter, avoiding fibre damage. This failure mode was unwanted and counteracted by tightly securing the specimens in a clamp with a 80 mm wide, round cutout. Upon release, the sledge accelerated until reaching the spring loaded arresting system, thereby disengaging the impacter, which would drop onto the specimen. Shortly before impact, the velocity was recorded by an infrared sensor. After rebound, the impacter was caught by the metal brace, which also served as a safety switch.

The impact force was recorded through strain gauges in the impacter rod at a rate of 500 kHz, with the data converter returning the force at each sampling point. The obtained force data was characterised by a systematic offset error and continuous high-frequency background noise, which was filtered by the computer program. The raw impact data before and after processing is shown in Figure I.1. Displacement data is commonly obtained from high-speed camera imagery. This method however was deemed time intensive and inaccurate. It was decided to generate acceleration data from the measured forces and to integrate over time in order to obtain the velocity v and finally the displacement δ of the panel during contact with the impacter. This method appears to be relatively uncommon but was previously used by Jackson and Poe [116] and other authors.

With the drop tower only returning force over time, acceleration data was generated by dividing the force-time data by the measured mass m of the impacter device. The data was integrated using

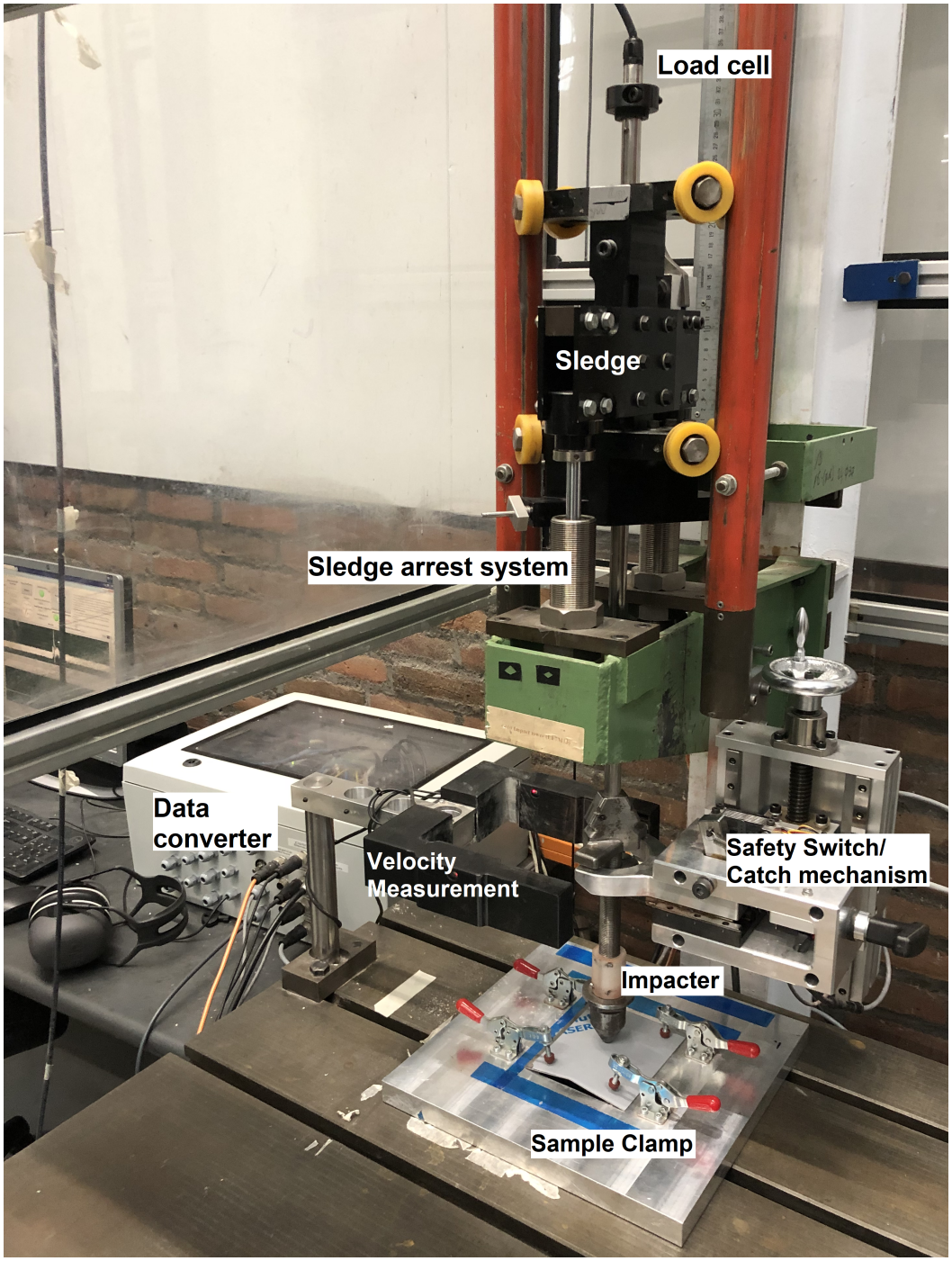

Figure 7.1: Impact tower setup

the trapezoidal method with

$$\begin{aligned} v\left(t_{n+1}\right) &= v\left(t_n\right) - \int_{t_n}^{t_{n+1}} a(t, v(t))\mathrm{d}t \\ &\approx \frac{1}{2} h\left(a\left(t_n, v\left(t_n\right)\right) + a\left(t_{n+1}, v\left(t_{n+1}\right)\right)\right) \end{aligned} \tag{7.1}$$

$$\begin{aligned} \delta\left(t_{n+1}\right) &= d\left(t_n\right) + \int_{t_n}^{t_{n+1}} d(t, v(t))\mathrm{d}t \\ &\approx \frac{1}{2} h\left(v\left(t_n, \delta\left(t_n\right)\right) + v\left(t_{n+1}, \delta\left(t_{n+1}\right)\right)\right) \end{aligned} \tag{7.2}$$

where the initial velocity v_0 was taken to be the incident velocity measured by the setup. The initial displacement was 0. The step size h was taken at $2 \cdot 10^{-6}$ s as governed by the 500 kHz data sampling rate. Gravitational acceleration was neglected due to being small compared to the impact forces. Having generated the correlated force-displacement data, the impact energy was calculated from integrating over the displacement, again using the trapezoidal method.

7.3 Impact Characteristics

Impact tests at 4 different energy levels were conducted on each of the 5 impact composites listed in Table 7.1. The two Twaron based panels were tested twice at the highest energy level in order to increase the validity of the measurement. Generated from a TN-MLF21-PEI specimen impacted at medium load, typical impact behaviour is presented in the time-domain in Figure 7.2(a). It suffered delamination damage but no fibre fracture. In order to better interpret energetic processes, force data was later evaluated in terms of displacement, as shown in Figure 7.2(b).

The reaction force is characterised by continuous oscillations, which are attributed to slippage at the boundary [34]. Four different stages in the impact response are distinguished. Initially, the force increases linearly at a steep slope. This region appears to be material dependent and does not change with the impact load. The energy dissipated linear elastically is denoted E_i, marking the energy required to initiate damage. Beyond this point, absorption is driven by damage propagation energy E_p [28]. After reaching a local peak, the force drops rapidly with some specimens exhibiting a larger drop at high impact loads. The next stage in the impact response marks a plateau in the force, with the material continuing to deform. The load will drop after the maximum displacement and energy E_{max} are reached with this point marking the absorption of all the incipient impact energy E_{tot}. As E_{max} remains constant after perforation, this value is taken to be the perforation limit of the material. Panels which do not suffer penetration see a decrease in displacement resulting in rebound of the impacter through elastically stored energy E_{el}. The absorbed energy E_a is dissipated through damage and other non-conservative effects such as boundary condition friction. The energy equilibrium is defined as follows:

$$E_{\mathrm{max}} = E_{\mathrm{el}} + E_{\mathrm{a}} \tag{7.3}$$

The algorithm was used to record the various energy components. The ductility index (DI) [34] was then computed as

$$\mathrm{DI} = \frac{E_{\mathrm{p}}}{E_{\mathrm{i}}} \tag{7.4}$$

The coefficient of restitution (COR) [32] was calculated as follows.

$$COR = \sqrt{\frac{E_{el}}{E_{tot}}} \tag{7.5}$$

The algorithm used to process the data is shown in Appendix H.

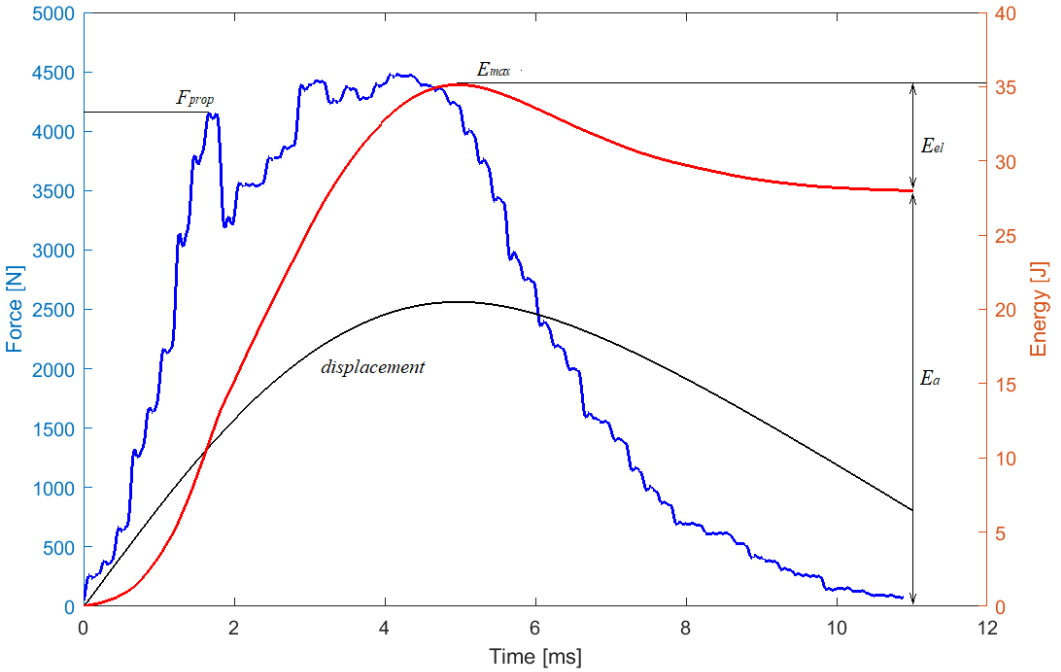

(a) Force, energy and displacement in the time domain

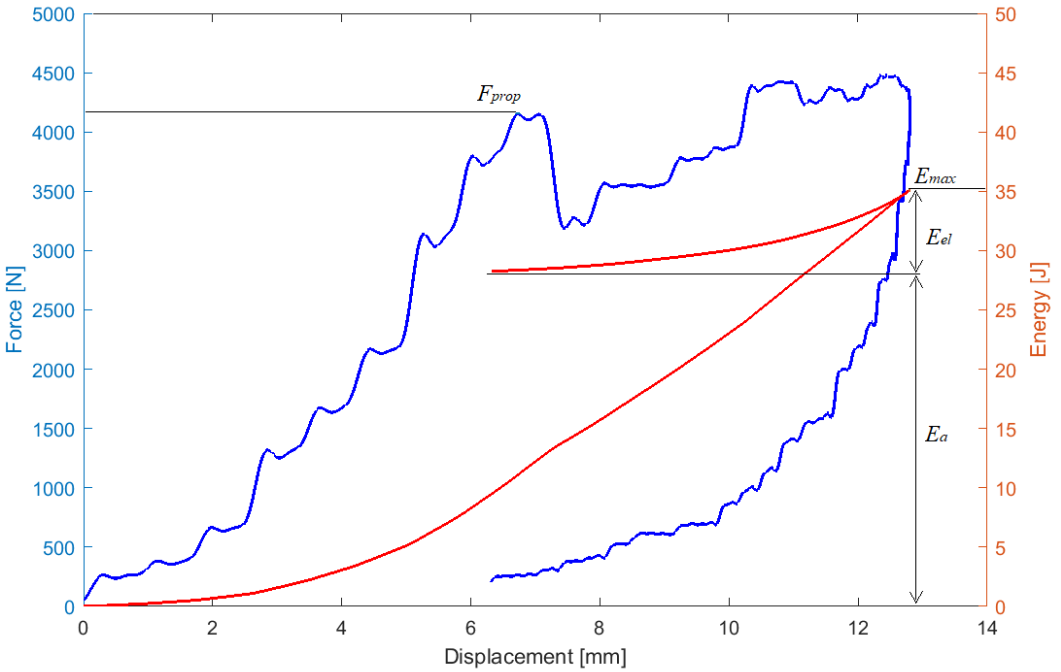

(b) Force and energy in the displacement domain

Figure 7.2: Composite material response during low-velocity impact event

Chapter 8

Results and Discussion

Impact tests were carried out to evaluate the effects of composite design parameter selection on impact performance. TW-T741-PPS (standard sizing) and TW-T736-PPS (epoxy sizing) were tested to evaluate the effect of changes in fibre matrix adhesion. These were also compared to the three Technora-MLF21 composites in order to show the influence of fibre degradation on the impact performance. Between the two PPS and the PEI based MLF21 laminates, the effects of matrix crystallinity and matrix material were compared. TN-MLF21-PEI appeared to have somewhat discoloured fibres, raising the concern that degradation may have occurred. Nonetheless, the panel appeared well consolidated with a somewhat higher-than-anticipated fibre volume fraction.

The force-displacement data of the Twaron based laminates and TN-MLF21-PEI is grouped in Figure 8.6 with the individual colours denoting the same impact energy level. The dashed red line denotes the second measurement conducted at the highest energy level in the Twaron composites. Load displacement data for the MLF21-PPS panels is shown in a similar fashion in Figure 8.7. The curves generally show good overlap, barring the abnormally high peak force in the dashed line in Figure 8.6(b). In each graph, the four energy dissipating regions are clearly distinguishable.

Some impact curves show steep, local peaks. The phenomenon is observed in the green line in Figure 8.6(a), where no apparent explanation could be found. The sudden break in the orange line of the same figure is attributed to the impacter and panel making contact with the support table, thus creating valid data only until that point. Markedly, contact with the table occurred at deformation of 20 mm, which coincided with the thickness of the support frame, thereby validating the method of generating displacement data. For later tests, the support frame was raised to avoid this issue. Figure 8.7(a) contains a peak in the high energy measurement denoted by the red line. This was caused by the sample being pulled from the clamps and locking itself up in the frame, causing a sudden increase in the stiffness response.

The impact specimens from each of the measurements are shown in Figure J.1. All of Twaron laminates show penetration from the lowest energy level onward, while the rightmost specimens have undergone perforation. The highest energy (rightmost) TN-MLF21-PEI specimen shows onsetting penetration, while neither of the TN-PPS specimens show any significant fibre damage. These specimens instead show global yielding and scratches from the edges of the clamping frame.

Ductility index and coefficient of restitution were calculated for each composite and at each of the energy levels. The parameters are shown in terms of absorbed energy E_a in Figure 8.4, with the marks denoting the individual data points. The DI is characterised by linear growth with E_a. This is apparent for materials loaded beyond the initial peak load, as the initiation energy remains constant, meaning the DI scales linearly with the propagation energy and therefore E_a. The linear relation was well reflected in the experiment but did not hold for the perforated samples.

8.1 Fibre type

Impact behaviour of the two fibre types used is compared in Figure 8.1. The Twaron laminates are matched to TN-MLF21-PEI as this was the only Technora based composite to exhibit comparable, valid impact behaviour. The figure shows the samples at high impact load, with the two TW-PPS composites being perforated and the TN-PEI composite undergoing penetration. Compared to the Twaron laminates, TN-PEI differs greatly in its response. As seen in Figure 8.5, the Technora composite has a higher impact stiffness and much higher peak load, which is clearly reflected in Figure 8.1. Similarly, energy absorption through damage progression is characterised by a much higher force plateau, but also a severe load drop after damage initiation. Unlike the perforated Twaron composites, the Technora sample shows some rebound.

Both of the Twaron based materials were penetrated at the lowest energy level and perforated at the highest. Both materials show only local failure phenomena, with penetration creating a pyramid shaped fracture area at the back surface (see Appendix J). The impacter produced fibre fracture in the two principal fibre directions with delaminations extending accross and beyond the entire damage area. The fracture surface in the penetrated TN-MLF21-PEI specimen differs from that in the Twaron composites in that it is more cone shaped and that the fibres appear to have fibrillated to a higher degree. Delaminations are much less apparent.

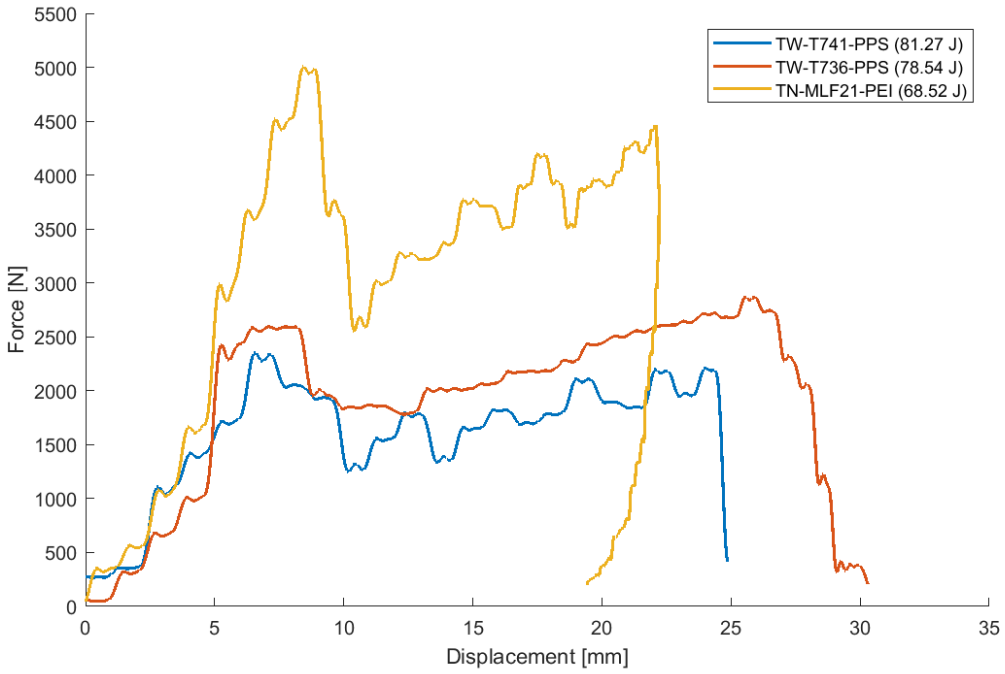

Figure 8.1: Impact response of TW-T741-PPS, TW-T736-PPS, and TN-MLF21-PEI at high load

While the higher impact stiffness is largely attributed to improved fibre matrix adhesion in the TN-PEI composite, the much higher peak load and and force plateau are clearly the results of the fibre condition. Due to its higher inherent fibre toughness, Technora is expected to exceed the energy absorption capacity of the Twaron 1000 yarn but the difference is far too small to explain the massively improved impact behaviour. Rather, the poor performance of the Twaron laminates shows the drastic effect of thermal degradation on the impact performance, massively reducing the tensile strength and therefore fibre toughness.

Recall that due to the processing conditions, the TW-PPS composites are projected to retain around 72% of their tensile strength while TN-PEI is rated at 82% strength retention. The difference in performance under impact is much larger, where the perforation energy of TW-T736-PPS is 58 J,

while TN-MLF21-PEI absorbed 68 J at penetration and stands to have a perforation limit of more than 100 J if the peak displacement is comparable to that of the Twaron composites. The highly detrimental effect of fibre degradation on impact is most likely the result of fibre embrittlement under thermal degradation. As seen in subsection 4.6.2, degradation reduces both tensile strength and strain, which results in an even larger reduction in toughness. This is reflected in the fracture behaviour of the impact composites, where the TW-PPS composites exhibited more localised damage modes comparable with GFRP, whereas TN-MLF21-PEI showed a round, global fracture area with the typical fibrillation seen in aramid fibres (see Appendix J).

Due to the high peak load, TN-MLF21-PEI absorbs large amounts of energy through linear elastic behaviour, hence producing a much lower DI than the Twaron composites at similar impact loads (see Figure 8.4(a)). The lower incline is explained by the much higher force plateau, where less damage propagation is required to absorb similar amounts of energy. As the impact tower was unable to produce the loads required to obtain perforation, the maximum index could not be obtained. It is however expected that perforation occurs at a lower DI than for the TW-PPS composites due to the large load drop (see Figure 8.1), which reduces the propagation energy in relation to the initiation energy.

Overall, the Technora composites produce lower ductility indices despite being much more energy absorbent than the Twaron laminates which reflects the observations of Ghaseminejhad and Parvizi-Majidi [77], who found the Ductility Index to be unrelated to the absolute impact performance of a material. However, global inspection of Figure 8.4(a) indicates similar behaviour between the Technora and Twaron composites, respectively. Contrary to this, changes in fibre-matrix adhesion and matrix material only create minor differences in the impact response. This shows that the fibre material is the principal parameter in governing the impact performance, while others may be selected secondarily in order to generate minor changes in material behaviour.

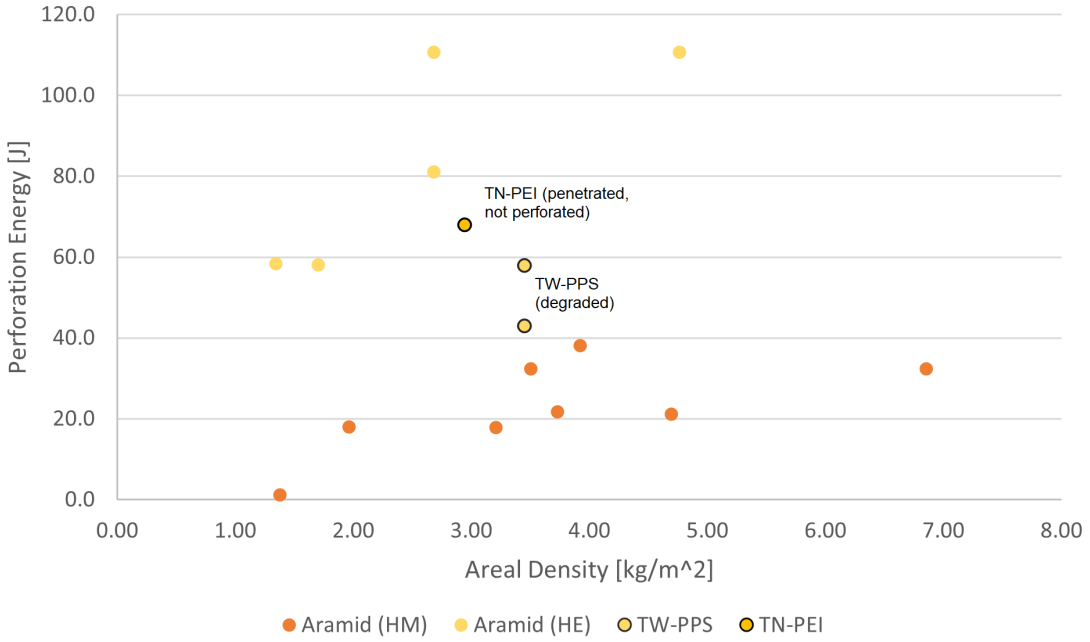

Figure 8.2: LVI-categorization of thermoplastic aramid laminates with respect to comparable aramid composites

Figure 8.2 rates the laminates of the present study by comparing with data obtained in the literature review. Both the TN-PEI and the TW-PPS laminates fall inbetween the ranges of high-modulus and high-elongation aramid, while Twaron 1000 and Technora both classify as high elongation fibres. The positioning of the TW-PPS composites indicates that the thermal degradation in Twaron yarn makes these materials unfeasible. Note that the TN-PEI laminate was no loaded to

perforation and is expected to exceed a failure energy of 100 J, placing it among the best performing materials despite undergoing some degradation. TN-PPS, which retains virtually all its strength is expected to perform even better but could not be tested under the present conditions. Nonetheless, their performance must be compared to that of Technora-Epoxy in order to evaluate whether added benefit is provided by using high-performance thermoplastic matrices.

8.2 Matrix Material

The properties of PEI vary greatly from these of PPS, where the properties of the latter can be modified by changing the crystallinity through the cooling rate. Their influence on impact performance is thought to be significant and was evaluated through comparing the three Technora MLF21 based composites.

All samples produced global damage from the lowest energy level onward, characterised by scratch marks from the frame and a delaminated strip running from the point of impact to the nearest edge of the panel as seen in Appendix J. This failure mode was attributed to cone formation creating an in-plane scissoring effect, where the material yields through interface failure before fibre damage can occur. Yielding is accompanied by significant slipping at the boundary conditions, creating a large amount of frictional work unrelated to the true material properties. Penetration was ultimately achieved at the maximum impact load with TN-MLF21-PEI. As seen in the image Figure J.1(c), this sample did not exhibit the typical delaminated strip seen in all other MLF21 composites. Generally, scissoring was less pronounced in the PEI sample, which exhibited localised fibre and matrix damage next to the global delaminated strip. These characteristics were not seen in the PPS based laminates, where neither of the two could be penetrated even after fully clamping the samples in a screw tightened frame. The effects of scissoring become increasingly visible at higher impact load, as seen in the highest energy curve of TN-MLF21-PPS-c. The sample was pulled out of the clamp and locked itself in the frame, resulting in the distinct load spike. Due to this unrealistic influence of the boundary condition, the validity of the test is largely limited to the linear elastic region, with the penetrated TN-MLF21-PEI sample being the exception.

Load displacement data for the TN-MLF21-PPS panels accross all 4 impact load levels is shown in Figure 8.7. The characteristics of all three Technora composites are compared for medium load impact in Figure 8.3. Clearly, behaviour in the TN-MLF21-PPS samples is very similar. The figure shows both identical maximum deflection and rebound, while the impact stiffness and peak load are found to be statistically indifferent, as previously established in Figure 8.5. Tn-MLF21-PEI behaves differently, showing both higher peak load, impact stiffness and force plateau. The higher toughness results in a higher fraction of energy absorbed in the early stages of the event, causing the notably lower peak displacement. Rebound is also more extensive in the PEI laminate, as would be expected from the higher E_{el} component. Figure 8.3 shows that the TN-PPS specimens have no distinguished load peak but a somewhat gradual decrease in impact stiffness before reaching the plateau region. Observe however that the TN-PEI sample in the same figure exhibits a sharper load drop despite undergoing the same fracture mode.

As the DI showed no difference between the MLF21-PPS materials, the coefficient of restitution was evaluated as an alternate viewpoint. Figure 8.4(b) shows the value in terms of E_a for the MLF21 laminates. In the propagation region, the COR follows power law behaviour [32], as reflected in the figure. The higher rebound deflection seen in TN-MLF21-PEI is evident accross the entire energy range and corroborates well with the low ductility index, attributing the material a high fraction of conservative energy dissipation. Between the MLF21-PPS laminates, no meaningful differences are observed.

With the two TN-MLF21-PPS composites showing virtually identical behaviour, no clear conclusions regarding the effect of heating rate on the interfacial and impact properties can be drawn. Differential scanning calorimetry was attempted to compare the crystallinity in the samples but provided no usable output. The actual degree of crystallinity then remains unknown.

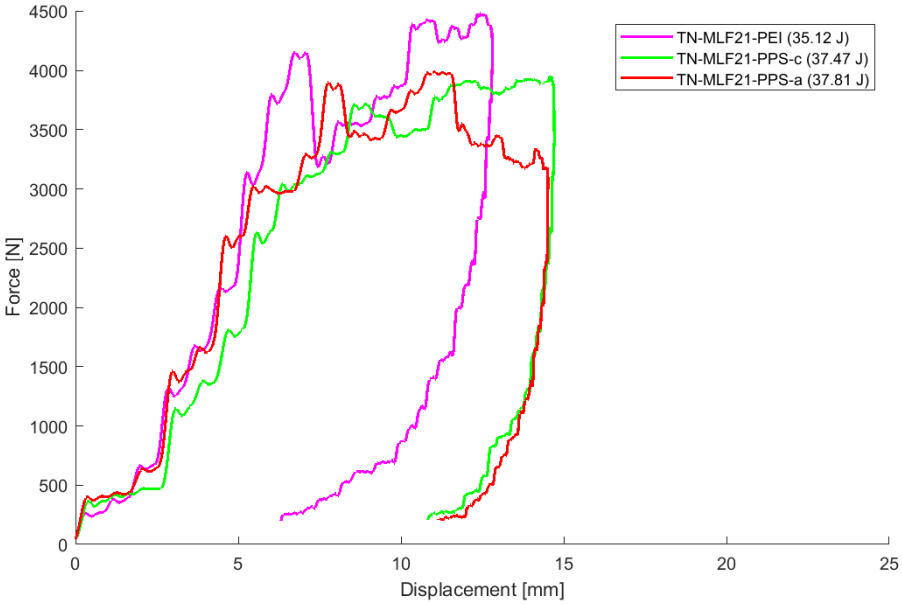

Figure 8.3: Comparison of impact behaviour in specimens impacted at similar energy level

The higher impact stiffness hints towards TN-PEI exhibiting better interfacial properties than the PPS based laminates. However, due to the absence of a clear peak load, the impact stiffness is not as much a reliable parameter. This is reflected in Figure 8.5, where the variance in the peak load is higher in the TN-PPS specimens. Other characteristics however support the notion of reduced fibre-matrix adhesion, notably the tendency towards localised fibre damage rather than scissoring. This tendency is reflected in the force-displacement behaviour, where the higher peak load in TN-PEI manifests its higher delamination threshold. The observed decrease in the impact stiffness at higher loads marks the onset of delamination and the sharper load drop seen in TN-PEI is thought to be due to the prevalence of fibre and matrix damage over scissoring. While the difference in interfacial properties could be clearly established, it remains unclear whether the poorer performance in TN-PPS is due to the inherent properties of the matrix or the slight presence of voids as observed in Table 7.1.

Due to the inconclusive impact results from the TN-MLF21-PPS specimens, it is impossible to make quantitative claims regarding their impact performance. However, their tendency to delaminate and overall ductile impact response strongly suggest ballistic composite-like behaviour and the potential for very high energy absorption, albeit at the cost of low out-of-plane properties. In section 8.1, TN-MLF21-PEI was shown to be a good performer despite undergoing some 20% strength reduction under processing. As the manufacturing cycle of PPS is shown to be much less detrimental to the Technora fibre's properties, it is thought that the true impact performance of TN-PPS is better than that of TN-PEI, despite the more brittle nature of PPS. In fact, several authors found only limited differences in the impact performance between various high-performance thermoplastics [76, 77, 78], whereas the fibre ductility was shown to be very influential in section 8.1. This indicates that the progressed degradation seen in TN-PEI outweighs the possible benefits in ductility. Focus should be put instead on improving the interfacial properties of TN-PPS, in order to maintain both high impact and out-of-plane properties.

In order to obtain valid results on the impact behaviour of TN-PPS, either higher fibre-matrix adhesion in the specimens or higher clamping forces in the fixture must be realised, where the latter method requires retesting of the other specimens due to the changed boundary conditions.

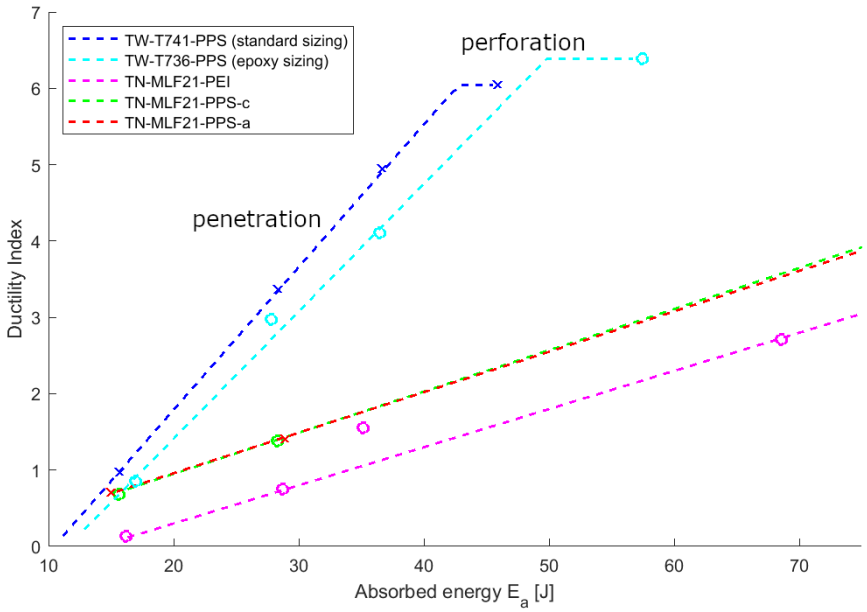

(a) Ductility index of impacted laminates in terms of absorbed energy. The data points correspond to the tests shown in Figure 8.6 and Figure 8.7

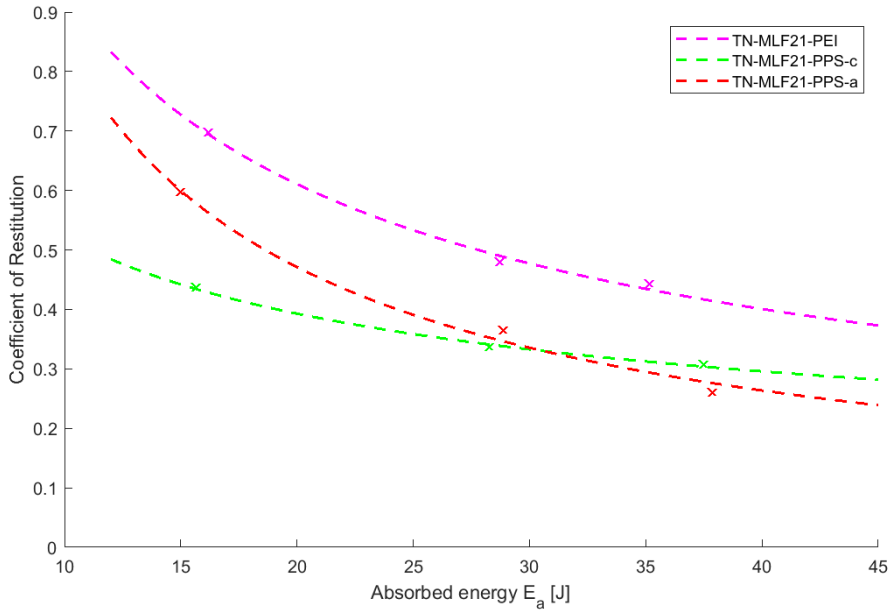

(b) Coefficient of restitution in terms of absorbed energy for TN-MLF21 laminates. The data points correspond to the tests shown in Figure 8.6 and Figure 8.7

Figure 8.4: Ductility index and Coefficient of restitution in terms of absorbed energy

8.3 Fibre-Matrix adhesion

Fibre-matrix adhesion was evaluated through the linear elastic region of the impact response, notably impact stiffness and peak load. The parameters are compared in Figure 8.5. The values were derived from the load displacement data shown in Figure 8.6 and Figure 8.7. The Twaron based composites were used to analyse the effect of adhesion on impact performance, while the interfacial adhesion of the Technora laminates was compared to see the effect of matrix material and crystallinity on the interface. Poor performance due to thermal degradation was expected in the Twaron composites but was accepted as the test only evaluated the influence of fibre matrix adhesion.

Thermogravimetric analysis (TGA) was conducted on the Twaron 1015 yarn used in the T736 composite in order to find the burn-off temperature of the epoxy sizing. The curve, shown in see Figure G.1, displays typical behaviour of aramid yarn in aerated atmosphere. The initial drop in mass is attributed to the natural water content in the yarn evaporating. Afterwards, the weight loss stagnates until rapidly increasing in the decomposition regime. The sizing makes out 0.75% of the fibre mass, meaning that burn-off should be noticeable in the data. No such weight drop is observed however and the TGA results are deemed inconclusive. It is unlikely that the decomposition temperature of the epoxy sizing is above that of the para-aramid.

The impact stiffness is closely linked to the static out-of plane properties [22], which in turn depend on the reinforcement stiffness and interfacial adhesion, among others [117]. As the reinforcements have comparable moduli, the impact stiffness is assumed to largely depend on the quality of the fibre-matrix interface. Between the two Twaron based laminates, TW-T736-PPS, using adhesion activated epoxy yarn, has a higher stiffness response. This strongly suggests that the sizing has some positive effect on the interfacial adhesion, despite being developed for use with thermoset matrix materials. Notably, the epoxy sized fibre composite had a lower fibre volume fraction than TW-T741-PPS (see Table 7.1), indicating that consolidation was poorer despite using the same consolidation cycle. It then appears that the improvements in adhesion outweighed the drawbacks of poorer consolidation, which are expected to lower the out-of-plane properties and therefore the impact stiffness.

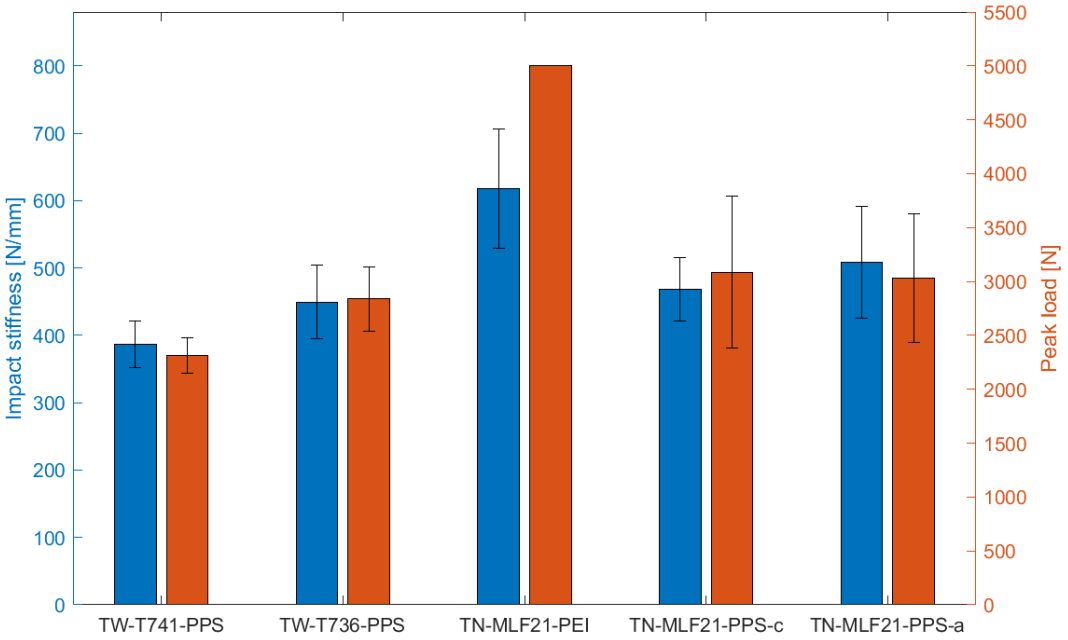

Figure 8.5: Impact stiffness and peak load of the low velocity impact tested composites

The difference in adhesion described in the Twaron laminates has a profound effect of the impact performance of the two otherwise identical composites. Their complete impact responses at perforation is compared in Figure 8.1. The higher peak load and impact stiffness of the adhesion activated composite, as observed in Figure 8.5, are clearly visible. Across all energy levels, TW-T741-PPS appears to produce a higher load drop after reaching peak force. The higher drop off results in a lower force plateau in the damage propagation region, as seen in Figure 8.1. The higher force plateau seen in the adhesion activated composite indicates higher fracture energy in crack propagation. Park and Seo [34] found an increase in K_{IC} fracture toughness with improved adhesion, which provides a likely explanation. As penetration in both samples was characterised by longitudinal and transverse crack growth, higher K_{IC} would result in more energy absorbed for the same crack length. Finally, the displacement at perforation is almost 20% higher in TW-T736-PPS, at 29 mm vs ca. 25 mm in TW-T741-PPS. This phenomenon is surprising when considering the higher impact stiffness of the material.

At similar energy levels, TW-T741-PPS continuously produces larger maximum deflections as reflected by the blue lines in Figure 8.6(a) and (b). This characteristic mirrors the more advanced damage propagation due to the lower peak load and force plateau. Consequently, compared to TW-T736-PPS, more energy is absorbed through damage propagation rather than in the initiation region. This results in a higher ductility index (ratio between initiation and propagation energy) for TW-T741-PPS at similar energy levels, as seen in Figure 8.4(a). However, the higher perforation displacement in the adhesion activated T736 composite results in a larger DI at perforation.

Overall, TW-T736-PPS is able to absorb much more energy than TW-T741-PPS due to higher impact stiffness, damage threshold, K_{IC} fracture toughness and maximum deflection. In fact, the improved interface results in higher energy absorption in every dissipating regime. The mean perforation energy of the two specimens was 58 J compared to 43 J in the composite with standard sizing, a 35% difference. This behaviour is contradictory to the findings of other studies, which universally observed reduced energy absorption in aramid composites with improved fibre-matrix adhesion [34, 81, 82, 83]. Kim and Mai argue that interface changes affect the dominant fracture mechanisms, where weaker fibre-matrix bonds favour the tough mechanism of pull-out [41]. The fracture surfaces of the Twaron composites however looked remarkably similar, suggesting that no such shift had occurred. Furthermore, the authors of these studies all modified the interface using either chemical or physical grafting methods. These effectively roughen the fibre surface but create some amount of damage in the process. It is likely that the reduction in impact performance is then caused by the reduced fibre strength rather than the improved bonding, which in the present study was found to positively affect energy absorption. This is supported by studies in which adhesion was modified through grafting of the matrix material rather than the fibres. Bandaru et al. used this method and also reported positive correlation between adhesion and impact performance [73, 74]. They found that stronger aramid-matrix interface increased the damage threshold, resulting in a higher fraction of the energy being absorbed in the initiation region. This is very well reflected by the experiment, where the fraction of energy dissipated in the initiation regime is consistently higher in TW-T736-PPS. Nonetheless, this hypothesis requires further validation, as small variations in processing conditions were also seen to affect the fibre strength.

In conclusion, improving the interface between aramid and thermoplastic matrix increases the energy absorption capacity. A higher degree of adhesion then appears beneficial to both the static as well as the impact performance of the laminate. However, due further experiments are required to confirm the universal applicability of this finding. Notably the applicability to non-degraded Technora yarn should be observed, as the Technora composites exhibited different impact response to the Twaron based ones.

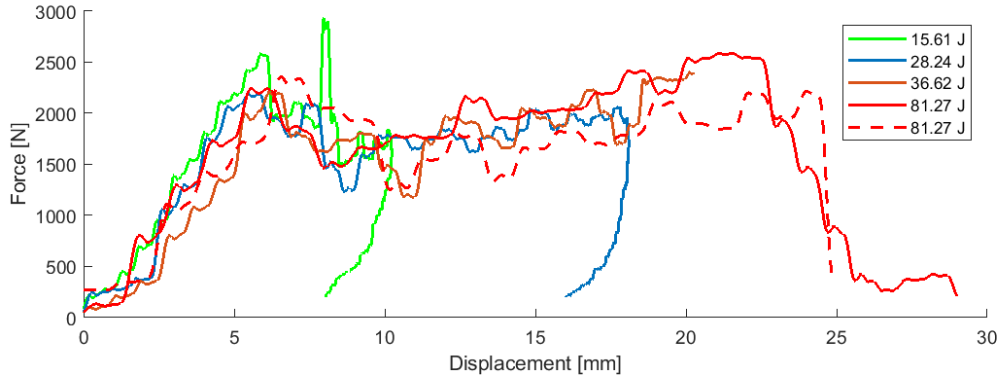

(a) TW-T741-PPS (standard sizing)

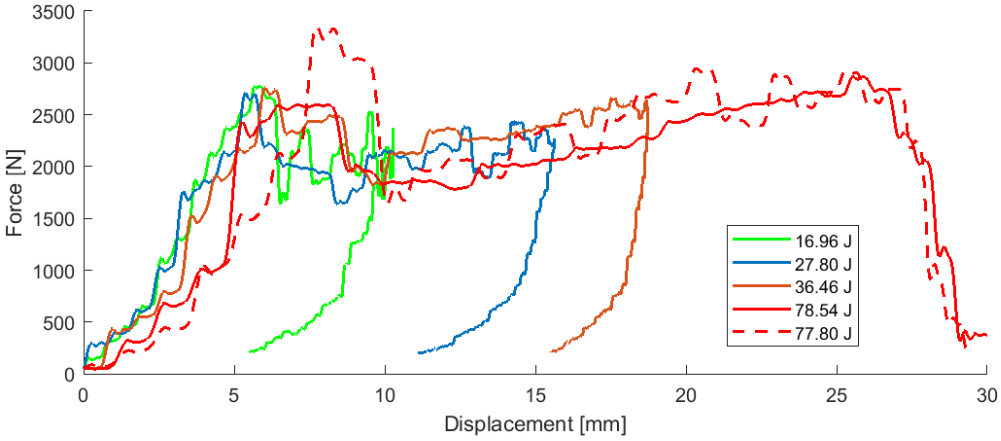

(b) TW-T736-PPS (epoxy sizing)

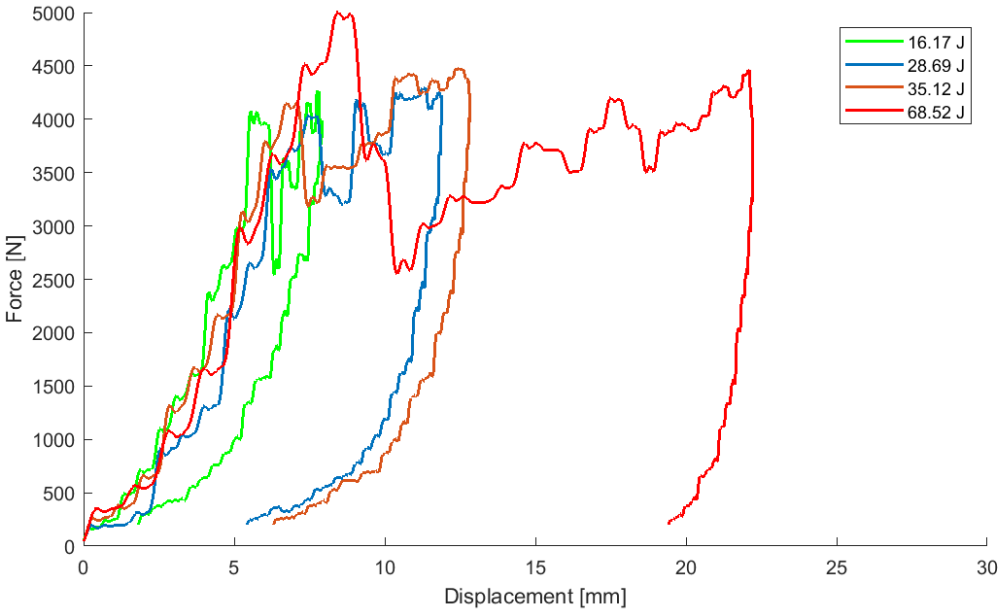

(c) TN-MLF21-PEI

Figure 8.6: LVI force-displacement behaviour over various energy levels

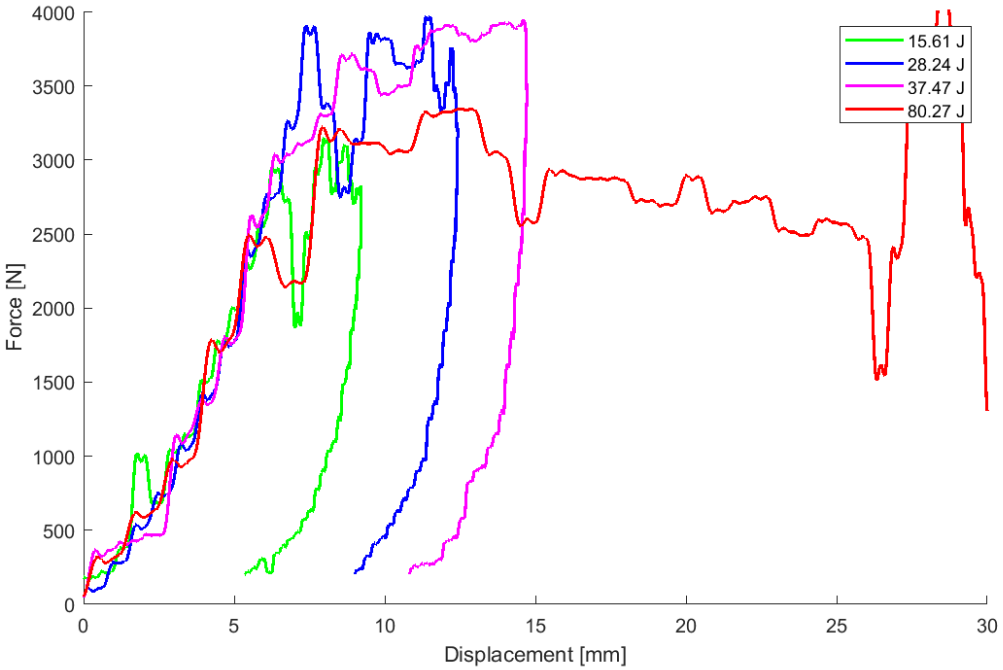

(a) TN-MLF21-PPS-c (slow cooling rate)

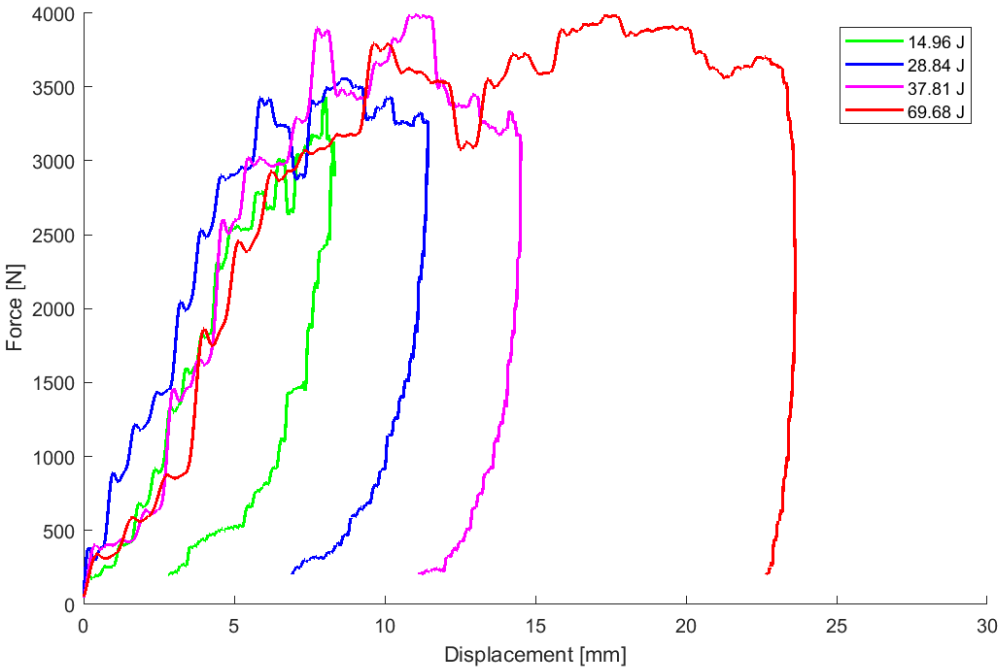

(b) TW-T736-PPS-a (fast cooling rate)

Figure 8.7: LVI force-displacement behaviour over various energy levels

Chapter 9

Conclusion

The impact performance of the newly developed materials was tested in a drop-weight tower. In view of fibre-matrix adhesion and matrix material, impact behaviour was analysed through force-displacement behaviour, ductility index and coefficient of restitution. An algorithm was used to determine impacter displacement based on fore-time data. Finally, it was attempted to classify material performance with respect to other, conventional composites as its impact strength is expected to eventually determine the usefullness of AFRTP.

Standard sizing Twaron T741 and adhesion activated T736 fabric compared the effects of the fibre matrix interface on imapact performance. Epoxy sizing used in conventional aramid composites was shown to work well with the application, greatly improving interfacial adhesion with the polymer. Technora reinforced PEI and PPS were used to evaluate matrix contribution to impact behaviour. Through changing the cooling rate, the crystallinity of the PPS matrix was varied in Technora PPS composites. Technora PEI, processed at a higher temperature, was used as a comparative means, with PEI being a more ductile, amorphous polymer.

As expected, Twaron laminates performed poorly due to fibre degradation under processing. The lower strength caused brittle, localised impact response. However, improved interface was shown to increase the perforation energy through higher impact stiffness, crack propagation fracture energy and maximum displacement. It is concluded that in poorly adhering aramid composites, gains in interfacial adhesion are beneficial to the impact strength due to higher fracture toughness in penetration. These findings are contradictory to the general rule of thumb, which suggests that there is a trade-off between interfacial adhesion and impact performance. While further experimentation is required to improve the general validity of this hypothesis, attempts should then be made at further improving the interfacial adhesion of AFRTP and the carry-over of these findings to Technora reinforced composites.

The different processing conditions of PPS and PEI made direct comparison of the two materials ambitious from the beginning. Differences in fibre-matrix adhesion and thermal degradation created secondary property differences unrelated to the matrix material itself. The impact data of the Technora-PPS composites was largely inconclusive due to low out-of-plane properties resulting in boundary condition effects rather than fibre damage. No clear differences could be established between the two and it was suspected that the degree of consolidation was insufficient. Penetration but not perforation was achieved in Technora-PEI, which had higher impact stiffness than the PPS based laminates. The perforation limit of the material was projected to be in excess of 100 J, placing it among the best performing composites of its areal density, despite having undergone some 20% strength loss during processing. Degradation in the Technora-PPS composites was expected to be much less severe, but the material's impact behaviour could not be characterised due to extensive delamination failure preventing penetration or perforation. Notably, this behaviour is similar to that of ballistic laminates, which in combination with aramid reinforcements are able to absorb very high amounts of energy. Most likely, the impact performance of Technora-PPS will be higher than that of

TN-PEI and the material is likely placed among the best performing structural composites. Improvements in the interface are however required in order to obtain acceptable out-of plane properties.

Chapter 10

Further Research

The research component focusing on the manufacturing of AFRTP composites gives a relatively complete image of the degradation mechanisms limiting the processing of aramid at high temperatures. The data provides guidelines on the expected strength loss for further research on these materials. Due to limited literature findings on the processing of these composites, the high degree of strength loss was somewhat unexpected and, out of necessity, shifted the main focus of the project from impact analysis to the understanding and mitigating degradation. The energy absorption potential of the material then remains somewhat unclear, largely due to the limited number of tests conducted.

It is desirable to reduce strength loss in Twaron and Technora reinforced thermoplastics during processing by as much as possible, as this will result in improved impact properties. While guidelines of degradation mitigation have been given for conventional processing methods, other, more innovative approaches could reduce heat exposure more extensively. Dissolving the matrix material before consolidation could eliminate the need to melt the polymer, potentially allowing for much shorter processing times and lower temperatures.

The feasibility of AFRTP largely depending on advantages in the specific impact performance over other composite materials. Further research is then required in the impact characterisation, notably in comparison with aramid composites using cheaper and easier-to-process matrices such as epoxy. A wide range of data is available on the performance of Twaron- or Kevlar-Epoxy but Technora has only sparsely been investigated as a composite reinforcement and the impact behaviour of Technora-Epoxy is virtually unknown. Categorising the impact performance requires a relatively large data set due to the multitude of composite design parameters. It is also expected that the impact performance of AFRTP may yet be improved drastically by optimising the fabric and layup for energy absorption. These parameters were not actively considered in the present study.

Characterisation of the out-of plane properties of AFRTP was not a main focus point and requires further attention. With many laminates showing signs of poor adhesion and bending properties, improving the interface should be a main focus point in future research. Structural performance is a main driver behind selecting high-performance thermoplastic resins, as pure impact composites do not require expensive matrices. Large improvements in fibre-matrix interaction were achieved with the epoxy sizing Twaron 1015 yarn and similar results are expected if appropriate sizings are used on Technora. The hypothesis of improved interface resulting in higher energy absorption should likewise be tested on the more ductile Technora composites.

Finally, as a novel material, the properties of AFRTP unrelated to impact have yet to be explored, especially under the aspect of intended use in aerospace applications.

Acknowledgements

At Teijin Aramid, I was given great freedom and responsibility during both my internship and the thesis project. Many colleagues showed great interest in my research, offering advice and help. Overall, I greatly enjoyed the working environment. Dr. Walter Nijhuis accompanied me over the entire period and remained closely involved with the project. I greatly respect his creative inputs and broad interest in research beyond his field of expertise. Dr. Ileana de Kleuver immediately became very involved in providing feedback and organisational assistance on the project. It was particularly through her that I felt valued at Teijin. Her and Dr. Jasper Biemolt's arrival brought with it a much welcome youthful atmosphere to the work floor. Ruud Berkel introduced me to the other, practical side of composite reserach. He remained involved through his help in the laboratory and with the logistics. Dr. Edwin Dommershuijzen, with years of experience on aramid fibre as a composite reinforcement, asked challenging questions and motivated me to view my own work critically. During the project, I learnt not to underestimate the complexity of supply chains and would have had trouble obtaining the right reinforcement materials without the regular efforts of Rüdiger Hartert. Lastly, I would like to thank Dirk-Jan Demkes and Dr. Sarah Saidi for their help in the laboratory.

Most students agree that the lab technicians in the Vliegtuighal are the the hardest working people in the faculty and my thesis work has certainly contributed to their workload. Thank you for the efforts Alexander, Dave, Victor and Durga. A special mention goes out to Ed Roessen, who took the time to optimise the process of milling aramid fibre composites, a particularly thankless task. Of course I am also grateful for the theoretical support to my Thesis, mostly provided by Dr. Julie Teuwen, who showed a lot of patience regarding my dislike for writing extensive reports. Dr. Kunal Masania and Dr. Rene Alderliesten, thank you in advance for chairing the committee.

With all lectures being held online, I only got to know most of my fellow students after starting my thesis. Thanks Jonas, Linde, Altay and Onur for making graduating a more sociable experience than could be expected. Thank you Clemens and Kunal for the many initiatives within the faculty group, notably taking your students on a trip to Paris. Hard work with the project group, including several late Tuesday evenings resulted in the strongest sandwich panel of 2022. Thanks for your great contributions, Ahaan, Marco and Kiva. Culinary and cleaning support during the more stressful periods of my thesis was largely provided by Jip and Roos, the best housemates I have had during my time in Delft. When I was on holiday, Justin and Tjeu selflessly looked after the house. Willem and Leon, thanks for having been there for the entire six years and Erik for joining somewhere along the way.

Finally, there is only my family left to thank for, who are of course in the end the people who got me here, most of all Mama, Papa and Jellie. Thanks for being around.

Bibliography

[1] R. Young and P. Lovell, *Introduction to Polymers: Third Edition*. United States: CRC Press, 3 ed., June 2011.

[2] O. Khondker, T. Fukui, M. Inoda, A. Nakai, and H. Hamada, "Fabrication and mechanical properties of aramid/nylon plain knitted composites," *Composites Part A: Applied Science and Manufacturing*, vol. 35, no. 10, pp. 1195–1205, 2004.

[3] V. Mahesh, S. Joladarashi, and S. M. Kulkarni, "A comprehensive review on material selection for polymer matrix composites subjected to impact load," *Defence Technology*, vol. 17, no. 1, pp. 257–277, 2021.

[4] P. Priyanka, A. Dixit, and H. S. Mali, "High strength kevlar fiber reinforced advanced textile composites," *Iranian Polymer Journal*, vol. 28, no. 7, pp. 621–638, 2019.

[5] J. Pepin, "Fiber-reinforced structures for turbine engine rotor fragment containment.," tech. rep., 1999.

[6] R. Gondaliya, D. Sypeck, and Z. Feng, "Improving damage tolerance of composite sandwich structure subjected to low velocity impact loading: Experimental analysis," 09 2016.

[7] W. Cantwell and J. Morton, "The impact resistance of composite materials — a review," *Composites*, vol. 22, no. 5, pp. 347–362, 1991.

[8] L. MatWeb, "Material property data," *MatWeb,[Online]. Available: http://www. matweb. com*, 2022.

[9] M. Cheng, W. Chen, and T. Weerasooriya, "Mechanical properties of kevlar® km2 single fiber," *J. Eng. Mater. Technol.*, vol. 127, no. 2, pp. 197–203, 2005.

[10] F. DuPont, "Kevlar aramid fiber technical guide," 2017.

[11] T. Aramid, "Twisted vs. resin impregnated/ untwisted proerpties of Twaron high modulus yarn," 2006. Unpublished confidantial document.

[12] B. Zhang, L. Jia, M. Tian, N. Ning, L. Zhang, and W. Wang, "Surface and interface modification of aramid fiber and its reinforcement for polymer composites: A review," *European Polymer Journal*, vol. 147, p. 110352, 2021.

[13] G. Faur-Csukat, "A study on the ballistic performance of composites," in *Macromolecular symposia*, vol. 239, pp. 217–226, Wiley Online Library, 2006.

[14] A. Searl, "Clearance of respirable para-aramid from rat lungs: Possible role of enzymatic degradation of para-aramid fibrils," *The Annals of Occupational Hygiene*, vol. 41, pp. 148–153, 1997. Proceedings of an International Symposium on Inhaled Particles.

[15] C. Chandrasekaran, "Testing of Rubber Lining," in *Anticorrosive Rubber Lining*, Plastics Design Library, pp. 165–172, William Andrew Publishing, 2017.

[16] M. Moure, I. Rubio, J. Aranda-Ruiz, J. Loya, and M. Rodriguez-Millan, "Analysis of impact energy absorption by lightweight aramid structures," *Composite Structures*, vol. 203, pp. 917–926, 2018.

[17] U. K. Vaidya, "Impact response of laminated and sandwich composites," in *Impact engineering of composite structures*, pp. 97–191, Springer, 2011.

[18] C. de Vos, "Design of an impact resistant composite material for application in future aircraft," 2021.

[19] T. J. Kang and C. Kim, "Energy-absorption mechanisms in kevlar multiaxial warp-knit fabric composites under impact loading," *Composites Science and Technology*, vol. 60, no. 5, pp. 773–784, 2000.

[20] J. J. Andrew, S. M. Srinivasan, A. Arockiarajan, and H. N. Dhakal, "Parameters influencing the impact response of fiber-reinforced polymer matrix composite materials: A critical review," *Composite Structures*, vol. 224, p. 111007, 2019.

[21] S. Abrate, *Impact engineering of composite structures*, vol. 526. Springer Science & Business Media, 2011.

[22] R. Olsson, "Mass criterion for wave controlled impact response of composite plates," *Composites Part A: Applied Science and Manufacturing*, vol. 31, no. 8, pp. 879–887, 2000.

[23] C. Kassapoglou, *Modeling the effect of damage in composite structures: Simplified approaches*. John Wiley & Sons, 2015.

[24] S. R. Reid and H. M. Wen, "Perforation of frp laminates and sandwich panels subjected to missile impact," in *Impact Behaviour of Fibre-Reinforced Composite Materials and Structures*, Woodhead Publishing Series in Composites Science and Engineering, pp. 239–279, Woodhead Publishing, 2000.

[25] W. Cantwell and J. Morton, "Comparison of the low and high velocity impact response of cfrp," *Composites*, vol. 20, no. 6, pp. 545–551, 1989.

[26] J. Artero-Guerrero, J. Pernas-Sanchez, J. Lopez-Puente, and D. Varas, "Experimental study of the impactor mass effect on the low velocity impact of carbon/epoxy woven laminates," *Composite Structures*, vol. 133, pp. 774–781, 2015.

[27] R. Karakuzu, E. Erbil, and M. Aktas, "Impact characterization of glass/epoxy composite plates: An experimental and numerical study," *Composites Part B: Engineering*, vol. 41, no. 5, pp. 388–395, 2010.

[28] S. Shah, S. Karuppanan, P. Megat-Yusoff, and Z. Sajid, "Impact resistance and damage tolerance of fiber reinforced composites: A review," *Composite Structures*, vol. 217, pp. 100–121, 2019.

[29] L. Sutherland and C. G. Soares, "Contact indentation of marine composites," *Composite Structures*, vol. 70, no. 3, pp. 287–294, 2005.

[30] D. ASTM, "7136," *Standard Test Method for Measuring the Damage Resistance of a Fibre-Reinforced Polymer Matrix Composite to a Drop-Weight Impact Event*, 2005.

[31] R.-M. Wang, S.-R. Zheng, and Y.-P. G. Zheng, *Polymer matrix composites and technology*. Elsevier, 2011.

[32] P. Feraboli and K. T. Kedward, "A new composite structure impact performance assessment program," *Composites Science and Technology*, vol. 66, no. 10, pp. 1336–1347, 2006.

[33] F. Chen and J. Hodgkinson, "Impact behaviour of composites with different fibre architecture," *Proceedings of the Institution of Mechanical Engineers, Part G: Journal of Aerospace Engineering*, vol. 223, no. 7, pp. 1009–1017, 2009.

[34] S.-J. Park and M.-K. Seo, "Chapter 7 - types of composites," in *Interface Science and Composites* (S.-J. Park and M.-K. Seo, eds.), vol. 18 of *Interface Science and Technology*, pp. 501–629, Elsevier, 2011.

[35] P. Cunniff, "Dimensionless parameters for optimization of textile based body armor systems," 01 1999.

[36] P. Hazell, A. Cowie, G. Kister, C. Stennett, and G. Cooper, "Penetration of a woven cfrp laminate by a high velocity steel sphere impacting at velocities of up to 1875m/s," *International Journal of Impact Engineering*, vol. 36, no. 9, pp. 1136–1142, 2009.

[37] W. Johnson, J. Masters, D. Wilson, M. Shaker, F. Ko, and J. Song, "Comparison of the low and high velocity impact response of kevlar fiber-reinforced epoxy composites," *Journal of Composites Technology Research - J COMPOS TECH RES*, vol. 21, 10 1999.

[38] G. Belingardi and R. Vadori, "Influence of the laminate thickness in low velocity impact behavior of composite material plate," *Composite Structures*, vol. 61, no. 1, pp. 27–38, 2003. Impact on Composites 2002.

[39] G. Caprino, V. Lopresto, C. Scarponi, and G. Briotti, "Influence of material thickness on the response of carbon-fabric/epoxy panels to low velocity impact," *Composites Science and Technology*, vol. 59, no. 15, pp. 2279–2286, 1999.

[40] S. Shrivastava, G. Tiwari, M. Iqbal, and P. Gupta, "The ballistic performance of thin aluminium plates against blunt-nosed projectile," *Materials Today: Proceedings*, vol. 21, pp. 1763–1771, 2020. International Symposium on Functional Materials (ISFM-2018): Energy and Biomedical Applications.

[41] J.-K. Kim and Y.-W. Mai, "High strength, high fracture toughness fibre composites with interface control—a review," *Composites Science and Technology*, vol. 41, no. 4, pp. 333–378, 1991.

[42] D. Phillips and A. Tetelman, "The fracture toughness of fibre composites," *Composites*, vol. 3, no. 5, pp. 216–223, 1972.

[43] T. Marston, A. G. Atkins, and D. K. Felbeck, "Interfacial fracture energy and the toughness of composites," *Journal of Materials Science*, vol. 9, no. 3, pp. 447–455, 1974.

[44] A. Atkins, "Intermittent bonding for high toughness/high strength composites," *J. Mater. Sci.*, vol. 10, 01 1975.

[45] A. Bergan, C. Dávila, F. Leone, J. Awerbuch, and T.-M. Tan, "A Mode I cohesive law characterization procedure for through-the-thickness crack propagation in composite laminates," *Composites Part B: Engineering*, vol. 94, pp. 338–349, 2016.

[46] J. A. Hinkley, "Interface effects in interlaminar fracture of thermoplastic composites," *Journal of Reinforced Plastics and Composites*, vol. 9, no. 5, pp. 470–476, 1990. Cited By :12.

[47] D. ASTM, "2344 standard test method for short-beam strength of polymer matrix composite materials and their laminates," *ASTM: West Conshohocken, PA, USA*, 2016.

[48] D. Arencón and J. I. Velasco, "Fracture toughness of polypropylene-based particulate composites," *Materials*, vol. 2, no. 4, pp. 2046–2094, 2009.

[49] S. Pinho, P. Robinson, and L. Iannucci, "Fracture toughness of the tensile and compressive fibre failure modes in laminated composites," *Composites Science and Technology*, vol. 66, no. 13, pp. 2069–2079, 2006.

[50] I. ASTM, "Standard test methods for plane-strain fracture toughness and strain energy release rate of plastic materials," *ASTM D5045-99*, 2007.

[51] N. Korbakov, H. Harel, Y. Feldman, and G. Marom, "Dielectric response of aramid fiber-reinforced peek," *Macromolecular Chemistry and Physics*, vol. 203, no. 16, pp. 2267–2272.

[52] I. Chang and J. Lees, "Recent development in thermoplastic composites: A review of matrix systems and processing methods," *Journal of Thermoplastic Composite Materials*, vol. 1, no. 3, pp. 277–296, 1988.

[53] V. Gupta, R. Mathur, T. Dhami, and O. Bahl, "Carbon/kevlar/peek thermoplastic composites," *High Performance Polymers - HIGH PERFORM POLYMERS*, vol. 14, pp. 285–292, 09 2002.

[54] S.-J. Park, M.-K. Seo, T.-J. Ma, and D.-R. Lee, "Effect of chemical treatment of kevlar fibers on mechanical interfacial properties of composites," *Journal of Colloid and Interface Science*, vol. 252, no. 1, pp. 249–255, 2002.

[55] X. Chen, *Advanced fibrous composite materials for ballistic protection*. Woodhead Publishing, 2016.

[56] A. Bhatnagar, *Lightweight ballistic composites: military and law-enforcement applications*. Woodhead Publishing, 2016.

[57] B. Jang, L. Chen, C. Wang, H. Lin, and R. Zee, "Impact resistance and energy absorption mechanisms in hybrid composites," *Composites Science and Technology*, vol. 34, no. 4, pp. 305–335, 1989.

[58] X. Wang, B. Hu, Y. Feng, F. Liang, J. Mo, J. Xiong, and Y. Qiu, "Low velocity impact properties of 3d woven basalt/aramid hybrid composites," *Composites Science and Technology*, vol. 68, no. 2, pp. 444–450, 2008.

[59] R. Park and J. Jang, "Impact behavior of aramid fiber/glass fiber hybrid composites: the effect of stacking sequence," *Polymer composites*, vol. 22, no. 1, pp. 80–89, 2001.

[60] M. Wardle, "Impact damage tolerance of composites reinforced with kevlar aramid fibers," in *Proceedings of ICCM-4 conference, Tokyo*, pp. 837–4, 1982.

[61] G. Dorey, G. Sidey, and J. Hutchings, "Impact properties of carbon fibre/kevlar 49 fibre hydrid composites," *Composites*, vol. 9, no. 1, pp. 25–32, 1978.

[62] K. Kaware and M. Kotambkar, "Low velocity impact response and influence of parameters to improve the damage resistance of composite structures/materials: a critical review," *International Journal of Crashworthiness*, vol. 0, no. 0, pp. 1–25, 2021.

[63] S. L. Valença, S. Griza, V. G. de Oliveira, E. M. Sussuchi, and F. G. C. de Cunha, "Evaluation of the mechanical behavior of epoxy composite reinforced with kevlar plain fabric and glass/kevlar hybrid fabric," *Composites Part B: Engineering*, vol. 70, pp. 1–8, 2015.

[64] A. Amirian, H. Rahmani, and H. Moeinkhah, "An experimental and numerical study of epoxy-based kevlar-basalt hybrid composites under high velocity impact," *Journal of Industrial Textiles*, p. 1528083721990902, 2021.

[65] A. K. Bandaru, S. Patel, Y. Sachan, R. Alagirusamy, N. Bhatnagar, and S. Ahmad, "Low velocity impact response of 3d angle-interlock kevlar/basalt reinforced polypropylene composites," *Materials Design*, vol. 105, pp. 323–332, 2016.

[66] M. Hazzard, S. Hallett, P. Curtis, L. Iannucci, and R. Trask, "Effect of fibre orientation on the low velocity impact response of thin dyneema® composite laminates," *International Journal of Impact Engineering*, vol. 100, 10 2016.

[67] F. Sarasini, J. Tirillò, M. Valente, L. Ferrante, S. Cioffi, S. Iannace, and L. Sorrentino, "Hybrid composites based on aramid and basalt woven fabrics: Impact damage modes and residual flexural properties," *Materials Design*, vol. 49, pp. 290–302, 2013.

[68] N. L. HANCOX, "1 - an overview of the impact behaviour of fibre-reinforced composites," in *Impact Behaviour of Fibre-Reinforced Composite Materials and Structures* (S. R. Reid and G. Zhou, eds.), Woodhead Publishing Series in Composites Science and Engineering, pp. 1–32, Woodhead Publishing, 2000.

[69] K. Rassiah, M. M. Ahmad, and A. Ali, "Ballistic impact performance of the layered and laminated composites: A review," *Pertanika Journal of Science and Technology*, vol. 23, no. 2, pp. 177–185, 2015.

[70] Y. Liang, X. Chen, and C. Soutis, "Review on manufacture of military composite helmet," *Applied Composite Materials*, pp. 1–19, 2021.

[71] M. I. Khan, M. Umair, R. Hussain, M. Karahan, and Y. Nawab, "Investigation of impact properties of para-aramid composites made with a thermoplastic-thermoset blend," *Journal of Thermoplastic Composite Materials*, p. 08927057211021464, 2021.

[72] E. E. Haro, J. A. Szpunar, and A. G. Odeshi, "Dynamic and ballistic impact behavior of biocomposite armors made of hdpe reinforced with chonta palm wood (bactris gasipaes) microparticles," *Defence Technology*, vol. 14, no. 3, pp. 238–249, 2018.

[73] A. K. Bandaru, V. V. Chavan, S. Ahmad, R. Alagirusamy, and N. Bhatnagar, "Ballistic impact response of kevlar® reinforced thermoplastic composite armors," *International Journal of Impact Engineering*, vol. 89, pp. 1–13, 2016.

[74] A. K. Bandaru, V. V. Chavan, S. Ahmad, R. Alagirusamy, and N. Bhatnagar, "Low velocity impact response of 2d and 3d kevlar/polypropylene composites," *International Journal of Impact Engineering*, vol. 93, pp. 136–143, 2016.

[75] N. Nayak, P. Sivaraman, A. Banerjee, V. Madhu, A. Dutta, V. Mishra, and B. Chakraborty, "Effect of matrix on the ballistic impact of aramid fabric composite laminates by armor piercing projectiles," *Polymer composites*, vol. 33, no. 3, pp. 443–450, 2012.

[76] S.-L. Gao and J.-K. Kim, "Cooling rate influences in carbon fibre/peek composites. part iii: impact damage performance," *Composites Part A: Applied Science and Manufacturing*, vol. 32, no. 6, pp. 775–785, 2001.

[77] M. Ghaseminejhad and A. Parvizi-Majidi, "Impact behaviour and damage tolerance of woven carbon fibre-reinforced thermoplastic composites," *Construction and Building Materials*, vol. 4, no. 4, pp. 194–207, 1990.

[78] B. Vieille, V. Casado, and C. Bouvet, "About the impact behavior of woven-ply carbon fiber-reinforced thermoplastic- and thermosetting-composites: A comparative study," *Composite Structures*, vol. 101, pp. 9–21, 2013.

[79] Z. Cheng, L. Zhang, C. Jiang, Y. Dai, C. Meng, L. Luo, and X. Liu, "Aramid fiber with excellent interfacial properties suitable for resin composite in a wide polarity range," *Chemical Engineering Journal*, vol. 347, pp. 483–492, 2018.

[80] T. Lin, S. Wu, J. Lai, and S. Shyu, "The effect of chemical treatment on reinforcement/matrix interaction in kevlar-fiber/bismaleimide composites," *Composites Science and Technology*, vol. 60, no. 9, pp. 1873–1878, 2000.

[81] D. Zheng, *Low velocity impact analysis of composite laminated plates*. PhD thesis, University of Akron, 2007.

[82] S. Yang, V. B. Chalivendra, and Y. K. Kim, "Fracture and impact characterization of novel auxetic kevlar®/epoxy laminated composites," *Composite Structures*, vol. 168, pp. 120–129, 2017.

[83] R. Park and J. Jang, "Impact behavior of aramid fiber/glass fiber hybrid composite: Evaluation of four-layer hybrid composites," *Journal of materials science*, vol. 36, no. 9, pp. 2359–2367, 2001.

[84] S. Saiello, J. Kenny, and L. Nicolais, "Interface morphology of carbon fibre/peek composites," *Journal of materials science*, vol. 25, no. 8, pp. 3493–3496, 1990.

[85] P. Potluri, P. Hogg, M. Arshad, D. Jetavat, and P. Jamshidi, "Influence of fibre architecture on impact damage tolerance in 3d woven composites," *Applied Composite Materials*, vol. 19, no. 5, pp. 799–812, 2012.

[86] G. Bibo, P. Hogg, and M. Kemp, "Mechanical characterisation of glass- and carbon-fibre-reinforced composites made with non-crimp fabrics," *Composites Science and Technology*, vol. 57, no. 9, pp. 1221–1241, 1997.

[87] M. Karahan and N. Karahan, "Influence of weaving structure and hybridization on the tensile properties of woven carbon-epoxy composites," *Journal of Reinforced Plastics and Composites*, vol. 33, no. 2, pp. 212–222, 2014.

[88] C. Evci, "Thickness-dependent energy dissipation characteristics of laminated composites subjected to low velocity impact," *Composite Structures*, vol. 133, pp. 508–521, 2015.

[89] J. Winkel and D. Adams, "Instrumented drop weight impact testing of cross-ply and fabric composites," *Composites*, vol. 16, no. 4, pp. 268–278, 1985.

[90] A. Sabet, N. Fagih, and M. H. Beheshty, "Effect of reinforcement type on high velocity impact response of grp plates using a sharp tip projectile," *International Journal of Impact Engineering*, vol. 38, no. 8, pp. 715–722, 2011.

[91] L. Francesconi and F. Aymerich, "Numerical simulation of the effect of stitching on the delamination resistance of laminated composites subjected to low-velocity impact," *Composite Structures*, vol. 159, pp. 110–120, 2017.

[92] R. Muñoz, F. Martínez-Hergueta, F. Gálvez, C. González, and J. LLorca, "Ballistic performance of hybrid 3d woven composites: Experiments and simulations," *Composite Structures*, vol. 127, pp. 141–151, 2015.

[93] A. Mouritz, "Ballistic impact and explosive blast resistance of stitched composites," *Composites Part B: Engineering*, vol. 32, no. 5, pp. 431–439, 2001.

[94] I. Gnaba, X. Legrand, P. Wang, and D. Soulat, "Literature review of tufted reinforcement for composite structures," *IOP Conference Series: Materials Science and Engineering*, vol. 254, p. 042011, 10 2017.

[95] M. Aktaş, H. Ersen Balcıoğlu, A. Aktaş, E. Türker, and M. Emin Deniz, "Impact and post impact behavior of layer fabric composites," *Composite Structures*, vol. 94, no. 9, pp. 2809–2818, 2012.

[96] R. Seltzer, C. González, R. Muñoz, J. LLorca, and T. Blanco-Varela, "X-ray microtomography analysis of the damage micromechanisms in 3d woven composites under low-velocity impact," *Composites Part A: Applied Science and Manufacturing*, vol. 45, pp. 49–60, 2013.

[97] J. Baucom and M. Zikry, "Low-velocity impact damage progression in woven e-glass composite systems," *Composites Part A: Applied Science and Manufacturing*, vol. 36, no. 5, pp. 658–664, 2005.

[98] R. Umer, H. Alhussein, J. Zhou, and W. Cantwell, "The mechanical properties of 3d woven composites," *Journal of Composite Materials*, vol. 51, no. 12, pp. 1703–1716, 2017.

[99] M. Aktaş, C. Atas, B. M. İçten, and R. Karakuzu, "An experimental investigation of the impact response of composite laminates," *Composite Structures*, vol. 87, no. 4, pp. 307–313, 2009.

[100] R. Sikarwar, V. Ramachandran, and N. Gupta, "Ballistic performance of kevlar/epoxy composite laminates," *Proceedings of the Indian National Science Academy*, vol. 79, p. 789, 01 2013.

[101] L. Grunenfelder, N. Suksangpanya, C. Salinas, G. Milliron, N. Yaraghi, S. Herrera, K. Evans-Lutterodt, S. Nutt, P. Zavattieri, and D. Kisailus, "Bio-inspired impact-resistant composites," *Acta Biomaterialia*, vol. 10, no. 9, pp. 3997–4008, 2014. Biomineralization.

[102] M. Quaresimin, M. Ricotta, L. Martello, and S. Mian, "Energy absorption in composite laminates under impact loading," *Composites Part B: Engineering*, vol. 44, no. 1, pp. 133–140, 2013.

[103] E. González, P. Maimí, P. Camanho, C. Lopes, and N. Blanco, "Effects of ply clustering in laminated composite plates under low-velocity impact loading," *Composites Science and Technology*, vol. 71, no. 6, pp. 805–817, 2011.

[104] D. Ginzburg, F. Pinto, O. Iervolino, and M. Meo, "Damage tolerance of bio-inspired helicoidal composites under low velocity impact," *Composite Structures*, vol. 161, pp. 187–203, 2017.

[105] C. Lopes, O. Seresta, Y. Coquet, Z. Gürdal, P. Camanho, and B. Thuis, "Low-velocity impact damage on dispersed stacking sequence laminates. part i: Experiments," *Composites Science and Technology*, vol. 69, no. 7, pp. 926–936, 2009.

[106] I. Zivkovic, P. Perisic, Z. Burzic, P. Uskokovic, and R. Aleksic, "Aramid fiber reinforced laminar thermoplastic composite materials," *Journal of Advanced Materials*, vol. 37, pp. 23–31, 10 2005.

[107] M. Kersemans, E. Verboven, J. Segers, S. Hedayatrasa, and W. V. Paepegem, "Non-destructive testing of composites by ultrasound, local defect resonance and thermography," *Multidisciplinary Digital Publishing Institute Proceedings*, vol. 2, no. 8, p. 554, 2018.

[108] A. D7269/D7269M-17, "Standard test methods for tensile testing of aramid yarns," 2017.

[109] A. D3039, "Standard test method for tensile properties of polymer matrix composite materials," *ASTM International: West Conshohocken, PA*, 2000.

[110] R. Klomp-de Boer and S. sterk, "Manufacturing and test results for Aramid/PEEK composites," *Netherlands Aerospace Center*, 2016. Unpublished confidantial document.

[111] E. Gerritzen-Willemsen, "About the feasibility of Twaron in a RIM process," *Teijin Aramid*, 2012. Unpublished confidantial document.

[112] S. Bourbigot, X. Flambard, and F. Poutch, "Study of the thermal degradation of high performance fibres—application to polybenzazole and p-aramid fibres," *Polymer Degradation and Stability*, vol. 74, no. 2, pp. 283–290, 2001.

[113] I. Curosu, M. Liebscher, S. Burk, H. Li, S. Hempel, N. Raak, H. Rohm, and V. Mechtcherine, "Influence of fiber type on the tensile behavior of high-strength strain-hardening cement-based composites (shcc) at elevated temperatures," *Materials Design*, vol. 198, p. 109397, 2021.

[114] A. A. Obaid, J. Deitzel, J. J.W. Gillespie, and J. Zheng, "The effects of environmental conditioning on tensile properties of high performance aramid fibers at near-ambient temperatures," *Journal of Composite Materials*, vol. 45, no. 11, pp. 1217–1231, 2011.

[115] A. D7136, "Standard test method for measuring the damage resistance of a fiber-reinforced polymer matrix composite to a drop-weight impact event," *ASTM International: West Conshohocken*, 2005.

[116] W. C. Jackson and C. Poe Jr, "The use of impact force as a scale parameter for the impact response of composite laminates," in *FAA, Ninth DOD (NASA) FAA Conference on Fibrous Composites in Structural Design, Volume 2*, 1992.

[117] B. Liu, A. Xu, and L. Bao, "Preparation of carbon fiber-reinforced thermoplastics with high fiber volume fraction and high heat-resistant properties," *Journal of Thermoplastic Composite Materials*, vol. 30, 10 2015.

[118] Y. Sudhir Sastry, P. R. Budarapu, Y. Krishna, and S. Devaraj, "Studies on ballistic impact of the composite panels," *Theoretical and Applied Fracture Mechanics*, vol. 72, pp. 2–12, 2014. Multiscale Modeling of Material Failure.

[119] A. K. Bandaru, S. Ahmad, and N. Bhatnagar, "Ballistic performance of hybrid thermoplastic composite armors reinforced with kevlar and basalt fabrics," *Composites Part A: Applied Science and Manufacturing*, vol. 97, pp. 151–165, 2017.

[120] N. Naik and P. Shrirao, "Composite structures under ballistic impact," *Composite Structures*, vol. 66, no. 1, pp. 579–590, 2004. Twelfth International Conference on Composite Structures.

[121] L. Sorrentino, D. S. de Vasconcellos, M. D'Auria, F. Sarasini, and J. Tirillò, "Effect of temperature on static and low velocity impact properties of thermoplastic composites," *Composites Part B: Engineering*, vol. 113, pp. 100–110, 2017.

[122] N. Shaari, A. Jumahat, and M. K. M. Razif, "Impact resistance properties of kevlar/glass fiber hybrid composite laminates," *Jurnal Teknologi*, vol. 76, no. 3, 2015.

[123] C. Evci and M. Gülgeç, "An experimental investigation on the impact response of composite materials," *International Journal of Impact Engineering*, vol. 43, pp. 40–51, 2012.

Appendix

Appendix A

Literature survey - Impact data collection

Reference	Matrix	Reinforcement	SEA relative to aramid	Comments
[118]	Epoxy	Kevlar	-	
		E-glass	-281%	
		Carbon	-41%	
[64]	Epoxy	Kevlar	-	Hybridisation increased EA over both materials
		Basalt	-36%	
		Kevlar-Basalt	14%	
[119]	PP	Kelvar 29	-	more aramid plies improved performance
		Basalt	-	
[120]	Epoxy	T300 Carbon	-	E-Glass had SEA of 150% higher than carbon
		E-glass	-	
[13]	Epoxy	Aramid	-	E-glass produced the same results as the aramid composite, S2-glass performed somewhat better
		E-glass	-1%	
		S2-glass	39%	
		Carbon	-468%	
[61]	Epoxy	Kevlar 49	-	252% better charpy impact test results
		T2 carbon	400%	
[121]	PEN	Twaron 2200	-	At 100°C Twaron had 75% better SEA than Basalt
		Basalt	-29.00%	
		CC160P carbon	-192.00%	
[59]	VE	Kevlar 29	-	Even larger difference in thicker laminate
		S2-glass	-747.55%	
[65]	PP	Kevlar 29	-	Hybridisation increased EA over both materials
		Basalt	-15.90%	
		K29-Basalt hybrid	29.30%	
[57]	Epoxy	Kevlar 49	-	Aramid deemed to perform poorly when impregnated with epoxy
		AW193P carbon	-39.20%	
		Glass	-45.20%	
[67]	Epoxy	Twaron 2200	-	Similar performance at same thickness
		Basalt	-40.70%	
		T2200-Basalt	-14.30%	

[122]	Epoxy	Kevlar 49 C-Glass K49-C-glass	- -128.30% -42.30%	Performance of hybrids according to rule of mixtures
[83]	VE	Kevlar 29 Kevlar 29 (treated) S2-glass	- -36.50% -813.00%	Removing the sizing improved EA by more than 30%
[123]	Epoxy	Aramid E-glass (UD) E-glass (woven)	- -333.80% -251.00%	
[13]	Epoxy	Aramid E-glass S2-glass Carbon	- 70.00% 400.00% -55.00%	E- and S2-glass outperformed the unspecified aramid by a significant margin
[89]	Epoxy	Kevlar 49 (woven) Kevlar 49 (UD) E-glass (woven) E-glass (UD) AS4 carbon (woven) AS4 carbon (UD)	- 0.00% 58.00% 176.40% 34.00% 12.00%	UD E-glass performed exceptionally well, questioned by authors

Table A.1: Studies on the relative specific energy absorption (SEA) of reinforcements with respect to aramid

Appendix B

Manufacturing and characterisation equipment

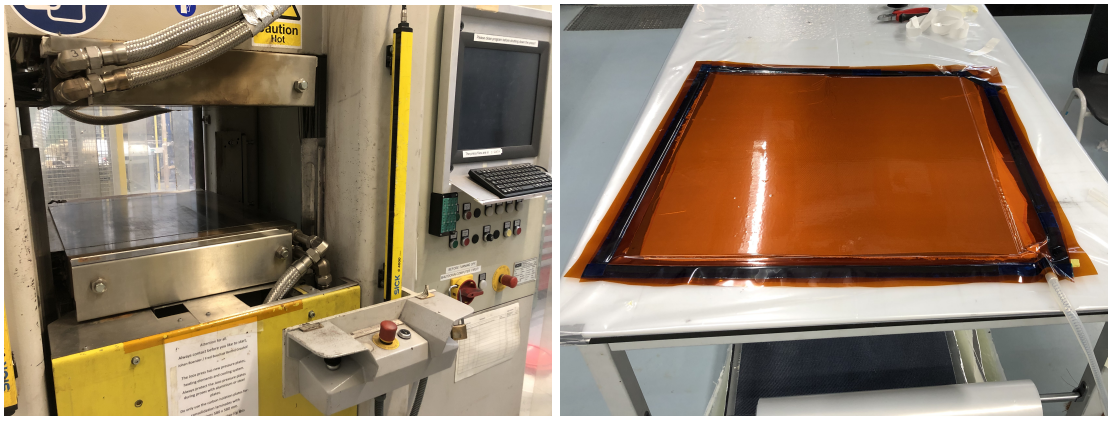

(a) Joos LAP 100 press (b) Panel encapsulated in Kapton vacuum bag

Figure B.1: Manufacturing equipment

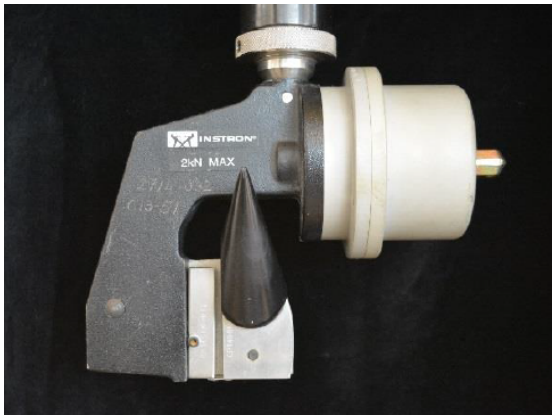

(a) Teijin aramid yarn tensile test clamp

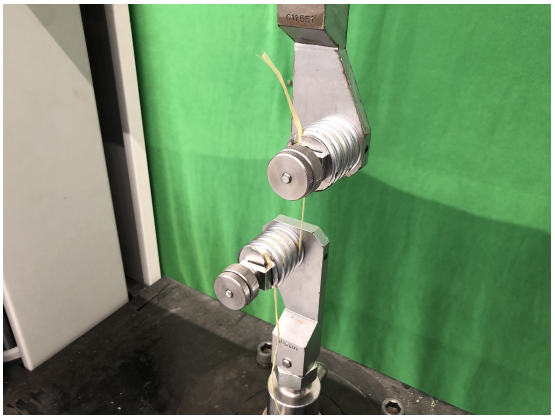

(b) TU Delft yarn tensile test setup

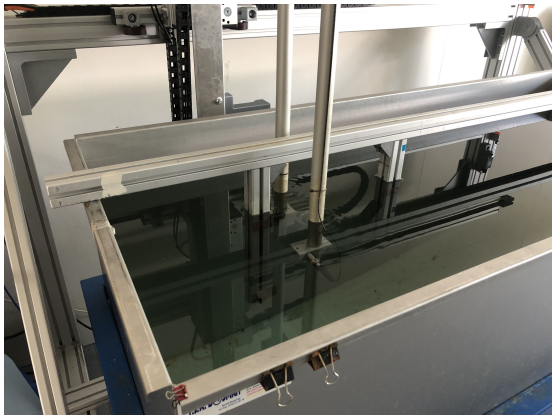

(c) C-scan test setup

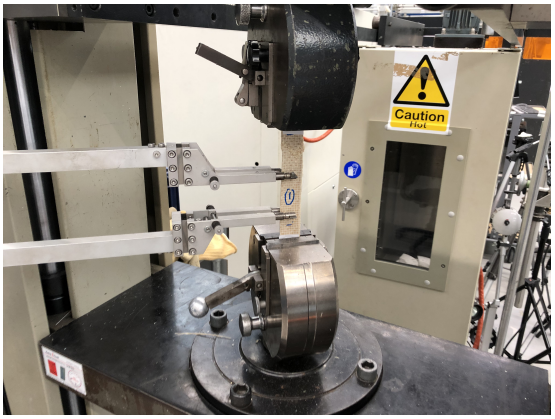

(d) Composites tensile test setup with extensometer

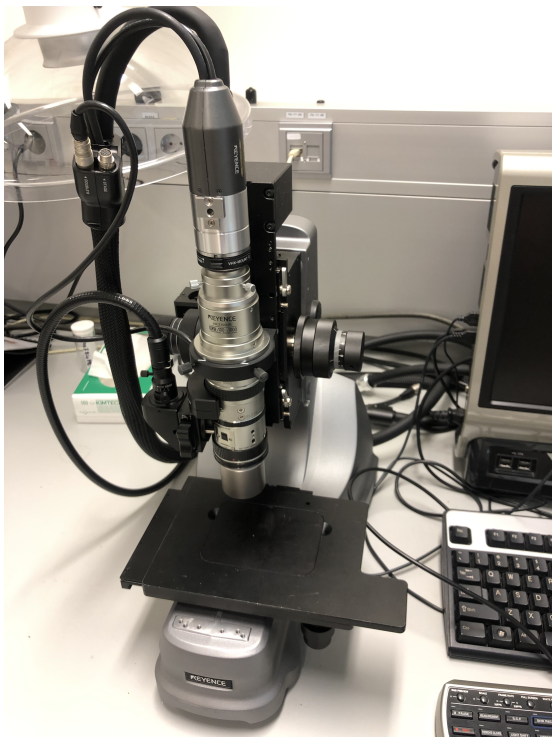

(e) Keyence VH-Z1000UR Microscope

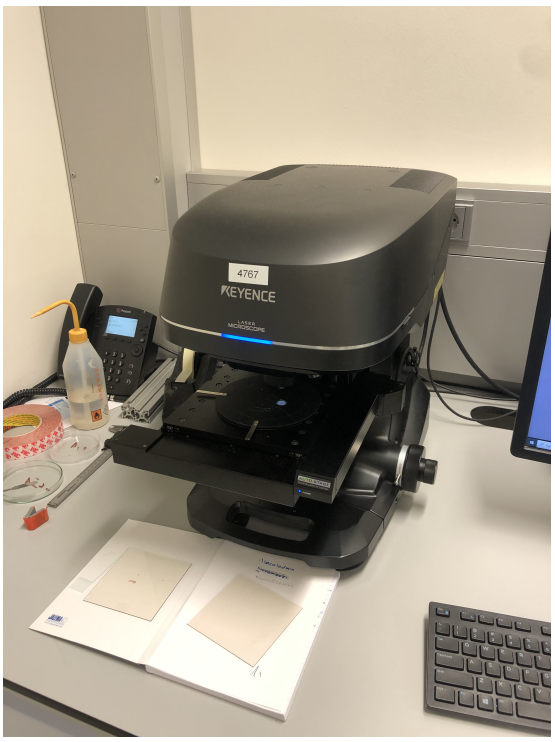

(f) Keyence VK-X1000 Microscope

Figure B.2: Characterisation equipment

Appendix C

Composite specimens

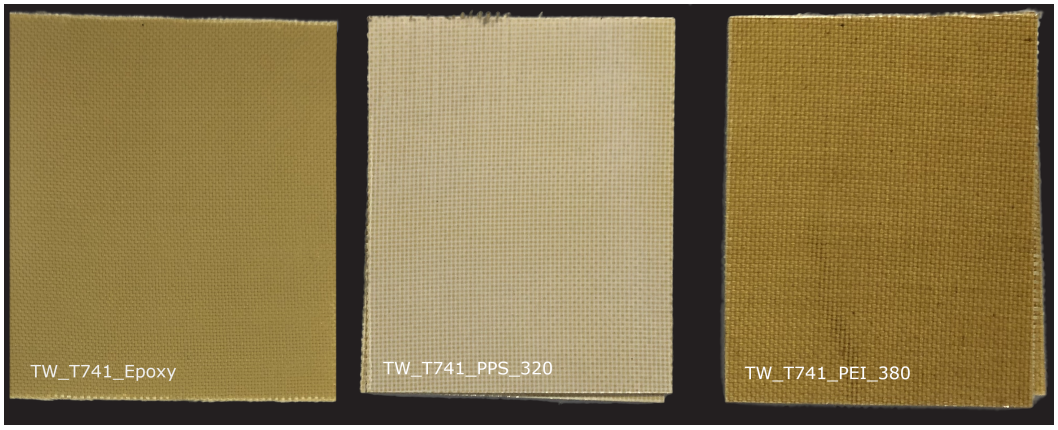

Figure C.1: T741 fabric reinforced panel specimens

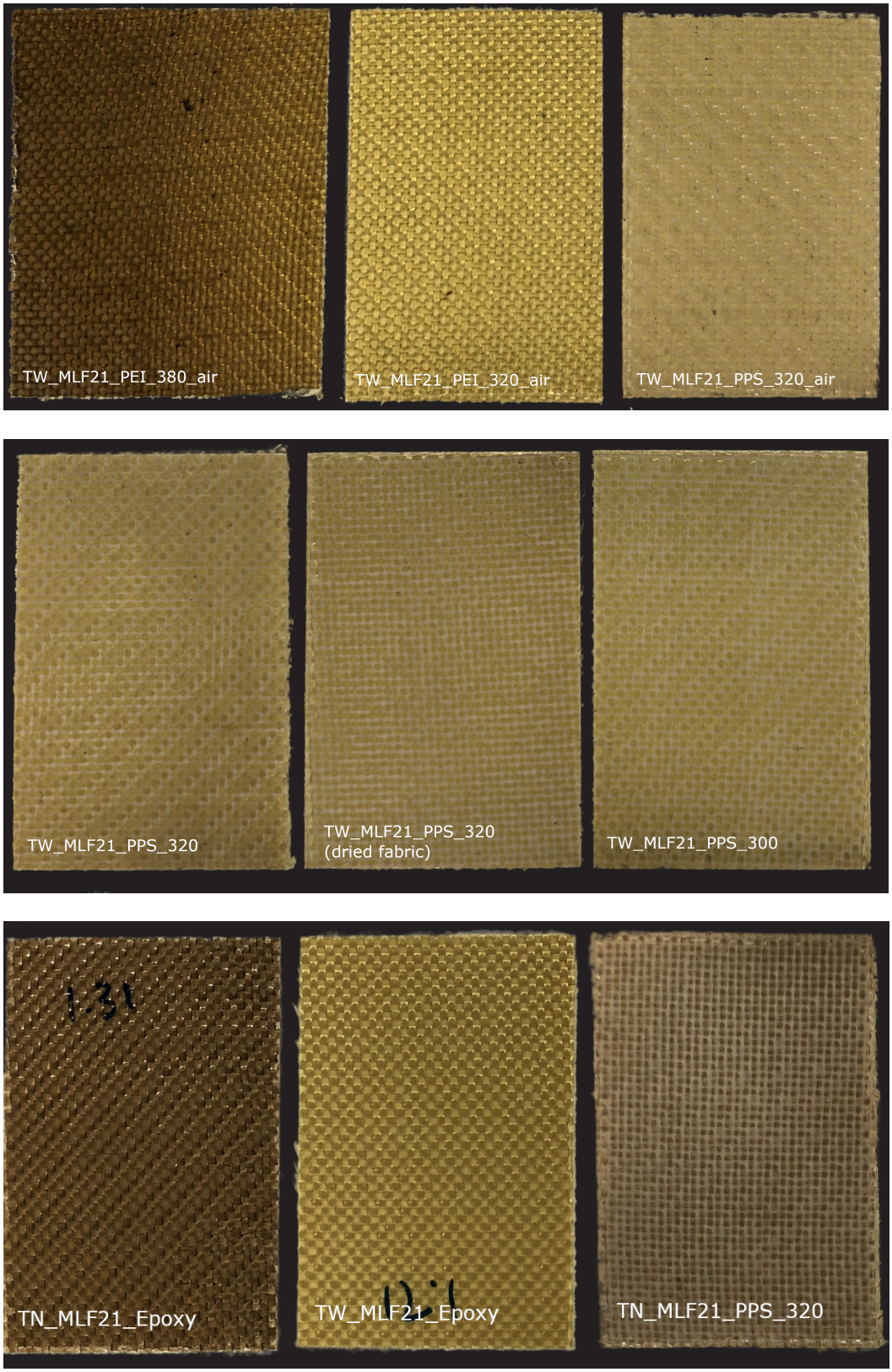

Figure C.2: MLF21 fabric reinforced panel specimens

Appendix D

Results of the fibre tensile tests

Table D.1: Retention of tensile strength for various aramid yarns after 15 min heat treatments

Yarn Type	Treatment	Duration	F_{break} [N]	STD [N]
Twaron 2200 (2000f)	None	-	611.1	28.9
	300°C air	15 min	367.6	31.8
	300°C N2		546.1	13.4
Twaron 2200 (1000f)	None	-	327.6	21.7
	300°C vacuum	15 min	318.1	8.9
Technora T200 (1000f) (old yarn)	None	-	225.0	29.42
	300°C vacuum	15 min	225.3	10.3
Twaron 2200 (1000f)	None	-	350.6	4.1
	300°C vacuum	60 min	314.1	8.2
	400°C vacuum		324.3	9.0
Technora T200 (1000f)	None	-	398.9	4.5
	300°C vacuum	60 min	383.5	10.3
	400°C vacuum		386.7	11.9
Twaron 1000	None	-	509.6	11.2
	PPS press cycle, 320°C vacuum, 10 bar	35 min	355.4	3.2

Appendix E

Tensile Specimens

(a) TW-MLF21-Epoxy

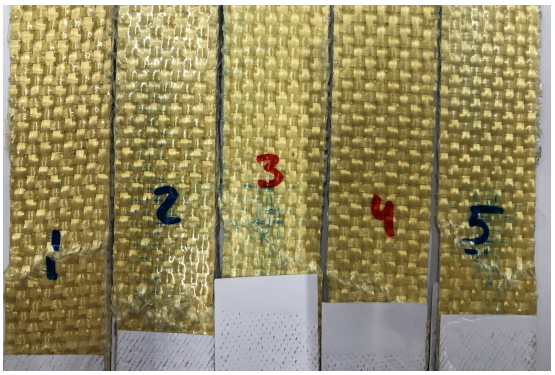

(b) TW-MLF21-PEI-320

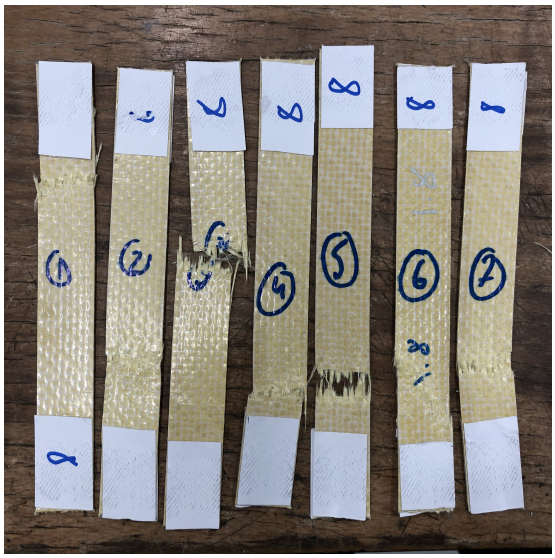

(c) TW-MLF21-PPS-320

(d) TN-MLF21-PPS-320

Figure E.1: Composite tensile specimens after fracture. Note the diagonal, ductile fracture surfaces seen in the poorly consolidated TW-MLF21-PEI-320 (b) compared to the brittle breaks in TW-MLF21-Epoxy (a). TW-MLF21-PPS-320 (c) and TW-MLF21-PPS-320 (d) show both failure modes

Appendix F

Microscopy Sample

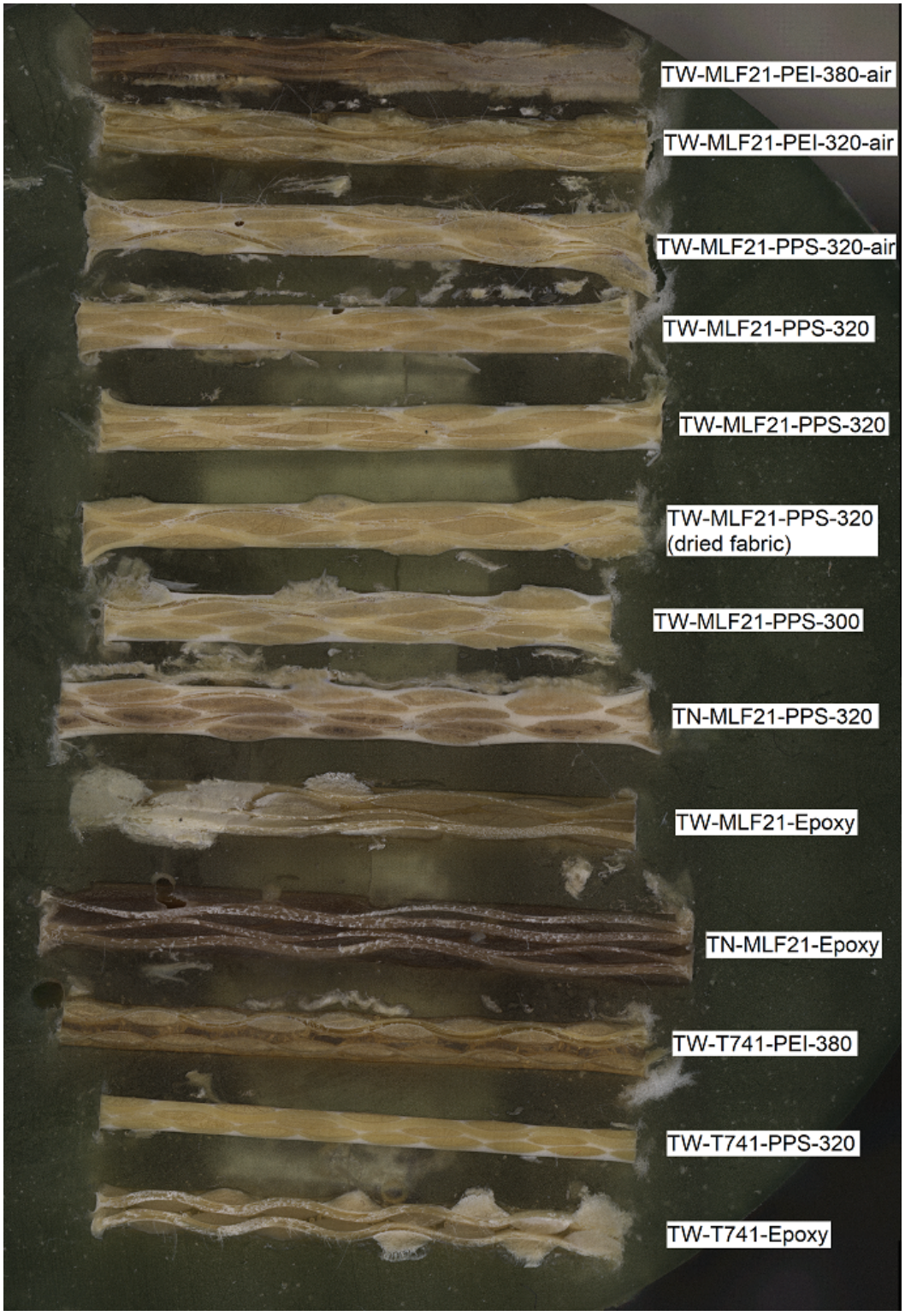

Figure F.1: Complete microscopy sample of process optimisation composites

Appendix G

Thermogravimetric analysis

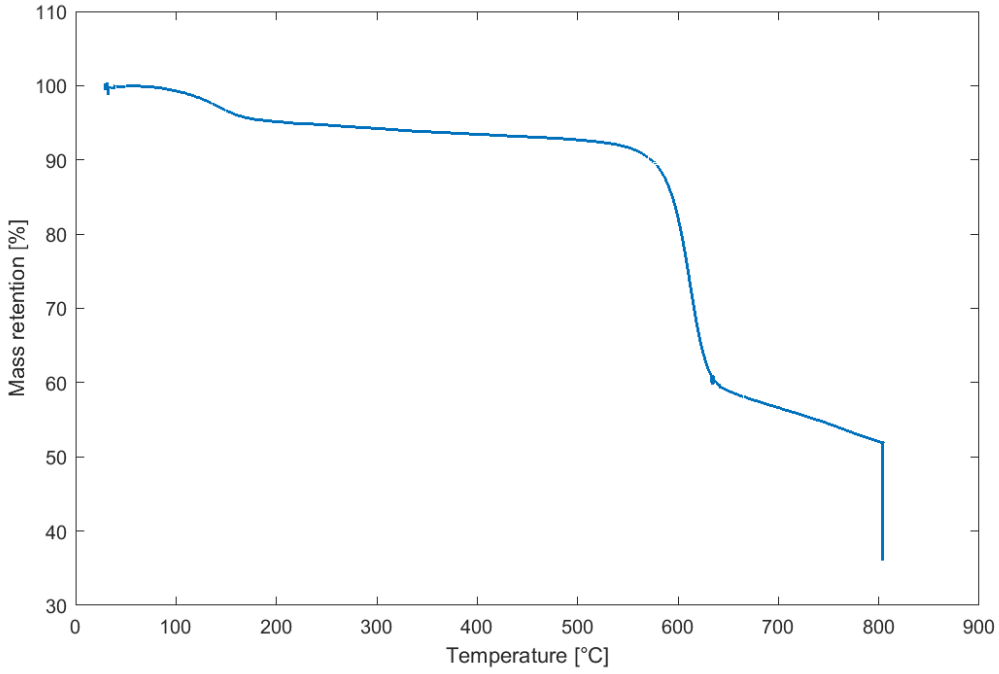

Figure G.1: Thermogravimetric curve of Twaron 1015 yarn used in T736 fabric

Appendix H

MATLAB Code

```
V = importdata('Velocity.xlsx');
nv = V.textdata;
V = V.data;                     % loading incident velocities

m0 = 1.4725;                    % impacter empty weight
mw = 2.3985;                    % added weight

load('Test3_comp')              % grouped, unprocessed force-time data of all specimens

for Spec = 1:5
    for i = 1:4
        N{i} = (sprintf('P3_%dx%i', Spec, i));              % selection of specimen
    end
    for a = 1:length(N)
        F = Data.(sprintf('%s%s%s', N{a}))(:, 3);           % creation of force data
        t = linspace(0, (length(F)-1)*2e-6, length(F))';    % creation of time data
        B = smoothdata(diff(smoothdata(F)));                % derivative of force data to identify point of contact
        for i = 3000:length(F)
            if abs(B(i+1000)) > 0.1                         % identification of start of event
                break
            end
        end
        for j = length(F):-1:i
            if abs(B(j-500)) > 0.01                         % identification of end of event
                break
            end
        end
        F = F(i:j)-min(mean(F(500:i)), mean(F(j:end)));     % removing data unrelated to event and nulling of force data
        t = t(i:j)-t(i);

        for i = 1:length(F)
            if F(i) > 50 && F(i+1000) > 1000                % identification of initial contact (continuuous rise in force)
                break
            end
        end
        for j = i+500:length(F)
            if F(j) < 15                                    % identification of last contact
                break
            end
        end
        F = F(i:j);                                         % removing data unrelated to event
        t = t(i:j)-t(i);
        Fce.(sprintf('%s%s%s', N{a})) = F;                  % storing processed force data
        tme.(sprintf('%s%s%s', N{a})) = t*1000;             % storing processed time data (ms)

        % integration
        acc = -F/(m0+mw);                                   % computation of acceleration-time data
        vel = V(nv == string(N{a}))+cumtrapz(t, acc);       % computaion of velocity-time data through trapezoidal integration
        d = cumtrapz(t, vel);                               % computation of displacement-time
        disp.(sprintf('%s%s%s', N{a})) = d*1000;            % storing processed displacement data (mm)

        for i = 400:length(F)
            if F(i) == max(F(i-100:i+100))
                Max_F(a, :) = [F(i), d(i), t(i)];           % identification of propagation initiation point
                break
            end
        end

        e.(sprintf('%s%s%s', N{a})) = cumtrapz(d, F);       % computing and storing energy-time data

        % Computing of various energies related to event: Impact energy (kinetic), E_max, E_el, E_abs, E_i, E_p
        E.(sprintf('P3_%d', Spec))(a, :) = [0.5*(m0+mw)*(V(nv == string(N{a})))^2, max(e.(sprintf('%s%s%s', N{a}))),
            max(e.(sprintf('%s%s%s', N{a})))-e.(sprintf('%s%s%s', N{a}))(end), e.(sprintf('%s%s%s', N{a}))(end),
            trapz(d(1:i), F(1:i)), trapz(d(i:end), F(i:end))];
        % Ductility Index (E_i/E_p)
        DI.(sprintf('P3_%d', Spec))(a) = trapz(d(i:end), F(i:end))/trapz(d(1:i), F(1:i));
        % Coefficient of resitution (sqrt(E_el/E_max))
        COR.(sprintf('P3_%d', Spec))(a) = sqrt(E.(sprintf('P3_%d', Spec))(a, 3)/(0.5*(m0+mw)*(V(nv == string(N{a})))^2));
    end
end
```

Figure H.1: Algorithm used to process impact data

Appendix I

Drop weight impact - data processing

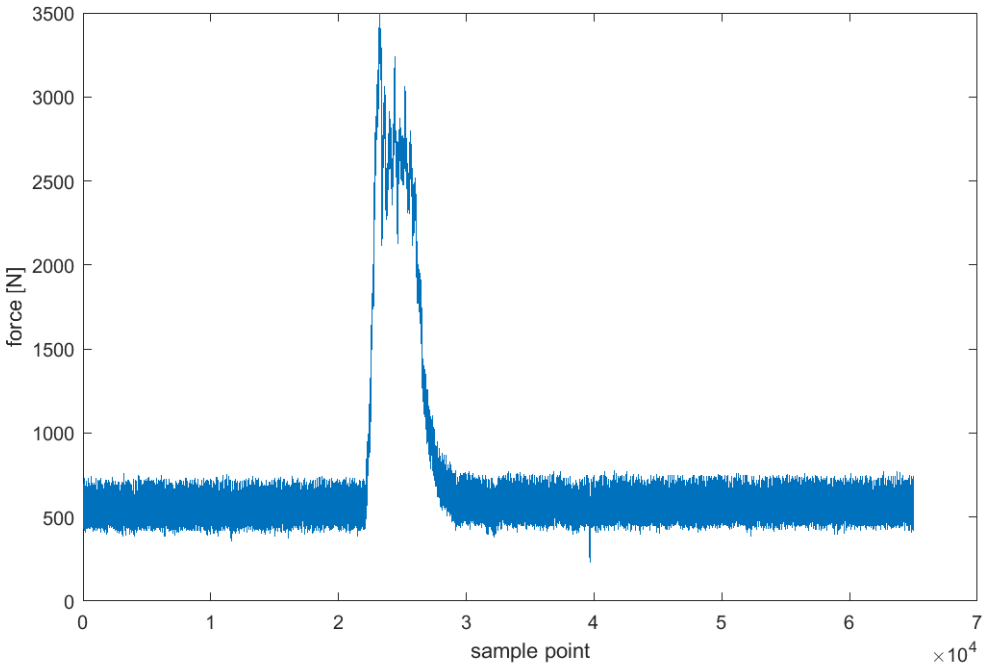

(a) Raw data as returned by drop impact setup

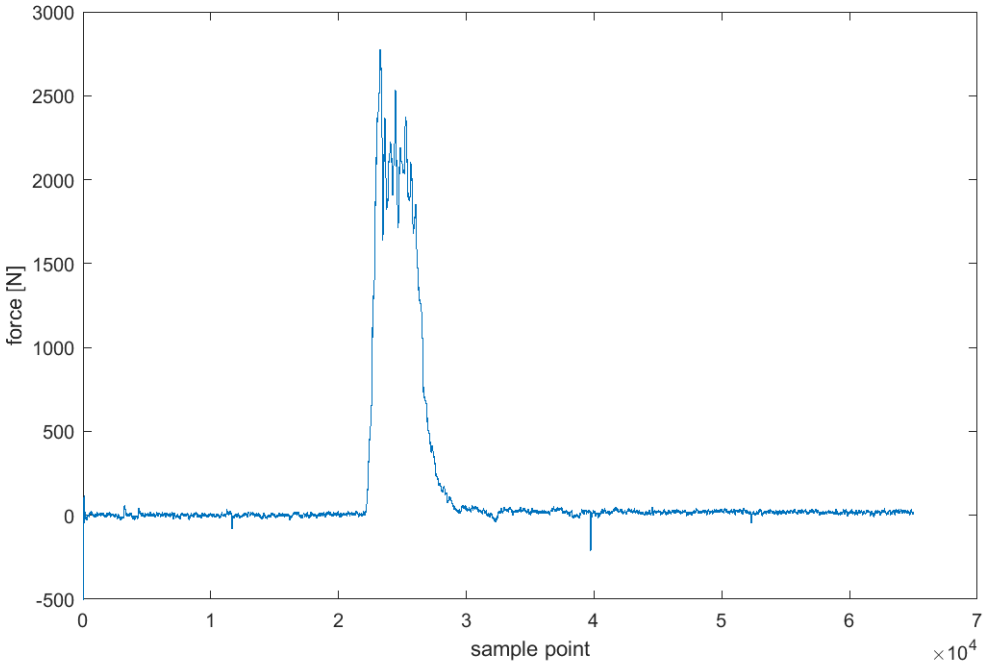

(b) Impact data after filtering and offset correction

Figure I.1: Data processing in low velocity impact

Appendix J

Impact Test Specimens

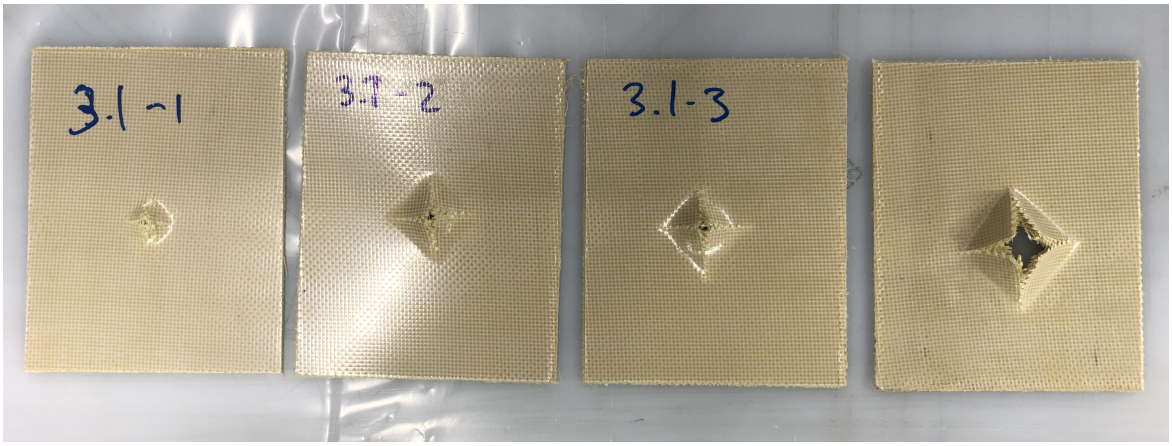

(a) TW-T741-PPS

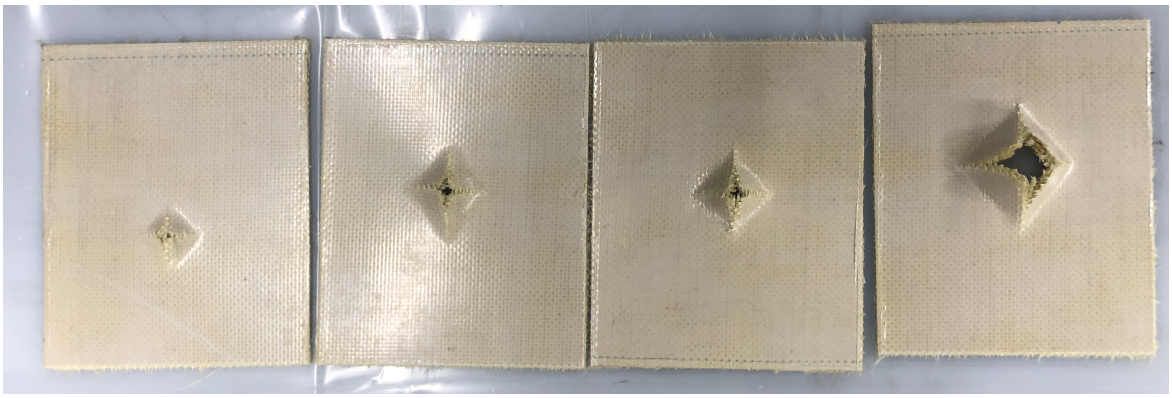

(b) TW-T736-PPS

Figure J.1: Test specimens impacted at increasing energy level

(c) TN-MLF21-PEI

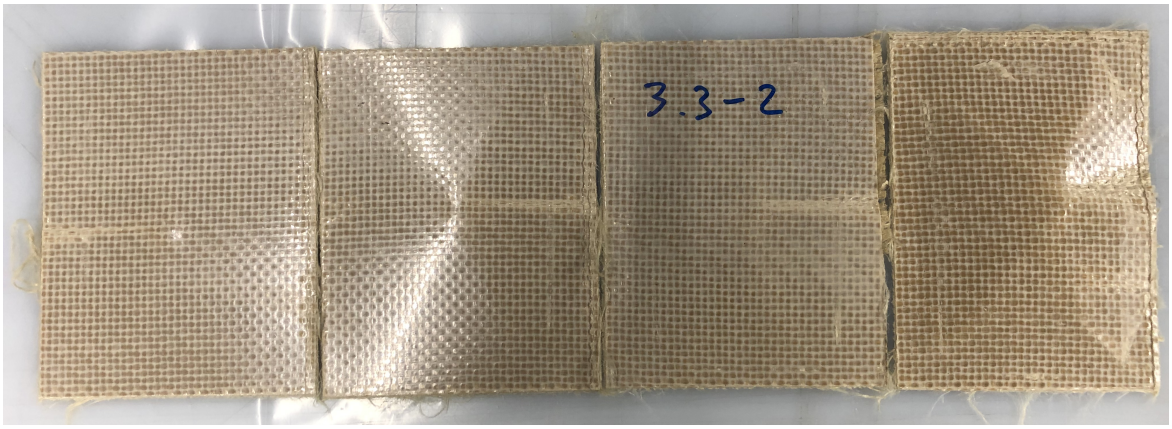

(d) TN-MLF21-PPS-c

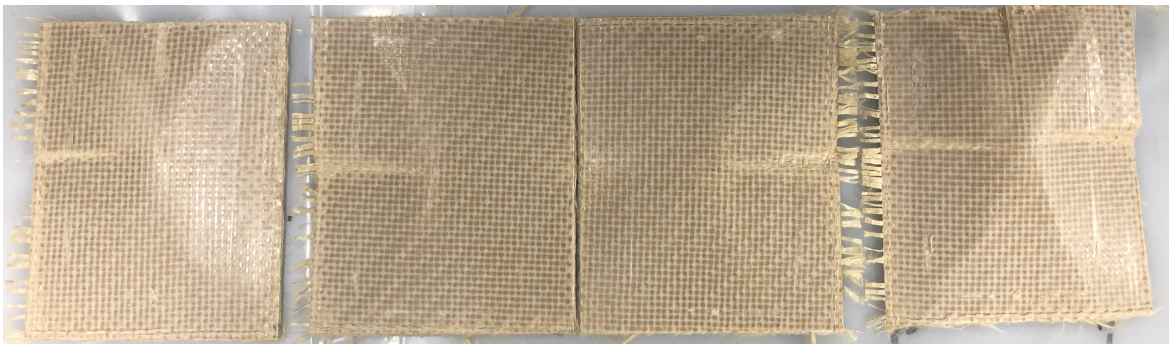

(e) TN-MLF21-PPS-a

Figure J.1: Test specimens impacted at increasing energy level